Advanced Microfabrication Techniques for the Development of Microfluidic-Based Artificial Placenta-Type Lung Assist Device

By

Neda Saraei

B.Sc.

A Thesis

Submitted to the School of Graduate Studies

in Partial Fulfilment of the Requirements for the Degree

Master of Applied Science in School of Biomedical Engineering

McMaster University

Advanced Microfabrication Techniques for the Development of Microfluidic-Based Artificial Placenta-Type Lung Assist Device

McMaster University, Master of Science (2023), Hamilton, Ontario, Canada

TITLE: Advanced Microfabrication Techniques for the Development of Microfluidic-Based Artificial Placenta-Type Lung Assist Device

AUTHOR: Neda Saraei

B.Sc.

SUPERVISOR: Professor P. Ravi Selvaganapathy

NUMBER OF PAGES: xi, 97

ABSTRACT

Preterm infants are at risk for respiratory distress syndrome (RDS) due to immature lungs, leading to notable neonatal mortality. About 10% of US births are premature. While mechanical ventilation is a common RDS treatment, it can cause complications. If it fails, extracorporeal membrane oxygenation (ECMO) is employed, but standard ECMO devices are not suited for preterm babies. The limitations of hollow fiber membrane oxygenators used in ECMO have spurred interest in an artificial placenta that connects to the umbilical cord and supports lung growth. Microfluidic blood oxygenators, with their biomimetic designs, have being explored for this purpose. This thesis advances microfabrication techniques for Lung Assist Devices (LADs), focusing on two main objectives: I. Improving Throughput for Elevated Blood Flow Rates: This section delves into refining Microfluidic Blood Oxygenators (MBOs) to accommodate greater blood flow rates. By combining parallel units, we increased throughput and optimized LAD designs. Newly designed MBOs, with an expanded gas exchange surface area, can manage blood flow rates up to 60 mL/min. Using these enhanced MBOs, we constructed a novel LAD achieving superior oxygenation compared to predecessors. Our in vitro tests confirmed that this LAD can sustain blood flow rates of up to 150 ml/min, elevating oxygen saturation by approximately 20%—equivalent to an oxygen transfer of 7.48 mL/min, a leading figure for AP-type devices. II. Hierarchically Designed Microchannels: The second objective revolves around developing microchannels with a hierarchical layout to mitigate stagnation and high shear stress regions. Traditional photolithography poses challenges at channel intersections, inducing clotting risks. We pioneered alternative microfabrication methods, yielding diverse microchannels and intricate hierarchical designs that emulate natural vascular networks devoid of dead zones. These advancements have propelled the microfabrication domain for artificial placenta-like LADs. Utilizing our method, we produced channels varying from hundreds to a few microns in height with a single exposure and an opal diffuser. Thin membranes (~60 µm top and ~45 µm bottom) were amalgamated, culminating in a total depth of about 200 µm. Such oxygenators excel in oxygenating blood even at intense flow rates of up to 15 mL/min per unit. Leveraging these hierarchically designed MBOs, we crafted a LAD supporting a flow rate of 100 mL/min, offering an oxygen transfer of 5.21 mL/min. Both LADs developed in this research proficiently support premature neonates weighing up to 2 kg. Notably, the priming volume of the LAD using the enhanced MBOs has been substantially minimized, underscoring its advancements over earlier models. Realizing these

objectives can transform neonatal care, addressing respiratory challenges in premature neonates and bolstering their chances for a healthier life.

ACKNOWLEDGMENT

I express my deepest gratitude to my advisor, Professor Ponnambalam Ravi Selvaganapathy, for the invaluable opportunity to work on this project and for his unwavering support and guidance over the past four years. His wisdom, dedication, and patience have been instrumental in our project's success and my personal growth.

I am grateful to all people involved in this project, who have supported and helped me through any steps of the project. Dr. John L. Brash, with his wonderful knowledge and experience, has been a guiding light. Dr. Gerhard Fusch's unconditional help and support throughout all my experiments. Dr. Niels Rochow's expertise and assistance in various aspects of the project have been greatly appreciated. Additionally, I must extend my thanks to Dr. Sask for her invaluable contributions. I am truly honored to have had the opportunity to collaborate with such a talented individuals. I am eagerly looking forward to our future collaborations.

Beyond the academic sphere, I owe a debt of gratitude to my parents, whose unwavering support, encouragement, and sacrifices have been the bedrock of my journey. My sisters, Shidokht and Parvin, alongside Reza, my brother, have been my steadfast anchors, always providing love, understanding, and insights that helped shape my perspectives. Shidokht, with her wisdom and poise, and Parvin, with her undying optimism and spirit, have been invaluable in my journey. Their collective love and encouragement, along with that of my parents, have been the driving force behind every step I took. Reza has been a pillar of strength, always there to offer support and motivation during challenging times. The collective support of my family has been instrumental in my achievements, and I am profoundly thankful for their presence in my life.

I would also like to express my deepest appreciation to my husband, Mohammadhossein. His unwavering love, encouragement, and understanding have been my anchor in both the highs and lows of my academic pursuits. His belief in me and his sacrifices have been the driving force behind my accomplishments. His unwavering support has allowed me to focus on my research with peace of mind, and for that, I am eternally grateful. Mohammadhossein's presence in my life has been a source of strength and inspiration, and I look forward to the continued journey together.

TABLE OF CONTENTS

LIST OF FIGURES

LIST OF TABLES

1. Chapter 1

Motivation and Organization

1.1 Introduction

Preterm infants often have underdeveloped lungs, which can lead to respiratory distress syndrome (RDS) because of an insufficient pulmonary surfactant. This results in increased neonatal mortality and morbidity. This condition is particularly dire for extremely premature infants born before 28 weeks of gestation, leading to a reduced survival rate. In the U.S., about 10% of the roughly 4 million births annually are premature, emphasizing the gravity of the situation[1]. Mechanical ventilation is the primary treatment for preterm babies with RDS. Despite its life-saving potential, it's invasive, requiring an endotracheal tube inserted through the mouth or nose. This can lead to complications, such as lung injury, bronchopulmonary dysplasia, and retinopathy, all of which might have long-term impacts[2]. If mechanical ventilation fails, extracorporeal membrane oxygenation (ECMO) becomes an alternative. In ECMO, the infant's blood is oxygenated outside the body. However, traditional ECMO devices, primarily designed for older children or adults, are not ideal for preterm infants. Their blood circuits have a large priming volume, almost equivalent to a neonate's total blood volume, which necessitates the use of donor blood and can lead to further complications. There are also concerns regarding uneven blood distribution that might result in dead zones or high-stress areas, causing hemolysis or clotting[3]. Hollow fiber membrane oxygenators (HFMO) are commonly used for ECMO. They consist of fibers within a plastic casing, facilitating gas exchange. Yet, they too have limitations, like plasma leakage. Hence, there's a growing interest in an artificial placenta (AP) that provides oxygenation while the infant's lungs mature. This device connects to the umbilical cord, reducing invasiveness, and operates without external pumps[4].

To meet these requirements, microfabrication techniques have been used to miniaturize AP blood oxygenators. Initial designs emphasized minimal priming volume, pumpless operation, and effective gas transfer which was introduced by Wu et al., a microfluidic single oxygenator unit

(SOU) for preterm infants[3]. This comprised a "blood vascular network" and a gas-permeable membrane. Although one SOU was not enough to provide adequate oxygen, multiple SOUs were combined, creating a more efficient lung assist device (LAD). More recently, Dabaghi et al. examined a microfluidic-based AP-type oxygenator using a newborn piglet model, which mimicked the conditions of neonatal babies with RDS[5]. This LAD, comprised of 16 stacked SOUs, was intended to support newborns with breathing difficulties, allowing them to breathe naturally while offering an extra means for oxygen transfer. The aim was to reduce the dependence on invasive mechanical ventilation and the associated side effects. Although the ideal design would connect the artificial placenta directly to a baby's umbilical vessels, the study used a piglet's carotid artery and jugular vein due to the model's limitations.

Over the last two decades, several microfluidic blood oxygenators (MBOs) have been created and tested, achieving efficient gas exchange due to their high surface-area-to-volume ratios[6]. They offer benefits like low priming volume, biomimetic blood vascular networks for uniform blood distribution, and the ability to use room air for gas transfer. These attributes make them promising alternatives to current commercial oxygenators. However, despite efforts to reduce priming volume and pressure drop while maximizing oxygenation efficiency, there is room for further improvement in increasing throughput, especially reasonable gas transfer at higher blood flow rates. Challenges for these devices include scaling up production for increasing throughput and manufacturing microchannels with more complex designs and geometries.

Enhancing the clinical viability of MBOs to match the performance of hollow fiber membrane oxygenators is challenging due to their limited throughput. Addressing this involves two key challenges:

I. **Enhancing throughput for higher blood flow rates:** Designing MBOs with a larger gas exchange surface is critical. This enhancement could be achieved by either expanding the size of the MBOs or by stacking multiple layers of these devices. Such design modifications can facilitate the total gas transfer at increased blood flow rates. However, several attempts to scale up a single-layer device to handle higher blood flow rates, while maintaining effective oxygen transfer, have been met with obstacles[6]. The inherent size constraints of photolithography techniques present a significant limitation. Current methods might only accommodate blood flow rates of 40–50 mL/min in a single-layer device, which has not been achieved yet. To increase throughput, it is

necessary to combine multiple units in parallel. By enhancing the throughput of MBOs, there is potential to reduce the need for numerous connectors in the final LAD assembly, leading to a more streamlined design.

II. **Microchannels with hierarchy designs for eliminating stagnation zones and high shear stress regions:** Reducing the hydraulic resistance in MBOs raises concerns about intersections between microchannels of varying heights. These intersections create dead zones and areas of high shear stress. The conventional solution is a photolithographic method that fabricates oxygenator designs with multiple channel heights by depositing several layers of photoresists of differing thicknesses. While this method produces channels of different heights, it also introduces stagnation areas and high shear stress points at the intersections. Such areas can result in blood clotting, posing a risk of device failure. Ideally, smooth transitions between channels, resembling a natural vascular network, would be preferred. However, achieving this is challenging with traditional photolithography due to its 2D constraints. Addressing these issues necessitates the development of alternative microfabrication methods. These new techniques should enable the crafting of microchannels with varied dimensions and complex hierarchical structures, thereby producing master molds with multiple heights without the associated negative effects of dead zones.

1.2 Research Objectives and Aims

The central objective of this thesis is to devise microfluidic blood oxygenators (MBOs) tailored for artificial placenta applications, integral in creating a neonatal lung assist device (LAD). The primary design criteria encompass MBOs with minimal hydraulic resistance for pumpless operation, a reduced priming volume to negate the necessity for blood transfusions, and the ability to operate efficiently in room air. The objective was achieved by tackling the subsequent aims, while also considering the previously mentioned constraints:

I. Scaling up the dimension of the previous generation of MBOs aiming to achieve equivalent gas transfer efficiency at higher blood flow rates under room air and oxygen-rich conditions.

II. Constructing a new LAD with the upscaled MBOs, aiming to decrease the quantity of MBOs and connectors required while enhancing gas transfer efficiency.

III. Enhancing the design and pioneering a new microfabrication technique to produce microchannels of diverse dimensions and intricate hierarchical designs with the goal of lowering

hydraulic resistance, mitigating high shear stress areas, and maintaining effective gas exchange efficiency.

IV. Building an LAD using MBOs with structured hierarchical microchannels, with the objective of minimizing the overall priming volume and reducing the number of MBOs needed.

1.3 Thesis outline

This thesis encompasses five chapters. Chapter 1 serves as an introduction, shedding light on the motivation and organization of the work. Chapter 2 offers a comprehensive review of the field and relevant literature. The concluding chapter, Chapter 5, wraps up the findings and sketches out potential avenues for future research. Here is a brief overview of these chapters:

I. Chapter 2 delves into the intricate workings of the lungs and the underlying causes of respiratory distress syndrome. Following this, the chapter evaluates diverse treatment strategies deployed in clinical settings. It then provides an insight into contemporary technologies before culminating in a comprehensive review of the evolution and progress of microfluidic oxygenators in academic research.

II. Chapter 3 delves into the creation of enlarged MBOs using 8-inch master molds and their application in building an LAD. It addresses Aim 1 and Aim 2, demonstrating that the newly introduced MBOs and LAD outperform their predecessors in terms of gas transfer. Utilizing the upscaled MBOs in the new LAD notably reduced the priming volume while achieving superior gas exchange rates.

III. Chapter 4 introduces a fabrication technique based on a modified photolithography process that utilizes SU8 photoresists to fabricate a MBO with hierarchy blood channels and double-sided gas transfer. This method employs a high-resolution mask and UV exposure unit to shape and form micro features. Instead of directly exposing a laid photoresist after alignment with a photolithography mask, the research suggests an innovative approach: the use of an optical light diffuser to indirectly expose the photoresist layer from the side of a transparent glass wafer. This technique disperses UV rays, facilitating exposure from the side where the photoresist is adhered to the glass wafer. Moreover, film photolithography masks are recommended over Cr masks, simplifying the fabrication process and providing flexibility for design adjustments. This chapter addresses both Aim 3 and Aim 4, unveiling MBOs with hierarchical blood channels.

IV. This chapter offers a comprehensive overview of the accomplishments presented in this thesis, concluding that microfluidic blood oxygenators possess significant potential for application as artificial placenta devices for blood oxygenation. Recommendations for future research directions are also provided. Future endeavors center on two primary strategies: (i) leveraging existing microfabrication techniques to enhance the gas exchange capabilities of microfluidic blood oxygenators, and (ii) exploring innovative fabrication methods like 3D printing to construct an artificial lung.

1.4 Contribution

The primary contributions of this thesis lie in the innovative microfabrication methods and their utilization in the design and advancement of microfluidic blood oxygenators. Within this work, the microfabrication of MBOs has been optimized and improved to facilitate the fabrication of scale-up MBOs for supporting higher blood flow rates while reaching better gas exchange rates. This enabled the assembly of a LAD with a smaller number of MBOs, which significantly reduced the number of MBOs and the overall priming volume. In addition, a new microfabrication technique that allows for the creation of oxygenators with hierarchical channels of varying heights and thin membranes on two sides has been introduced. This process aims to ensure smooth transitions between these channels, mirroring the continuity found in natural vascular networks. A notable achievement of this advanced fabrication strategy was the formation of slender membranes in areas designated for gas exchange microchannels, a necessity given that some of the broader channels reached heights of up to 600 μm. Significantly, the microchannels designed for gas exchange have an average height of approximately 100 μm. This necessitates a distinct fabrication approach for MBOs that facilitate double-sided gas transfer diffusion.

1.5 References:

[1] CDC, “Premature Birth,” *Centers for Disease Control and Prevention*, Nov. 01, 2022. https://www.cdc.gov/reproductivehealth/features/premature-birth/index.html (accessed Aug. 23, 2023).

[2] T. Pham, L. J. Brochard, and A. S. Slutsky, “Mechanical Ventilation: State of the Art,” *Mayo Clinic Proceedings*, vol. 92, no. 9, pp. 1382–1400, Sep. 2017, doi: 10.1016/j.mayocp.2017.05.004.

[3] W.-I. Wu *et al.*, “Lung assist device: development of microfluidic oxygenators for preterm infants with respiratory failure,” *Lab Chip*, vol. 13, no. 13, p. 2641, 2013, doi: 10.1039/c3lc41417e.

[4] M. C. Annesini, L. Marrelli, V. Piemonte, and L. Turchetti, “Blood Oxygenators and Artificial Lungs,” in *Artificial Organ Engineering*, M. C. Annesini, L. Marrelli, V. Piemonte, and L. Turchetti, Eds., London: Springer, 2017, pp. 117–161. doi: 10.1007/978-1-4471-6443-2_6.

[5] M. Dabaghi *et al.*, “A Pumpless Microfluidic Neonatal Lung Assist Device for Support of Preterm Neonates in Respiratory Distress,” *Adv. Sci.*, vol. 7, no. 21, p. 2001860, Nov. 2020, doi: 10.1002/advs.202001860.

[6] M. Dabaghi *et al.*, “Miniaturization of Artificial Lungs toward Portability,” *Advanced Materials Technologies*, vol. 5, no. 7, p. 2000136, 2020, doi: 10.1002/admt.202000136.

2. Chapter 2: Introduction

2.1 Lung and its function

The human respiratory system is a marvel of precision, responsible for the crucial exchange of oxygen and carbon dioxide that sustains life. Central to this complex process are the lungs, two spongy organs located in the chest cavity. Found on either side of the heart and protected by the rib cage, the lungs boast a conical shape, comprising three lobes in the right lung and two in the left. A branching network of bronchi leads to smaller bronchioles, culminating in microscopic air sacs called alveoli, which play a pivotal role in gas exchange[1]. As passive organs, the lungs rely on pressure changes to draw air in and expel it from the body. The diaphragm, a dome-shaped muscle beneath the lungs, is crucial in this process. When it contracts and moves downward, the chest cavity expands, creating negative pressure inside the lungs. This induces inhalation, as air is drawn in through the nose or mouth, passing through the trachea and bronchi, eventually reaching the alveoli. Exhalation occurs when the diaphragm relaxes, and the lungs passively recoil, forcing air out[1]. The lungs' primary function lies in facilitating the exchange of gases between inhaled air and the bloodstream[2]. As air reaches the alveoli, oxygen molecules diffuse through the thin alveolar walls and into surrounding capillaries. Oxygen then binds with hemoglobin in red blood cells, transporting it throughout the body to nourish cells and tissues. In tandem, carbon dioxide, a byproduct of cellular respiration, diffuses from the blood into the alveoli and is subsequently exhaled[2]. Surfactant, a crucial substance lining the alveoli, minimizes surface tension within them, preventing collapse during exhalation and ensuring they remain open for efficient gas exchange[3]. This unique property reduces the effort required for lung inflation during each breath. Lung capacity, signifying the volume of air the lungs can hold, and ventilation, indicating the rate of air movement, are vital factors in respiratory health[3], [4]. Breathing is regulated by the autonomic nervous system, continuously monitoring blood oxygen and carbon dioxide levels[5]. Sensors in arteries and the brainstem detect changes and adjust the breathing rate and depth accordingly. Furthermore, the brain's respiratory centers respond to factors like blood pH levels, ensuring a delicate balance between oxygen and carbon dioxide is maintained.

2.2 Respiratory failure in preterm and term neonates

Respiratory Distress Syndrome (RDS), also known as hyaline membrane disease, is a critical condition that primarily affects premature newborns[6]. It occurs due to their underdeveloped lungs, specifically the insufficient production of surfactant – a vital substance that prevents alveoli (air sacs) from collapsing during exhalation[7]–[9]. Premature babies, born before 37 weeks of gestation, often struggle to produce enough surfactant as its production typically increases in the final trimester[10]. This lack of surfactant leads to the collapse of alveoli, making breathing challenging for these infants. Typical symptoms of RDS include rapid, shallow breathing, visible chest retractions, grunting during exhalation, and cyanosis (bluish skin color) due to low oxygen levels in the bloodstream[11]. Diagnosing RDS involves thorough clinical assessment, medical history review, and chest X-rays revealing distinct lung patterns[12]. Immediate intervention is crucial, with affected infants often requiring admission to neonatal intensive care units (NICUs) for specialized care and monitoring[12]. RDS causes breathing difficulties due to the underdeveloped lungs and insufficient surfactant production. Consequently, premature infants with RDS encounter the following challenges in breathing: (I) Alveolar Collapse: The absence of surfactant leads to alveolar collapse and impaired airway maintenance during breathing. (II) Increased Respiratory Effort: To compensate for the collapsed alveoli, babies must exert more effort during each breath, leading to rapid and shallow breathing. (III) Impaired Gas Exchange: The compromised alveoli impede effective oxygen and carbon dioxide exchange, leading to decreased blood oxygen levels. (IV) Lung Stiffness: Underdeveloped lung tissue contributes to increased lung stiffness, making ventilation more difficult. (V) Risk of Respiratory Failure: In severe cases, inadequate oxygen levels and carbon dioxide retention can lead to respiratory failure, requiring immediate medical attention[13]–[15].

2.3 The treatments for respiratory distress syndrome

Premature infants with RDS often receive specialized care in neonatal intensive care units (NICUs). Treatment may involve respiratory support, such as continuous positive airway pressure (CPAP)[16], [17], mechanical ventilation[18]–[20], and exogenous surfactant administration[21]–[23], to assist lung function until the baby's lungs mature enough to produce surfactant naturally. Prognosis varies based on the condition's severity and the gestational age at birth. With proper medical care, many infants with RDS can recover and develop normally. ECMO (Extracorporeal

Membrane Oxygenation) is employed in certain cases to treat RDS when standard therapies prove inadequate or when the condition is particularly severe[24], [25]. ECMO is a life-saving technique that provides temporary respiratory and, in some instances, circulatory support by circumventing the lungs and/or heart to oxygenate the blood and eliminate carbon dioxide[25]. In specific instances of RDS, such as in premature infants with extremely underdeveloped lungs, traditional ventilator support may not suffice to maintain sufficient oxygen levels and remove carbon dioxide from the blood[25]. ECMO becomes an option as a rescue therapy when conventional ventilation proves ineffective. RDS can inflict significant harm on the alveoli, resulting in profound respiratory compromise[26], [27]. ECMO supports gas exchange through an artificial membrane that oxygenates the blood outside the body, granting the damaged lungs a chance to rest and recuperate. Mechanical ventilation, especially with high pressures, can at times worsen lung injury, leading to ventilator-induced lung injury (VILI)[28], [29]. ECMO offers a gentler form of lung support, reducing the risk of further harm to fragile lung tissue. In certain instances, especially in newborns, RDS may ameliorate over time as the lungs mature and produce more surfactant[30], [31]. ECMO serves as a temporary bridge, supporting the infant's respiratory needs until the lungs sufficiently recover to sustain gas exchange independently. In some situations, RDS may coincide with other medical conditions or complications, making it challenging to manage with standard treatments alone[32], [33]. ECMO provides vital support during the treatment of these complex cases. It is essential to recognize that ECMO is a highly specialized and invasive procedure, not without risks. It necessitates a skilled multidisciplinary team and specialized equipment. ECMO is typically considered a last resort when other treatments have been exhausted, or when the condition is life-threatening[34]. According to the World Health Organization (WHO), RDS is a leading cause of respiratory distress in premature infants, especially those born before 28 weeks of gestation. In 2015, it was estimated that about 10% of all newborns worldwide suffer from RDS, with higher rates in low-income countries where access to specialized care may be limited[35]. In the United States, RDS is a significant health concern, particularly for premature babies[35], [36]. The Centers for Disease Control and Prevention (CDC) reported that in 2019, about 8.3% of all births in the U.S. were preterm (born before 37 weeks of gestation), and many of these preterm infants may be at risk of developing RDS[37].

As mentioned earlier, mechanical ventilation and ECMO are vital interventions used to treat babies suffering from RDS. However, they have distinct limitations that must be carefully considered in

neonatal care. Prolonged use of mechanical ventilation with high pressures can cause ventilator-induced lung injury, further damaging the delicate and underdeveloped lung tissue in premature infants[28], [38]. Administering high levels of oxygen during mechanical ventilation may lead to oxygen toxicity, harming the lungs and potentially causing long-term issues[39]. Mechanical ventilation can result in barotrauma, causing damage due to excessive air pressure and possibly leading to conditions like pneumothorax[40]. Infants on mechanical ventilation face a higher risk of developing ventilator-associated infections, complicating their already delicate condition[41], [42]. Prolonged reliance on the ventilator may make the baby dependent on it for breathing, making the process of weaning off the support challenging. Also, ECMO involves cannulating large blood vessels, posing the risk of infection, bleeding, and vascular complications[43]. Not all medical centers have the specialized equipment and skilled teams required for ECMO, leading to potential treatment delays. ECMO increases the risk of blood clot formation and bleeding, necessitating careful management of anticoagulation[44], [45]. ECMO is a complex and costly procedure, impacting healthcare expenses significantly. Moreover, ECMO is intended as temporary support. Prolonged use may lead to complications, demanding a careful transition to other respiratory support or gradual weaning off ECMO when appropriate[45], [46]. While both mechanical ventilation and ECMO are indispensable in managing RDS and saving neonates' lives, doctors must carefully weigh these limitations and consider individual circumstances to determine the best treatment approach for optimal outcomes.

2.4 Artificial placenta: a different approach for treating RDS

To address many challenges and limitations of the current treatments for RDS, Artificial placenta and artificial womb devices have been invented. Artificial placenta and artificial womb devices offer potential life-saving support to neonates with RDS by emulating the functions of the natural placenta and womb[47]–[49]. Although these innovative technologies are still in the research phase and not widely used in clinical settings, they hold promise for improving outcomes for premature babies, especially those with severe RDS. The artificial placenta aims to enhance gas exchange and oxygen delivery outside the womb via the umbilical cords in a less invasive manner, providing a more efficient alternative to conventional mechanical ventilation[50], [51]. By redirecting the baby's blood through a specialized membrane that oxygenates the blood and eliminates carbon dioxide, this device can potentially reduce the risk of ventilator-induced lung injury and allow the

underdeveloped lungs of neonates with RDS to rest and recover[52]. An artificial womb, also known as an extra-uterine support system, seeks to create an environment that closely resembles conditions inside the mother's womb[53], [54]. By providing a fluid-filled, temperature-controlled space, premature babies can continue developing outside the womb[55]. This environment aims to support lung maturation and minimize complications associated with RDS. By replicating the womb's conditions, the artificial womb aims to foster lung growth and surfactant production, potentially reducing the severity of RDS and improving the overall health and survival prospects of premature infants[55], [56]. It is essential to acknowledge that both artificial placenta and artificial womb devices are still subjects of ongoing research and not yet widely available for clinical use. However, their potential to offer an alternative to conventional treatments and possibly mitigate respiratory distress in neonates makes them promising advancements in the care of premature infants.

2.5 Blood oxygenators

2.5.1 The history of blood oxygenators

The history of blood oxygenators has been a journey of continuous innovation and development, starting in the mid-20th century and progressing to the present with cutting-edge advancements. Early experiments conducted in the 1940s and 1950s involved exposing blood to oxygen in controlled laboratory settings, paving the way for the exploration of gas exchange processes outside the body[57]. A groundbreaking milestone in the field occurred in 1953 when Dr. John Gibbon Jr. successfully developed the heart-lung machine, famously known as the Gibbon machine[57], [58]. This landmark invention allowed the support of the first-ever open-heart surgery by temporarily taking over the functions of the heart and lungs during the procedure. This remarkable achievement revolutionized cardiac surgery and opened doors for further research into blood oxygenation technologies[58]. In the 1960s, the introduction of hollow fiber oxygenators marked a significant breakthrough in extracorporeal circulation[59], [60]. These hollow fiber membranes, made from biocompatible materials like polypropylene or polymethylpentene, offered a vast surface area and excellent gas-permeable properties[60]. As a result, these oxygenators proved to be highly efficient in oxygenating the blood and effectively removing carbon dioxide during cardiopulmonary bypass surgeries. This advancement significantly improved patient outcomes and reduced complications during critical medical procedures. As medical knowledge continued to expand, the concept of

ECMO emerged in the 1970s[59]–[61]. ECMO represented a groundbreaking technology that provided temporary respiratory and/or circulatory support to critically ill patients. By utilizing blood oxygenators outside the body to perform gas exchange, ECMO played a pivotal role in neonatal intensive care units (NICUs) and critical care settings, offering life-saving support to patients with severe respiratory or cardiac failure[47], [61], [62]. The 1980s witnessed further advancements in blood oxygenator design, focusing on enhancing membrane materials and technology[62]. These improvements resulted in better biocompatibility and gas exchange efficiency, minimizing complications and ensuring more successful medical procedures[62]. In the late 20th and early 21st centuries, blood oxygenators continued to evolve with a strong emphasis on miniaturization and specialization[62], [63]. This progress allowed for their utilization in an even broader range of medical scenarios, including pediatric surgeries and minimally invasive procedures, thereby extending the benefits of blood oxygenation to a wider patient population.

In the case of artificial placenta application, the baby's blood is directed through the blood oxygenator, where it comes into contact with a continuous supply of oxygenated gas devoid of carbon dioxide. During this process, oxygen diffuses from the gas into the blood, while carbon dioxide diffuses from the blood into the gas, effectively oxygenating the blood and removing waste carbon dioxide. Subsequently, the oxygenated blood is returned to the baby's body.

2.5.2 Modern blood oxygenators

In clinical settings, two main types of blood oxygenators are utilized to facilitate gas exchange during medical procedures: hollow fiber oxygenators and flat-sheet membrane oxygenators[62]. Hollow fiber oxygenators are the most commonly used type in hospitals, hollow fiber oxygenators, consist of numerous tiny, hollow fibers made from biocompatible materials like polypropylene or polymethylpentene[62], [64]. In modern hollow fiber oxygenators, blood flows through the hollow cores of these fibers, while oxygen-rich gas circulates around the outer side. Gas exchange occurs through the walls of the hollow fibers, enabling oxygen to diffuse into the blood and carbon dioxide to diffuse out[62]. Hollow fiber oxygenators are prevalent in cardiopulmonary bypass during open-heart surgeries and in ECMO for patients with severe respiratory or cardiac issues. Flat-sheet membrane oxygenators, also known as plate or disc oxygenators, flat-sheet membrane oxygenators are employed in specific clinical scenarios[62], [65]. They consist of flat, thin membranes made from biocompatible materials. Blood flows over one side of the membrane, and oxygen-rich gas

flows on the other side. Gas exchange occurs through the membrane, allowing oxygen to transfer from the gas to the blood and carbon dioxide to transfer from the blood to the gas[65], [66]. Flat-sheet membrane oxygenators are commonly used in pediatric surgeries or for patients with particular medical conditions where their design and size offer advantages. Both types of blood oxygenators serve the crucial purpose of oxygenating the blood and removing carbon dioxide, providing essential support in critical medical situations. However, the use of hollow fiber oxygenators have become more standard and common in the last few decades.

Hollow fiber oxygenators, while effective in supporting gas exchange in various clinical situations, have certain limitations when used for premature babies with RDS. Hollow fiber oxygenators require a specific amount of priming volume (fluid) for proper functioning and to remove air bubbles[63], [67]. In premature babies, especially those with low blood volumes (low birth weights), the priming volume can be relatively significant compared to their overall blood volume, potentially leading to hemodilution and fluid-related complications[67]–[69]. The high surface area of hollow fiber oxygenators can cause blood trauma, triggering the clotting cascade and platelet consumption. This increases the risk of blood clot formation and hemolysis (breakdown of red blood cells)[67]. The artificial surfaces of hollow fibers can trigger an inflammatory response in premature babies' immature immune systems. This may lead to the release of inflammatory mediators and compromise the baby's overall health. Hollow fiber oxygenators may have limitations in their gas exchange efficiency, particularly in severe cases of RDS in premature babies. Insufficient gas exchange can result in inadequate oxygenation and incomplete removal of carbon dioxide from the blood. Premature babies are more prone to coagulation and clotting issues, and the use of hollow fiber oxygenators may exacerbate these problems due to their large surface area and interaction with foreign surfaces[70], [71]. The blood trauma and hemodilution caused by hollow fiber oxygenators may necessitate more frequent blood transfusions for premature babies, which carries its own set of risks[72], [73]. To address some of these limitations, especially high priming volume and non-optimal gas transfer efficiency, microfabrication techniques and technologies have been utilized to help ensure the best possible outcomes for these vulnerable infants[74]–[76].

2.6 Microfluidic blood oxygenators: the advent of a new era

Microfluidic blood oxygenators (MBOs) are state-of-the-art medical devices designed to enable gas exchange in the blood at a microscale level using microfabrication technologies. Unlike traditional blood oxygenators that utilize hollow fibers or flat-sheet membranes, microfluidic oxygenators operate on a much smaller scale, typically at the micrometer level [77]. These devices consist of microfluidic channels or networks of microchannels. The blood flows through these tiny channels, while an oxygen-rich gas or oxygenating gas (room air or a gas with higher oxygen content than room air) is circulated on the other side. This enables gas exchange at the interface between the blood and the blood, allowing oxygen to diffuse into the blood and carbon dioxide to diffuse out[63], [78]. MBOs offer numerous advantages over conventional oxygenators. They provide enhanced gas exchange efficiency due to their larger surface area-to-volume ratio, reducing blood trauma and the risk of clotting or hemolysis. Additionally, they have a smaller priming volume, making them well-suited for neonatal applications, and their precise and controlled nature may offer personalized treatment options[79], [80]. Though still in the research and development phase, ongoing research in microfabrication techniques and biocompatible materials holds significant promise for integrating microfluidic oxygenators into critical care, neonatal medicine, and other medical fields [63]. Their compact, portable design makes them suitable for diverse medical settings, presenting an exciting avenue for future medical advancements.

The majorities of developed MBOs are comprised of three main components: the blood side flow manifold, the gas side flow manifold, and a thin gas-permeable membrane as depicted in Figure 2.2.1 [63]. The blood side manifold consists of microfluidic channels, resembling the structure and function of natural lungs to ensure efficient gas exchange. Meanwhile, the gas side manifold uniformly delivers gases like oxygen or air in proximity to the gas-permeable membrane. Microfabrication techniques are employed to design blood flow paths and manifolds that reduce high shear stress zones and stagnant regions, resulting in lower resistance to blood flow and decreased pressure drops across the device. In some oxygenators, the gas side manifold is omitted to allow exposure to ambient air or oxygen. Membranes play a crucial role in MBOs, physically separating the blood side from the gas side while enabling rapid gas exchange. Polydimethylsiloxane (PDMS) is the preferred material for MBO membrane fabrication due to its high permeability and ease of use.

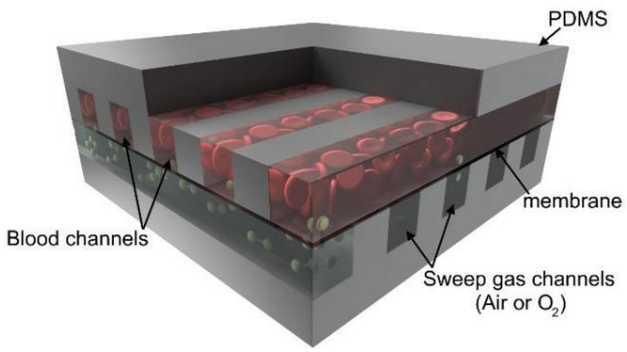

Figure 2.2.1: A 3D schematic view of MBOs made of three the blood side flow manifold, the gas side flow manifold, and a thin gas-permeable membrane. Reproduced with the permission[63].

2.6.1 The choice of materials for microfluidic blood oxygenators

When selecting materials for blood oxygenators, it's crucial to ensure they meet specific criteria. These devices play a pivotal role in aiding respiratory functions, and their efficiency, safety, and durability hinge on the properties of their constituent materials. Here are the essential properties these materials should exhibit[81]:

(1) gas permeability: The membrane must be precisely designed to facilitate an unhindered flow of gases. Its pores need to be slightly larger than the O_2 molecules, measuring at 0.346 nm, and CO_2 molecules at 0.33 nm. This ensures the seamless exchange of these crucial gases, mimicking the natural respiratory process.

(2) resistance to blood and plasma: Ensuring the integrity of the membrane is vital. It must serve as an effective barrier to blood, keeping it separate and preventing any unwanted mixing with gases. Minimizing plasma leakage is also crucial, as this can affect the overall efficiency and safety of the oxygenation process.

(3) material malleability and strength: The foundational materials chosen for these membranes should not only be malleable but robust. Given the continuous movement of blood, the membranes will experience a consistent shear force, especially with an average blood flow pressure of about 0.053 MPa. This demands that the material possesses commendable mechanical strength.

(4) stability and resistance: Beyond just functioning, the membrane materials need to be resilient in various environments. They should offer thermal stability, which means they can operate effectively in different temperature ranges. Additionally, their resistance to chemicals, both acidic and basic, microbial degradation, and oxidative processes ensures longevity. Furthermore, being able to withstand sterilization processes like autoclaving indicates a higher degree of durability.

(5) biocompatibility: Perhaps one of the most crucial criteria is that the material shouldn't react negatively with the biological environment it's placed in. This includes avoiding triggering any inflammatory responses. It's imperative to ensure that the material doesn't induce clotting, activate unwanted enzymatic reactions, or stimulate an immune response, guaranteeing the patient's safety.

Selecting membranes for blood oxygenation involves distinguishing between porous and non-porous types. Most of these membranes should feature nanopores to facilitate adequate gas transfer. Notable materials in this category include polypropylene (PP), poly-4-methylpentene (PMP), polyvinylidene difluoride (PVDF), polysulfone (PS), and polyethersulfone (PES). Conversely, silicone-based materials, when rendered sufficiently thin, can serve as gas-permeable membranes even without incorporating porosity.

PDMS, which is a type of silicone-based polymer, stands out as the preferred material for microfabrication and microfluidics due to its exceptional combination of advantageous properties, making it an ideal choice for a wide range of applications. In the realm of medical and biological applications, PDMS's high biocompatibility is of utmost importance, ensuring safe interactions with living tissues and cells[82]–[84]. This property makes PDMS-based devices suitable for handling diverse biological samples, including blood or cells. Moreover, PDMS's optical transparency in the visible and near-infrared regions enables researchers to easily visualize and study biological processes, cells, and fluid flows within microdevices, utilizing advanced microscopy techniques[85]. Most importantly, PDMS's exceptional gas permeability is particularly advantageous in microfluidics, as it facilitates efficient gas exchange applications like oxygenation or carbon dioxide removal[63], [86]. By enabling efficient gas diffusion across its surface, PDMS ensures proper gas exchange during biological or chemical reactions[87], [88]. Furthermore, PDMS's excellent reproducibility allows it to be molded and replicated with precision, ensuring consistent quality and performance of microfluidic devices during mass production, making them suitable for both research and commercial use. Moreover, the cost-effectiveness of PDMS sets it

apart from other materials used in microfabrication, making it accessible to researchers and laboratories with limited budgets[89], [90]. The flexible and elastic nature of PDMS is a highly valued characteristic, allowing it to deform without compromising structural integrity. This quality facilitates the fabrication, assembly, and sealing of PDMS-based microfluidic devices, catering to a wide variety of microfluidic applications[91]–[94]. However, this natural property of PDMS caused some issues and challenges in the fabrication of MBOs, which lacked the gas compartments to encounter the differential pressure exerted by the blood compartment, leading to membrane bulging and deformation, and finally device failure[74].

To PDMS be used as a gas-permeable membrane, it should be fabricated in the form of a thin film[95], [96]. The easiest tool to manufacture a thin PDMS layer or film is spin-coating. PDMS membranes are created using a spin-coating technique, where a mixture of PDMS base and curing agent in a 10:1 ratio is applied onto a flat substrate, typically a silane-coated silicon wafer to reduce stickiness and ease delamination[96]–[98]. The coated substrate is then cured either in an oven or on a hot-plate. The 10:1 ratio of PDMS base to curing agent is preferred over other ratios for several reasons in the fabrication of PDMS membranes and microfluidic devices: (I) optimal cross-linking: The 10:1 ratio provides a suitable balance between the number of cross-links and chain lengths in the resulting PDMS network. This ensures a stable and robust membrane while maintaining desired mechanical properties like flexibility and elasticity[99]. (II) Easy mixing: The 10:1 ratio simplifies the mixing process of PDMS components, leading to consistent and reproducible results during fabrication. (III) Minimized uncured PDMS: Excess curing agent may lead to unreacted or uncured PDMS in the final product, affecting membrane properties. The uncured PDMS molecules can eventually leak to the biological fluid such as blood in the case of blood oxygenators, increasing the chance of cytotoxicity. The 10:1 ratio reduces the presence of uncured PDMS, ensuring a fully cured and functional membrane[100]–[102]. (IV) Reduced swelling: PDMS membranes can absorb compounds from the environment, causing swelling and altering properties. The 10:1 ratio helps minimizes this issue, resulting in more reliable and stable membranes while not compromising the gas exchange properties of the final product[96], [101], [103]. (V) Consistent permeability: The 10:1 ratio has been extensively studied and optimized for various applications, ensuring predictable and consistent permeability results. Overall, the 10:1 ratio strikes a balance between cross-linking, ease of fabrication, and desirable properties, making it the preferred choice for PDMS-based microfluidic devices and membranes in research and practical applications.

The gas permeability of PDMS membranes can be significantly affected by a range of parameters: (1) Curing ratio: The proportion of PDMS base to curing agent used during fabrication plays a critical role. Lowering the curing agent ratio enhances permeability by reducing cross-linked chains, allowing gases to diffuse more easily. However, it may also increase membrane elasticity and vulnerability to deflection and rupture under pressure[96], [104]. As mentioned above, the 10:1 ratio was mostly used for fabricating MBOs, however, the impact of varying PDMS ratios has not been widely studied for MBOs, especially modern MBOs. (2) Curing temperature: The temperature at which the PDMS membrane is cured influences its permeability. Higher curing temperatures can result in greater permeability to specific gases compared to lower temperatures. Different gases may exhibit varying diffusion rates in PDMS membranes, impacting permeability. Membranes cured at 75 °C have shown higher permeability to CO_2, N_2, and CH_4 compared to those cured at temperatures ranging from 25 °C to 150 °C[105], [106]. (3) Membrane thickness: Generally, membrane thickness has a limited impact on permeability. Permeability mainly depends on the diffusion coefficient and solubility of gases, which are inherent material properties independent of thickness. Nevertheless, thinner PDMS membranes may facilitate higher oxygen flux, benefiting microfabricated designs for oxygenation[96], [96], [107]. (4) The source of PDMS or silicone-based material: The selection of PDMS material, including grade and brand, can affect gas permeability. Different PDMS materials may possess varied gas diffusivity and solubility properties, resulting in differences in membrane permeability. (5) Gas type: The specific gas under consideration for permeability analysis also plays a role. Different gases may display distinct diffusion rates and solubility in PDMS membranes, leading to variations in permeability. For instance, PDMS membranes are more permeable to CO_2 compared to O_2.[95], [108]–[110] (6) Environmental conditions: The surrounding environment can influence membrane permeability. Factors such as temperature, humidity, and the presence of other gases or solvents may impact gas diffusion through the membrane. Conventionally, the environmental factor had been ignored due to the fact that gas transfer is mostly dominated by the diffusion of gases through blood rather than the diffusion of gases through the membranes.

Despite some early research exploring the use of other porous membranes, like polycarbonate with different porosities, they were found to cause plasma leakage, preventing further use. An alternative approach to tackle the leaking issues involved coating a thin layer of PDMS on these porous membranes to improve bonding with PDMS microchannel features, reducing leakage and device

failure[63], [68]. However, this method did not show a noticeable improvement in oxygenation compared to nonporous PDMS membranes. Another interesting avenue explored to enhance oxygen diffusion through PDMS membranes is using patterned or nonpatterned micropores[111]–[115]. Nonetheless, it is important to note that creating a porous PDMS membrane is challenging and has scalability limitations. More recently, a new category known as "composite membrane" has emerged for MBOs. This involved reinforcing PDMS with ultrathin stainless-steel mesh or a porous polytetrafluoroethylene (PTFE) membrane with high porosity to increase the mechanical strength of the composite PDMS membrane[74], [75], [79].

In summary, PDMS plays a crucial role in MBOs due to its ease of fabrication and high gas transfer capabilities, making it the dominant material in this area. Although the majority of ongoing research has focused on improving the design of MBOs, it might be needed to explore innovative techniques to enhance oxygen diffusion and address limitations associated with using porous membranes in conjunction with PDMS.

2.6.2 History of microfluidic blood oxygenators

In the last 15 years, many different designs and configurations of MBOs had been introduced. In the early stages, MBOs, similar to traditional hollow fibre membranes, relied on an oxygen-rich environment to effectively oxygenate the blood. The first generation of MBOs was introduced by Lee et al. where they conducted theoretical studies to evaluate diverse MBO designs with varying heights and geometries[116]. Some of these designs were subsequently fabricated and validated experimentally, including configurations with an array of straight rectangular microchannels and others with microscale support posts placed in a wide rectangular channel. The use of support posts aimed to enhance the effective gas exchange surface area without increasing the device size. However, despite the low pressure drop facilitating pumpless operation, these devices couldn't fully oxygenate blood at an acceptable flow rate, indicating inadequate oxygen transfer for clinical purposes due to their small size. Moreover, relying on pure oxygen as the ventilation source made these designs complex and less suitable for a portable artificial lung format[117], [118].

In 2010, Hoganson and colleagues[119] developed a micro-machined artificial lung with a microvascular network of blood channels and alveolar chambers for enhanced gas exchange. However, despite its low pressure drop and high operating flow rate, the device exhibited a lower oxygen flux compared to another device. It required pressurized 100% oxygen, making it resource-

intensive and bulky. Additionally, the design inefficiently used only 30% of the nominal area, rendering it unsuitable as a lung assist device.

Potkay et al.[120] developed an early microfluidic device with a nonporous PDMS membrane (15 µm thickness) and microcapillaries (20 and 10 µm height) using air as the sweep gas. This can be considered as one of the earliest effort to eliminate the need of oxygen as the sweep gas for MBOs. To imitate natural lung branching, the blood compartment microchannels were created with varying heights (140, 60, and 20 or 10 µm). Artificial microcapillaries on the blood side were 88 µm wide and spaced 88 µm apart. Support posts in the gas side prevented membrane collapse, resulting in a 20% reduction in the effective surface area. Larger channels (140 and 60 µm height) facilitated blood distribution with lower pressure drop, while smaller channels (10 or 20 µm height) ensured efficient gas exchange. The total surface area, including all branching channels and microcapillaries, was 24 cm^2. Devices with 20 µm tall and 10 µm tall microcapillaries had active gas exchange surface areas of 2.34 and 1.67 cm^2, respectively. Porcine blood was used to test all devices, while air was supplied as the ventilating gas. The highest oxygen uptake achieved was approximately 0.04 mL min^{-1} at a blood flow rate of 1.5 mL min^{-1}, with a corresponding pressure drop of around 500 mmHg. Over time, the pressure drop on the blood side increased due to clot formation in the small artificial capillaries. After approximately 3 hours of operation, less than 10% of the artificial microcapillaries were clogged. Despite using air instead of pure oxygen, the device demonstrated similar or better efficiency compared to other available artificial lungs, thanks to the reduction in oxygen diffusion resistance in the blood side (as the size of the blood channels was in the range of 10–20 µm, comparable to the size of red blood cells, allowing oxygen molecules to reach red blood cells promptly after entering the blood). The introduction of channels with different heights was the main strategy to reduce hydraulic resistance. However, this approach would cause the creation of dead zones in the regions where channels with different height met.

Kniazeva et al.[121] devised a multi-layer MBO inspired by the natural vasculature design to optimize blood flow with reduced resistance. They conducted experiments with various membrane thicknesses (11, 26, 46, 59, 83, and 120 µm) to understand how varying membrane thickness would impact gas transfer. This was the first time that the impact of PDMS membranes with different thickness on gas exchange was studied. The MBOs consisted of 3, 5, or 10 bilayers, each containing a blood vascular microchannel network and an oxygen channel separated by a thin membrane. In

the first prototype introduced by this research group, phosphate-buffered saline (PBS) instead of blood was used to assess gas transfer efficiency[121]. In a subsequent study, the same research group led by Borenstein tested a ten-bilayer configuration of the previously developed device, using bovine blood in 2012[122]. Each ten-transfer-module device, along with its inlets and outlets, was connected to central vertical channels for blood and gas inflow and outflow. The devices had 50 or 100 µm tall channels and 30 or 117 µm thick membranes. Whole bovine blood was used at varying flow rates of 1–10 mL/min. The highest oxygen transfer reported was 0.275 mL/min1 at a blood flow rate of 10 mL/min for the ten-transfer-module device with 50 µm tall blood channels and 30 µm thick membranes. The study revealed that increasing the number of layers, using thinner membranes, and shortening the blood vascular networks improved gas transfer. However, reducing the height of blood vascular networks resulted in a lower priming volume but higher pressure drops. To evaluate the resistance of the vascular networks in single and ten-layer transfer modules, DI water was used, and no pressure drop was observed for those devices perfused with blood[122]. Nevertheless, the pressure drop was still significant when tested with water, making this MBO design unsuitable for pumpless operation.

In 2013, Wu et al.[68] introduced a microvascular network featuring square pillars, which had a unique characteristic of being exposed to room air instead of oxygen. The study investigated various membrane types. The device's unique design offered portability by eliminating the need for a ventilating gas supply. It featured a single-sided membrane design with an 80 µm tall blood vascular network comprising 500 µm square pillars. Four different membrane designs were tested, including a 20 µm thick nonporous PDMS membrane, a porous PDMS membrane, and two porous polycarbonate membranes with thicknesses of 6 µm and pore sizes of 0.1 and 0.05 µm respectively. To minimize pressure drop due to sharp bends in blood flow direction, a new fluidic interconnection design with tapered inlets and outlets was introduced. The total gas exchange surface area measured 15.26 cm^2, and the priming volume was 0.122 mL, resulted in a surface-to-volume ratio of 125 cm^{-1}. The porous PDMS membrane demonstrated the highest gas transfer performance among the four membranes. This advancement shows great promise for enhanced portability and efficiency in oxygenation devices. The oxygenator demonstrated remarkable gas exchange rates of 1.46 µL/min/cm^2 for O_2 and 5.27 µL/min/cm^2 for CO_2, operating at a blood flow rate of 4 ml/min with a porous PDMS membrane. Notably, these devices exhibited minimal pressure drop (32 - 60 mmHg) during operation and effectively utilized ambient air for blood

oxygenation. Consequently, these devices show promising potential for utilization in lung assist applications.

The work done by Rieper et al.[123] could be considered as one of the groundbreaking in the field, where they introduced a novel microfluidic multilayer extracorporeal gas exchange device with double-sided gas diffusion for the first time. The device's design involved stacking ten blood and 11 air layers and they constructed and tested various devices with different layers. The blood compartment featured an array of 40 parallel microchannels, each 1 mm wide and separated by 500 µm wide ridges. To separate the blood side from the gas side, a 90 µm thick PDMS membrane was employed. The resulting total gas exchange surface area for their device measured 120 cm^2 per layer, with a priming volume of approximately 0.7 mL. For ventilation, the device could utilize pure oxygen or air. During experimentation with porcine blood, a seven-layer device demonstrated impressive oxygen uptake rates of 0.3 and 0.156 mL/min for pure oxygen and air, respectively, at a blood flow rate of 5 mL/min. When the blood flow rate was increased to 15 mL/min, the pressure drop reached 80 mmHg. The authors estimated that to achieve an oxygen transfer rate of 250 mL/min for adult artificial lungs, a device with 833 blood compartment layers would be necessary, resulting in a significant priming volume of 580 mL[123]. Despite achieving an impressive blood flow rate of 50 mL/min in the microfluidic blood oxygenator, there are notable concerns regarding the fabrication method. The use of wire electrical discharge machining to create the mold for the blood compartment's steel sheet may not yield the smooth channel walls required to prevent hemolysis and thrombotic reactions on surfaces. Additionally, the device's design lacks optimization through flow distribution analysis or shear stress analysis, potentially resulting in stagnation or high shear zones that could exceed the blood coagulation threshold. Nevertheless, this research represents a significant advancement in the field of microfluidic blood oxygenators, opening up new possibilities for enhanced gas exchange in extracorporeal applications.

Gimbel et al.[78] from Borenstein's research group, introduced a multilayer microfluidic blood oxygenator with an expanded vascular network design inspired by their previous works[121], [122] that had larger gas exchange surface area. Similar to the earlier versions, the developed device in the work was consisted of stacking14 transfer modules in parallel, achieving a larger gas exchange surface area of 46.2 cm^2. Gas transfer was evaluated using heparinized bovine blood, and the device exhibited an impressive oxygen uptake of 1.2 mL/min at a blood flow rate of 25 mL/min. Notably,

the expanded MBO showed no reported pressure drop. To enhance hemocompatibility, human endothelial cells were coated in the blood vascular network, reducing blood clot formations without affecting oxygen uptake. This research presents promising advancements in microfluidic blood oxygenators, potentially improving gas exchange in medical applications.

In their recent study[124], they tested a scaled version of a microfluidic oxygenator that achieved an impressive oxygen transfer rate of 500 mL/min/m2 in its 14-layer configuration. The devices were constructed from layers of PDMS with advanced designs aimed at optimizing oxygen transfer rates. Despite the advances, at flow rates exceeding 8 mL/min, the pressure drop increased significantly, reaching up to 150 mmHg, and a wall shear rate of 4000 1/s was noted. These findings indicate the challenges that arise as the device scales. The research concludes that while the 14-layer device's oxygen transfer efficiency surpassed previous records, challenges like the elevated pressure drop and wall shear rate need to be addressed in future designs. Advanced fabrication techniques might offer solutions to balance efficiency and minimize pressure drops.

Later, the same research group changed the design of their MBOs aiming to improve the hemocompatibility of their devices[125]. Conventional lithographic techniques using single photoresist thickness or etch depth produce channels that increase in width but maintain a fixed depth. This results in wide, shallow trunk lines for blood transport to external devices. Additionally, vertical manifolds in stacked layers have transitions with abrupt 90-degree angles where blood flows, leading to potential clot formation, which microfluidic designs aim to prevent. They designed manifold conduits with tapered bottom surfaces, preventing sudden channel depth changes—a major flow disturbance in traditional microfluidic devices. The RAD1 and RAD2 devices comprise a blood/vascular layer, a gas layer, and an intervening gas transfer membrane. In vitro measurements for oxygen and carbon dioxide removal rates were conducted on both single transfer layer and multi-layer RAD1 devices. The RAD1 design showcased an oxygen transfer capacity of 5 volume percent at blood flow rates around 5 mL per minute per layer. A RAD2 device with elongated channels was subsequently designed to target enhanced CO2 removal, with blood flow rates analogous to hemodialysis processes. At a 20 volume percent CO2 transfer, the RAD2 device would necessitate 133 layers for achieving 80 mL/min CO2 removal with a blood flow rate of 400 mL/min. Significantly, no major clotting was observed within the microfluidic device, suggesting potential for stable operational performance[125].

This work highlighted the utility of high-precision CNC machining in creating branching networks that replicate crucial elements of natural blood circulation. While the microchannels still exhibit the rectangular structure seen in previous microfluidic oxygenator studies, this research uniquely incorporates smoothly varying depth branching channels in both horizontal and vertical distribution manifolds. Such features ensure the avoidance of flow disturbances usually caused by abrupt changes in channel depth, especially at entry and exit points. This paves the way for scaling up to devices suitable for clinical application.

Further they optimized and scaled up their design[126]. This new work focused on two primary advancements in microfluidic oxygenators: a unique three-dimensional microfluidic architecture and a design supporting blood flow rates up to 30 mL/min. Constructed from three layers (oxygen gas channels, branching blood channels, and a thin PDMS membrane), its design mitigates pressure drops while ensuring efficient oxygen transfer. The devices underwent rigorous testing involving oxygen transfer studies, using methods like heated blood rockers and pressure sensors, and hemocompatibility assessments in an ex vivo setup with heparinized swine blood.

In testing[126], the microfluidic oxygenator exhibited its highest oxygen transfer capacity at a 30 mL/min blood flow rate, achieving over 3.3 volume percent. However, the observed pressure drop of 93 mm Hg is slightly high for optimal ECMO circuits. Hemocompatibility tests revealed that three out of five devices maintained proper function for a 6-hour circulation, whereas two faced blockages prematurely. Nevertheless, there were no significant differences in key parameters like platelet count when comparing microfluidic oxygenators to control circuits, suggesting favorable hemocompatibility. The device's capability to sustain a 30 mL/min blood flow rate is especially notable since it closely mimics in vivo vasculature dynamics. Conclusively, the developed microfluidic oxygenator shows immense promise in enhancing the safety and efficacy of ECMO procedures, holding the potential to become an integral part of next-generation extracorporeal organ support technology.

The same research group introduced a microfluidic oxygenator device inspired by physiological patterns, designed to replicate natural blood flow not only within individual layers but throughout a multi-layered arrangement[127]. The combination of multiple layers in this microchannel device is achieved through a three-dimensional, physiologically inspired distribution manifold, ensuring a consistent flow throughout the entire stack, with a particular emphasis on the critical entry and

exit areas. They have plans to assess hemocompatibility and conduct large animal studies using these prototypes. The design was influenced by a computational finite element analysis tool (COMSOL), targeting both the optimization of blood flow patterns and gas transfer efficiency. Their design of the vascular network layer focuses on achieving a smooth, laminar flow, aiming to minimize disruptions from the inlet to the outlet manifold, even when navigating the expansive parallel array of gas transfer channels. In their tests, the device displayed proficient blood distribution across its eight layers, a feat made possible by the manifold's design and a balanced flow distribution system. Their findings underscore the potential of microfluidic oxygenator technology, suggesting possible technical upper hands over traditional HFM devices due to its capacity to guide blood through precise, physiologically inspired microchannel networks. Over recent years, there has been a notable push towards improving microfluidic systems, primarily due to their unique design features, such as shallow blood channels and slim gas transfer membranes. However, while these features seem promising, the methods currently employed to create these devices face certain challenges. These include ensuring smooth transitions at channel junctions and within distribution manifolds[127].

Leveraging their refined design of MBOs, they introduced the pioneering clinical-scale microfluidic respiratory assist device[128]. This novel creation effectively exhibited oxygen transfer capabilities at a blood flow rate of 750 mL/min. Conceived as a superior replacement to traditional ECMO systems, this device doesn't rely on the external circulation of blood through a hollow fiber membrane oxygenator. Delving into the results, they revealed a device intricately structured with 736 distinct oxygenation channels. These channels measure 9.1 cm in length, 500 μm across, and have a depth of 160 μm. Every layer possesses a prime volume of 14.7 mL, and it reaches a residence time of 8.8 seconds at a blood flow rate of 100 mL/min. To facilitate uniform flow distribution, the oxygenation channels are linked through a dual-tier bifurcating channel mechanism. These channels converge into more expansive distribution pathways dubbed as "fingers," which further integrate into a wider "trunk" channel. Precision-engineered transitions at each joining point ensure fluidity in the flow dynamics. Highlighting the device's relevance, they emphasized its unprecedented size and capability, making it a strong alternative to traditional ECMO devices. They contrasted their invention with previous microfluidic ECMO versions, which suffered from limited blood flow rates and lacked animal model evaluations. Summarizing, they presented an impressive microfluidic respiratory assist device, effectively tested on larger animals,

achieving a notable blood flow rate of 750 mL/min[128]. At the heart of their breakthrough lies the device's extensive microfluidic layout, replete with intricate 3D microchannel branching. With the positive outcomes and their vanguard stance in ECMO advancements, they hold a bright outlook for future progress. They predict further refinement in the 3D branching design and the incorporation of surface enhancements, aiming to craft comprehensive adult oxygenators to expand ECMO treatment applications.

Borenstein's research team presented a microfluidic system that integrated blood oxygenators and hemodialysis mechanisms within a single cartridge[129]. During their tests, it was consistently noted that the system maintained an oxygen transfer volume percentage close to 6.5%. This consistency showed that the oxygenating efficiency of the device was stable, even when there were changes in the ultrafiltration rate (UFR). Yet, they identified certain inconsistencies in hematocrit measurements. They postulated that these discrepancies might arise from difficulties in securing evenly mixed samples. One of the primary trends they identified was that the removal of plasma water led to a predictable rise in the recorded hematocrit values during the test sessions. They also highlighted an issue with the method of blood introduction to the device. Employing a syringe, which lacks the mixing advantages of a peristaltic pump equipped with a blood bag on a rocker, could have contributed to these inconsistencies. Their findings showed that for optimal system performance, it was best to maintain a flow rate in the range of 0.4-0.6 mL/min for plasma water. Notably, the mean permeability they recorded during their trials was only 13.5% of the initially anticipated value, showcasing some unexpected results[129].

Their pioneering work provides the inaugural demonstration of concurrent oxygenation and ultrafiltration (UF) in a microfluidic setting, offering a foundational model for prospective devices aimed at addressing multiple-organ failure. By evaluating the outcomes from the dual-layer design of their prototype, they believe it's possible to infer its scalability for larger clinical uses. They underline the significance of seamlessly merging multiple organ support functions to cater to the needs of severely ill patients. However, inherent challenges persist, especially when it comes to fusing intricate systems like ECMO and renal replacement therapy. Their innovative approach introduces a prototype that marries a microfluidic oxygenator and UF apparatus in a side-by-side arrangement, directing blood efficiently into individual layers of a unified device. Their

breakthroughs point towards the future creation of a clinical tool capable of delivering modifiable fluid removal paired with robust oxygenation within a single integrated system[129].

In a recent work, Potkay's research group employed their established mathematical models to shape μALs (microfluidic artificial lungs) with varying capillary heights, ensuring a steady flow rate and pressure drop[130]. Their objective was to delve into how capillary dimensions influenced device efficacy. Their empirical findings were based on benchtop trials using bovine whole blood, aiming to measure pressure drop and gas exchange rates. From these experiments, it became evident that the in vitro pressure drops in designs with 60 and 100 μm capillary heights were quite similar, albeit both being less than theoretical predictions. This highlighted the precision of their mathematical and CFD models in forecasting pressure drops across diverse design blueprints. Another notable discovery was the uniformity in gas exchange efficiency across all tested models. However, designs incorporating taller capillaries (60 and 100 μm) demonstrated increased pressure drops relative to the 30 μm capillary design[130]. Their analytical commentary underscored significant observations. Gas exchange proved to be exceptionally effective at shorter capillary heights, necessitating a reduced gas exchange surface to meet targeted blood flow. With an increase in capillary height, the essential blood distribution channel's length shortened, thereby decreasing the overall surface in contact with blood and the priming volume. A key observation they pinpointed was that the ideal scenario, minimizing both surface area and priming volume, materialized when capillaries were around 42 μm tall[130]. Conclusively, they innovated three μAL designs with varied channel dimensions but equivalent physiological attributes. Among these, the model with 60 μm capillaries had the minimal blood-contacting surface and priming volume, though it exposed blood to the most intense shear forces. These revelations pave the way for subsequent studies aimed at refining blood flow channels, pushing the boundaries of μAL biocompatibility[130].

Lachaux et. al. introduced a technique, enabling them to ensure each 4-inch tri-layer unit's integrity, even when the membrane was reduced to a mere 15 μm thickness, and it could handle elevated blood flow rates. [131]. One single unit oxygenator could support a blood flow rate of up to 25 mL/min. The team was focused on improving flow rates without sacrificing oxygenation, suggesting that an increase in scale might be the key. They utilized Murray's law to determine the widths of their tree-like branching structures, achieving 200 μm for the tiniest microcapillaries.

This intricate design ensured that flow was uniformly distributed across the capillaries, minimizing shear stress at each connection. They strategically selected dimensions for their branching designs to optimize shear stress and fluid resistance, in line with the expanded principles of Murray's law. Through their experimentation, they sought to validate their advanced blood capillary design using endothelial cells. For this, they turned to cord blood Endothelial colony-forming cells, underscoring their enhanced performance and accessibility compared to adult versions. Over the course of 12 days, they monitored cell growth on the device. From day one, these cells began colonizing the device's surface, and they observed a consistent cellular presence throughout the study. Impressively, they achieved complete endothelialization of the single tri-layer device across the entire experiment[131].

In their concluding remarks, they highlighted the development of a compact PDMS microfluidic oxygenator tailored for maximum gas exchange efficiency. When tested with swine venous blood, the results were promising in both oxygenating and decarbonating functions. Their design's uniqueness lies in its capacity for stacking multiple 4-inch tri-layer units, thereby increasing flow rate without diminishing the performance of an individual unit. In real terms, a standalone oxygenator unit could sustain blood flow rates as high as 25 ml/min while maintaining efficient gas exchange even when pushed to 15 ml/min. With a five-unit combined setup, they achieved remarkable performance, oxygenating and decarbonating at flow rates reaching 80 ml/min. They signaled their ambition to conduct further in vivo tests with an increased stack of these tri-layer oxygenators in the future[131].

In the study by Dabaghi et. al.[63], a newborn piglet model was tested with microfluidic-based artificial type oxygenator that they developed earlier[79]. The effectiveness of the LAD was initially determined through in vitro tests. Further in vivo tests on a piglet model demonstrated that the LAD could alleviate respiratory distress in piglets similar in size to neonatal babies. During in vitro testing using bovine blood, the LAD's gas exchange performance was analyzed in both an oxygen-rich environment and standard room air. The oxygen saturation levels were set at specific parameters, and after passing the deoxygenated blood through the device, oxygen levels were measured at the outlet. This LAD, made up of 16 stacked MBOs, was assessed on a newborn piglet, aiming to assist neonates with respiratory failure. The device was designed to let infants breathe normally while simultaneously providing an additional avenue for gas exchange. This could

potentially avert the long-term side effects caused by over-reliance on mechanical ventilation. The initial design concept envisions the artificial placenta being connected directly to the neonate's umbilical vessels. Still, due to the limitations of the piglet model used in this study, the carotid artery and jugular vein were employed as alternatives. In conclusion, the development of a pumpless LAD offered hope for preterm neonates suffering from respiratory ailments. Its gas exchange capabilities were confirmed through in vitro tests. Additionally, an innovative technique was established to coat surfaces that come into contact with blood. The device's efficacy in facilitating gas exchange was further confirmed when it was connected to a newborn piglet, showing consistency with the in vitro findings. As the LAD continues to be refined, focus will be on its hemocompatibility, biocompatibility, and potential for direct connections to the umbilical vessels.

Dabaghi et. al. introduced a novel microfluidic blood oxygenator with four-sided blood channels for gas transfer[132]. This new design features closed gas chambers on each side of the blood channel, aiming to improve gas transfer efficiency. Through various techniques like photolithography and spin-coating, the devices were fabricated and then tested using heparinized bovine blood. The findings showed that the new fsMBO design had enhanced oxygenation performance, especially at higher flow rates, compared to the conventional dsMBO design. Additionally, the study revealed that slight variations in the device's channel height did not drastically impact its gas exchange capabilities. In conclusion, the innovative microfluidic blood oxygenator design with closed air chambers offers a promising alternative to traditional hollow fiber-based oxygenators, demonstrating improved performance at increased flow rates. However, MBOs developed in this work only could support low blood flow rates. Indeed, there is a need for future work to scale up the size of these MBOs to reach higher blood flow rates.

2.7 References:

[1] J. E. Cotes, D. J. Chinn, and M. R. Miller, *Lung Function: Physiology, Measurement and Application in Medicine*. John Wiley & Sons, 2009.

[2] C. C. W. Hsia, D. M. Hyde, and E. R. Weibel, "Lung Structure and the Intrinsic Challenges of Gas Exchange," *Compr Physiol*, vol. 6, no. 2, pp. 827–895, Mar. 2016, doi: 10.1002/cphy.c150028.

[3] J. A. Zasadzinski, J. Ding, H. E. Warriner, F. Bringezu, and A. J. Waring, "The physics and physiology of lung surfactants," *Current Opinion in Colloid & Interface Science*, vol. 6, no. 5, pp. 506–513, Nov. 2001, doi: 10.1016/S1359-0294(01)00124-8.

[4] S. A. Rooney, S. L. Young, and C. R. Mendelson, "Molecular and cellular processing of lung surfactant1," *The FASEB Journal*, vol. 8, no. 12, pp. 957–967, 1994, doi: 10.1096/fasebj.8.12.8088461.

[5] P. J. Barnes, "The third nervous system in the lung: physiology and clinical perspectives.," *Thorax*, vol. 39, no. 8, pp. 561–567, Aug. 1984.

[6] M. A. Matthay, L. B. Ware, and G. A. Zimmerman, "The acute respiratory distress syndrome," *J Clin Invest*, vol. 122, no. 8, pp. 2731–2740, Aug. 2012, doi: 10.1172/JCI60331.

[7] M. A. Matthay *et al.*, "Acute respiratory distress syndrome," *Nat Rev Dis Primers*, vol. 5, no. 1, Art. no. 1, Mar. 2019, doi: 10.1038/s41572-019-0069-0.

[8] B. T. Thompson, R. C. Chambers, and K. D. Liu, "Acute Respiratory Distress Syndrome," *New England Journal of Medicine*, vol. 377, no. 6, pp. 562–572, Aug. 2017, doi: 10.1056/NEJMra1608077.

[9] L. B. Ware and M. A. Matthay, "The Acute Respiratory Distress Syndrome," *New England Journal of Medicine*, vol. 342, no. 18, pp. 1334–1349, May 2000, doi: 10.1056/NEJM200005043421806.

[10] D. Morniroli *et al.*, "Beyond survival: the lasting effects of premature birth," *Front Pediatr*, vol. 11, p. 1213243, Jul. 2023, doi: 10.3389/fped.2023.1213243.

[11] N. DeMarco, J. Twynstra, M. B. Ospina, M. Darrington, C. Whippey, and J. A. Seabrook, "Prevalence of Low Birth Weight, Premature Birth, and Stillbirth Among Pregnant Adolescents in Canada: A Systematic Review and Meta-analysis," *Journal of Pediatric and Adolescent Gynecology*, vol. 34, no. 4, pp. 530–537, Aug. 2021, doi: 10.1016/j.jpag.2021.03.003.

[12] P. Pelosi *et al.*, "Personalized mechanical ventilation in acute respiratory distress syndrome," *Critical Care*, vol. 25, no. 1, p. 250, Jul. 2021, doi: 10.1186/s13054-021-03686-3.

[13] "Premature Birth Complications Top Cause of Death in Children Younger Than 5 Years | Pregnancy | JAMA | JAMA Network." https://jamanetwork.com/journals/jama/article-abstract/2091316 (accessed Aug. 23, 2023).

[14] T. M. Randis, "Complications Associated with Premature Birth," *AMA Journal of Ethics*, vol. 10, no. 10, pp. 647–650, Oct. 2008, doi: 10.1001/virtualmentor.2008.10.10.cprl1-0810.

[15] E. B. Hysinger and J. C. Woods, "Seeing Premature Lung Disease: Hyperpolarized Xe Magnetic Resonance Imaging," *Am J Respir Crit Care Med*, vol. 207, no. 1, pp. 15–16, Jan. 2023, doi: 10.1164/rccm.202208-1612ED.

[16] O. Chowdhury, C. J. Wedderburn, D. Duffy, and A. Greenough, "CPAP review," *Eur J Pediatr*, vol. 171, no. 10, pp. 1441–1448, Oct. 2012, doi: 10.1007/s00431-011-1648-6.

[17] S. Gupta and S. M. Donn, "Continuous positive airway pressure: Physiology and comparison of devices," *Seminars in Fetal and Neonatal Medicine*, vol. 21, no. 3, pp. 204–211, Jun. 2016, doi: 10.1016/j.siny.2016.02.009.

[18] G. Yue, J. Wang, H. Li, B. Li, and R. Ju, "Risk Factors of Mechanical Ventilation in Premature Infants During Hospitalization," *Therapeutics and Clinical Risk Management*, vol. 17, pp. 777–787, Dec. 2021, doi: 10.2147/TCRM.S318272.

[19] E. E. Williams and A. Greenough, "Lung Protection During Mechanical Ventilation in the Premature Infant," *Clinics in Perinatology*, vol. 48, no. 4, pp. 869–880, Dec. 2021, doi: 10.1016/j.clp.2021.08.006.

[20] T. Pham, L. J. Brochard, and A. S. Slutsky, "Mechanical Ventilation: State of the Art," *Mayo Clinic Proceedings*, vol. 92, no. 9, pp. 1382–1400, Sep. 2017, doi: 10.1016/j.mayocp.2017.05.004.

[21] S. Gupta and S. M. Donn, “Novel Approaches to Surfactant Administration,” *Critical Care Research and Practice*, vol. 2012, p. e278483, Dec. 2012, doi: 10.1155/2012/278483.

[22] J. E. H. Bunt *et al.*, “Treatment with exogenous surfactant stimulates endogenous surfactant synthesis in premature infants with respiratory distress syndrome,” *Critical Care Medicine*, vol. 28, no. 10, p. 3383, Oct. 2000.

[23] G. K. Suresh and R. F. Soll, “CURRENT SURFACTANT USE IN PREMATURE INFANTS,” *Clinics in Perinatology*, vol. 28, no. 3, pp. 671–694, Sep. 2001, doi: 10.1016/S0095-5108(05)70112-3.

[24] M. Schoberer *et al.*, “Fifty Years of Work on the Artificial Placenta: Milestones in the History of Extracorporeal Support of the Premature Newborn,” *Artificial Organs*, vol. 36, no. 6, pp. 512–516, 2012, doi: 10.1111/j.1525-1594.2011.01404.x.

[25] D. G. Blauvelt, E. N. Abada, P. Oishi, and S. Roy, “Advances in extracorporeal membrane oxygenator design for artificial placenta technology,” *Artificial Organs*, vol. 45, no. 3, pp. 205–221, 2021, doi: 10.1111/aor.13827.

[26] G. A. Agrons, S. E. Courtney, J. T. Stocker, and R. I. Markowitz, “Lung Disease in Premature Neonates: Radiologic-Pathologic Correlation,” *RadioGraphics*, vol. 25, no. 4, pp. 1047–1073, Jul. 2005, doi: 10.1148/rg.254055019.

[27] C. McPherson and J. A. Wambach, “Prevention and Treatment of Respiratory Distress Syndrome in Preterm Neonates,” *Neonatal Netw*, vol. 37, no. 3, pp. 169–177, May 2018, doi: 10.1891/0730-0832.37.3.169.

[28] M. A. Attar and S. M. Donn, “Mechanisms of ventilator-induced lung injury in premature infants,” *Seminars in Neonatology*, vol. 7, no. 5, pp. 353–360, Oct. 2002, doi: 10.1053/siny.2002.0129.

[29] C. G. Carvalho, R. C. Silveira, and R. S. Procianoy, “Ventilator-induced lung injury in preterm infants,” *Rev. bras. ter. intensiva*, vol. 25, pp. 319–326, Dec. 2013, doi: 10.5935/0103-507X.20130054.

[30] C. Dani, I. Corsini, J. Cangemi, V. Vangi, and S. Pratesi, "Nitric oxide for the treatment of preterm infants with severe RDS and pulmonary hypertension," *Pediatric Pulmonology*, vol. 52, no. 11, pp. 1461–1468, 2017, doi: 10.1002/ppul.23843.

[31] S. Arnon, T. Dolfin, I. Litmanovitz, R. Regev, S. Bauer, and M. Fejgin, "Preterm labour at 34–36 weeks of gestation: should it be arrested?," *Paediatric and Perinatal Epidemiology*, vol. 15, no. 3, pp. 252–256, 2001, doi: 10.1046/j.1365-3016.2001.00357.x.

[32] V. Catanzarite, D. Willms, D. Wong, C. Landers, L. Cousins, and D. Schrimmer, "Acute respiratory distress syndrome in pregnancy and the puerperium: causes, courses, and outcomes," *Obstetrics & Gynecology*, vol. 97, no. 5, Part 1, pp. 760–764, May 2001, doi: 10.1016/S0029-7844(00)01231-X.

[33] H. Sun *et al.*, "Characteristics of Respiratory Distress Syndrome in Infants of Different Gestational Ages," *Lung*, vol. 191, no. 4, pp. 425–433, Aug. 2013, doi: 10.1007/s00408-013-9475-3.

[34] W. Butt and G. MacLaren, "Extracorporeal membrane oxygenation," *F1000Prime Rep*, vol. 5, p. 55, Dec. 2013, doi: 10.12703/P5-55.

[35] S. Yadav, B. Lee, and R. Kamity, "Neonatal Respiratory Distress Syndrome," in *StatPearls*, Treasure Island (FL): StatPearls Publishing, 2023. Accessed: Aug. 23, 2023. [Online]. Available: http://www.ncbi.nlm.nih.gov/books/NBK560779/

[36] J. Dyer, "Neonatal Respiratory Distress Syndrome: Tackling A Worldwide Problem," *P T*, vol. 44, no. 1, pp. 12–14, Jan. 2019.

[37] CDC, "Premature Birth," *Centers for Disease Control and Prevention*, Nov. 01, 2022. https://www.cdc.gov/reproductivehealth/features/premature-birth/index.html (accessed Aug. 23, 2023).

[38] "Chronic Lung Disease after Premature Birth | NEJM." https://www.nejm.org/doi/full/10.1056/NEJMra067279?casa_token=GAD7VtQCxhQAAAAA:ydVZt2IBlz51I8ttK9o5YCs2q1p47ek5GLiEC6KClTMn7-z6IKgDtzHqFUcPhY8tEeJt-1BjaUsXeQ (accessed Aug. 24, 2023).

[39] B. Weinberger, D. L. Laskin, D. E. Heck, and J. D. Laskin, "Oxygen Toxicity in Premature Infants," *Toxicology and Applied Pharmacology*, vol. 181, no. 1, pp. 60–67, May 2002, doi: 10.1006/taap.2002.9387.

[40] A. Malek, N. Afzali, M. Meshkat, and N. H. Yazdi, "Pneumothorax after Mechanical Ventilation in Newborns," *Iran J Pediatr*, vol. 21, no. 1, pp. 45–50, Mar. 2011.

[41] Khattab, "Ventilator-associated pneumonia in the neonatal intensive care unit." https://www.mmj.eg.net/article.asp?issn=1110-2098;year=2014;volume=27;issue=1;spage=73;epage=77;aulast=Khattab (accessed Aug. 24, 2023).

[42] M. Cernada, M. Brugada, S. Golombek, and M. Vento, "Ventilator-Associated Pneumonia in Neonatal Patients: An Update," *Neonatology*, vol. 105, no. 2, pp. 98–107, Nov. 2013, doi: 10.1159/000355539.

[43] S. K. Pooboni and K. M. Gulla, "Vascular access in ECMO," *Indian J Thorac Cardiovasc Surg*, vol. 37, no. 2, pp. 221–231, Apr. 2021, doi: 10.1007/s12055-020-00999-w.

[44] S. Zeibi Shirejini, J. Carberry, Z. K. McQuilten, A. J. C. Burrell, S. D. Gregory, and C. E. Hagemeyer, "Current and future strategies to monitor and manage coagulation in ECMO patients," *Thrombosis Journal*, vol. 21, no. 1, p. 11, Jan. 2023, doi: 10.1186/s12959-023-00452-z.

[45] K. Rais Bahrami and K. P. Van Meurs, "ECMO for neonatal respiratory failure," *Seminars in Perinatology*, vol. 29, no. 1, pp. 15–23, Feb. 2005, doi: 10.1053/j.semperi.2005.02.004.

[46] E. Lüsebrink *et al.*, "Update on Weaning from Veno-Arterial Extracorporeal Membrane Oxygenation," *Journal of Clinical Medicine*, vol. 9, no. 4, Art. no. 4, Apr. 2020, doi: 10.3390/jcm9040992.

[47] A. W. Flake, F. R. De Bie, D. A. Munson, and C. Feudtner, "The artificial placenta and EXTEND technologies: one of these things is not like the other," *J Perinatol*, pp. 1–6, Jul. 2023, doi: 10.1038/s41372-023-01716-2.

[48] "The artificial womb - Bulletti - 2011 - Annals of the New York Academy of Sciences - Wiley Online Library."

[49] S. K. Kukora, G. B. Mychaliska, and E. M. Weiss, “Ethical challenges in first-in-human trials of the artificial placenta and artificial womb: not all technologies are created equally, ethically,” *J Perinatol*, pp. 1–6, Jul. 2023, doi: 10.1038/s41372-023-01713-5.

[50] S. D. Bird, “Artificial placenta: Analysis of recent progress,” *European Journal of Obstetrics & Gynecology and Reproductive Biology*, vol. 208, pp. 61–70, Jan. 2017, doi: 10.1016/j.ejogrb.2016.11.005.

[51] “Artificial placenta: Recent advances and potential clinical applications - Metelo-Coimbra - 2016 - Pediatric Pulmonology - Wiley Online Library.”.

[52] H. Usuda *et al.*, “Artificial placenta technology: History, potential and perception,” *Placenta*, Oct. 2022, doi: 10.1016/j.placenta.2022.10.003.

[53] E. A. Partridge, M. G. Davey, and A. W. Flake, “Development of the Artificial Womb,” *Curr Stem Cell Rep*, vol. 4, no. 1, pp. 69–73, Mar. 2018, doi: 10.1007/s40778-018-0120-1.

[54] E. C. Romanis, “Artificial womb technology and the frontiers of human reproduction: conceptual differences and potential implications,” *Journal of Medical Ethics*, vol. 44, no. 11, pp. 751–755, Nov. 2018, doi: 10.1136/medethics-2018-104910.

[55] “An extra-uterine system to physiologically support the extreme premature lamb | Nature Communications.” https://www.nature.com/articles/ncomms15112 (accessed Aug. 24, 2023).

[56] E. C. Romanis, “Artificial womb technology and clinical translation: Innovative treatment or medical research?,” *Bioethics*, vol. 34, no. 4, pp. 392–402, 2020, doi: 10.1111/bioe.12701.

[57] H. Iwahashi, K. Yuri, and Y. Nosé, “Development of the oxygenator: past, present, and future,” *J Artif Organs*, vol. 7, no. 3, pp. 111–120, Sep. 2004, doi: 10.1007/s10047-004-0268-6.

[58] M. W. Lim, “The history of extracorporeal oxygenators*,” *Anaesthesia*, vol. 61, no. 10, pp. 984–995, 2006, doi: 10.1111/j.1365-2044.2006.04781.x.

[59] O. O. Teber *et al.*, “Polymeric hollow fiber membrane oxygenators as artificial lungs: A review,” *Biochemical Engineering Journal*, vol. 180, p. 108340, Mar. 2022, doi: 10.1016/j.bej.2022.108340.

[60] T. He *et al.*, "Membranes for extracorporeal membrane oxygenator (ECMO): History, preparation, modification and mass transfer," *Chinese Journal of Chemical Engineering*, vol. 49, pp. 46–75, Sep. 2022, doi: 10.1016/j.cjche.2022.05.027.

[61] W. S. Haworth, "The development of the modern oxygenator," *The Annals of Thoracic Surgery*, vol. 76, no. 6, pp. S2216–S2219, Dec. 2003, doi: 10.1016/j.athoracsur.2003.09.012.

[62] M. C. Annesini, L. Marrelli, V. Piemonte, and L. Turchetti, "Blood Oxygenators and Artificial Lungs," in *Artificial Organ Engineering*, M. C. Annesini, L. Marrelli, V. Piemonte, and L. Turchetti, Eds., London: Springer, 2017, pp. 117–161. doi: 10.1007/978-1-4471-6443-2_6.

[63] M. Dabaghi *et al.*, "Miniaturization of Artificial Lungs toward Portability," *Advanced Materials Technologies*, vol. 5, no. 7, p. 2000136, 2020, doi: 10.1002/admt.202000136.

[64] P. J. Featherstone and C. M. Ball, "The Early History of Extracorporeal Membrane Oxygenation," *Anaesth Intensive Care*, vol. 46, no. 6, pp. 555–557, Nov. 2018, doi: 10.1177/0310057X1804600601.

[65] S. R. Wickramasinghe, A. R. Goerke, J. D. Garcia, and B. Han, "Designing Blood Oxygenators," *Annals of the New York Academy of Sciences*, vol. 984, no. 1, pp. 502–514, 2003, doi: 10.1111/j.1749-6632.2003.tb06023.x.

[66] S. R. Wickramasinghe, J. D. Garcia, and B. Han, "Mass and momentum transfer in hollow fibre blood oxygenators," *Journal of Membrane Science*, vol. 208, no. 1, pp. 247–256, Oct. 2002, doi: 10.1016/S0376-7388(02)00281-8.

[67] N. Rochow *et al.*, "Artificial Placenta - Lung Assist Devices for Term and Preterm Newborns with Respiratory Failure," *Int J Artif Organs*, vol. 36, no. 6, pp. 377–391, Jun. 2013, doi: 10.5301/ijao.5000195.

[68] W.-I. Wu *et al.*, "Lung assist device: development of microfluidic oxygenators for preterm infants with respiratory failure," *Lab Chip*, vol. 13, no. 13, p. 2641, 2013, doi: 10.1039/c3lc41417e.

[69] J. Arens *et al.*, "NeonatOx: A Pumpless Extracorporeal Lung Support for Premature Neonates," *Artificial Organs*, vol. 35, no. 11, pp. 997–1001, 2011, doi: 10.1111/j.1525-1594.2011.01324.x.

[70] A. Payot, S. Gendron, F. Lefebvre, and H. Doucet, "Deciding to resuscitate extremely premature babies: How do parents and neonatologists engage in the decision?," *Social Science & Medicine*, vol. 64, no. 7, pp. 1487–1500, Apr. 2007, doi: 10.1016/j.socscimed.2006.11.016.

[71] D. Patel, "The Fighting Journey of a Premature Baby: A Systemic Review of Developmental and Neurological Complications of the Premature Baby," *Honors Undergraduate Theses*, Jan. 2021, [Online]. Available: https://stars.library.ucf.edu/honorstheses/946

[72] K. J. Collard, S. Godeck, and J. E. Holley, "Blood transfusion and pulmonary lipid peroxidation in ventilated premature babies," *Pediatric Pulmonology*, vol. 39, no. 3, pp. 257–261, 2005, doi: 10.1002/ppul.20190.

[73] S. D. Keene, R. M. Patel, B. K. Stansfield, J. Davis, C. D. Josephson, and A. M. Winkler, "Blood product transfusion and mortality in neonatal extracorporeal membrane oxygenation," *Transfusion*, vol. 60, no. 2, pp. 262–268, 2020, doi: 10.1111/trf.15626.

[74] H. Matharoo *et al.*, "Steel reinforced composite silicone membranes and its integration to microfluidic oxygenators for high performance gas exchange," *Biomicrofluidics*, vol. 12, no. 1, p. 014107, Jan. 2018, doi: 10.1063/1.5014028.

[75] M. Dabaghi *et al.*, "An artificial placenta type microfluidic blood oxygenator with double-sided gas transfer microchannels and its integration as a neonatal lung assist device," *Biomicrofluidics*, vol. 12, no. 4, p. 044101, Jul. 2018, doi: 10.1063/1.5034791.

[76] M. Dabaghi *et al.*, "An ultra-thin, all PDMS-based microfluidic lung assist device with high oxygenation capacity," *Biomicrofluidics*, vol. 13, no. 3, p. 034116, May 2019, doi: 10.1063/1.5091492.

[77] J. A. Potkay, "The promise of microfluidic artificial lungs," *Lab Chip*, vol. 14, no. 21, pp. 4122–4138, 2014, doi: 10.1039/C4LC00828F.

[78] A. A. Gimbel, E. Flores, A. Koo, G. García-Cardeña, and J. T. Borenstein, "Development of a biomimetic microfluidic oxygen transfer device," *Lab on a Chip*, vol. 16, no. 17, pp. 3227–3234, 2016, doi: 10.1039/C6LC00641H.

[79] M. Dabaghi *et al.*, "An ultra-thin highly flexible microfluidic device for blood oxygenation," *Lab Chip*, vol. 18, no. 24, pp. 3780–3789, 2018, doi: 10.1039/C8LC01083H.

[80] N. Rochow *et al.*, "An Integrated Array of Microfluidic Oxygenators as a Neonatal Lung Assist Device: In Vitro Characterization and In Vivo Demonstration: Neonatal Lung Assist Device," *Artificial Organs*, vol. 38, no. 10, pp. 856–866, Oct. 2014, doi: 10.1111/aor.12269.

[81] D. Sheng, X. Li, C. Sun, J. Zhou, and X. Feng, "The separation membranes in artificial organs," *Materials Chemistry Frontiers*, vol. 7, no. 17, pp. 3455–3474, 2023, doi: 10.1039/D3QM00255A.

[82] K. J. Regehr *et al.*, "Biological implications of polydimethylsiloxane-based microfluidic cell culture," *Lab on a Chip*, vol. 9, no. 15, pp. 2132–2139, 2009, doi: 10.1039/B903043C.

[83] T. Fujii, "PDMS-based microfluidic devices for biomedical applications," *Microelectronic Engineering*, vol. 61–62, pp. 907–914, Jul. 2002, doi: 10.1016/S0167-9317(02)00494-X.

[84] K. Raj M and S. Chakraborty, "PDMS microfluidics: A mini review," *Journal of Applied Polymer Science*, vol. 137, no. 27, p. 48958, 2020, doi: 10.1002/app.48958.

[85] E. Berthier, E. W. K. Young, and D. Beebe, "Engineers are from PDMS-land, Biologists are from Polystyrenia," *Lab on a Chip*, vol. 12, no. 7, pp. 1224–1237, 2012, doi: 10.1039/C2LC20982A.

[86] G. G. Morbioli, N. C. Speller, and A. M. Stockton, "A practical guide to rapid-prototyping of PDMS-based microfluidic devices: A tutorial," *Analytica Chimica Acta*, vol. 1135, pp. 150–174, Oct. 2020, doi: 10.1016/j.aca.2020.09.013.

[87] A. J. Thompson, L. J. Ma, T. J. Plegue, and J. A. Potkay, "Design Analysis and Optimization of a Single-Layer PDMS Microfluidic Artificial Lung," *IEEE Trans. Biomed. Eng.*, vol. 66, no. 4, pp. 1082–1093, Apr. 2019, doi: 10.1109/TBME.2018.2866782.

[88] G. Narendran, S. Z. Hoque, N. S. Satpathi, K. N. Nampoothiri, and A. K. Sen, "PDMS membrane-based flexible bi-layer microfluidic device for blood oxygenation," *J. Micromech. Microeng.*, vol. 32, no. 9, p. 094001, Jul. 2022, doi: 10.1088/1361-6439/ac7ea6.

[89] "Microfluidic devices fabricated in Poly(dimethylsiloxane) for biological studies - Sia - 2003 - ELECTROPHORESIS - Wiley Online Library." https://analyticalsciencejournals.onlinelibrary.wiley.com/doi/abs/10.1002/elps.200305584?casa_token=Hh5PMSwPK-IAAAAA:XpEM504OTclCn-

hJQcmznDCkTdQVXf4EKhmZmp0BcTfaGDl7WFkbC4s-P8xUOA8AB9AF9qPSc-n1_A (accessed Aug. 25, 2023).

[90] A. Shakeri, S. Khan, and T. F. Didar, "Conventional and emerging strategies for the fabrication and functionalization of PDMS-based microfluidic devices," *Lab on a Chip*, vol. 21, no. 16, pp. 3053–3075, 2021, doi: 10.1039/D1LC00288K.

[91] L. Tang and N. Yoon Lee, "A facile route for irreversible bonding of plastic-PDMS hybrid microdevices at room temperature," *Lab on a Chip*, vol. 10, no. 10, pp. 1274–1280, 2010, doi: 10.1039/B924753J.

[92] K. S. Lee and R. J. Ram, "Plastic–PDMS bonding for high pressure hydrolytically stable active microfluidics," *Lab on a Chip*, vol. 9, no. 11, pp. 1618–1624, 2009, doi: 10.1039/B820924C.

[93] K. Haubert, T. Drier, and D. Beebe, "PDMS bonding by means of a portable, low-cost corona system," *Lab Chip*, vol. 6, no. 12, pp. 1548–1549, Nov. 2006, doi: 10.1039/B610567J.

[94] A. Borók, K. Laboda, and A. Bonyár, "PDMS Bonding Technologies for Microfluidic Applications: A Review," *Biosensors*, vol. 11, no. 8, Art. no. 8, Aug. 2021, doi: 10.3390/bios11080292.

[95] F. Wu, L. Li, Z. Xu, S. Tan, and Z. Zhang, "Transport study of pure and mixed gases through PDMS membrane," *Chemical Engineering Journal*, vol. 117, no. 1, pp. 51–59, Mar. 2006, doi: 10.1016/j.cej.2005.12.010.

[96] G. Firpo, E. Angeli, L. Repetto, and U. Valbusa, "Permeability thickness dependence of polydimethylsiloxane (PDMS) membranes," *Journal of Membrane Science*, vol. 481, pp. 1–8, May 2015, doi: 10.1016/j.memsci.2014.12.043.

[97] Z. Si *et al.*, "The Ultrafast and Continuous Fabrication of a Polydimethylsiloxane Membrane by Ultraviolet-Induced Polymerization," *Angewandte Chemie*, vol. 131, no. 48, pp. 17335–17339, 2019, doi: 10.1002/ange.201908386.

[98] A. L. Thangawng, R. S. Ruoff, M. A. Swartz, and M. R. Glucksberg, "An ultra-thin PDMS membrane as a bio/micro–nano interface: fabrication and characterization," *Biomed Microdevices*, vol. 9, no. 4, pp. 587–595, Aug. 2007, doi: 10.1007/s10544-007-9070-6.

[99] W. S. Lee, K. S. Yeo, A. Andriyana, Y. G. Shee, and F. R. Mahamd Adikan, “Effect of cyclic compression and curing agent concentration on the stabilization of mechanical properties of PDMS elastomer,” *Materials & Design*, vol. 96, pp. 470–475, Apr. 2016, doi: 10.1016/j.matdes.2016.02.049.

[100] Z. Wang, A. A. Volinsky, and N. D. Gallant, “Crosslinking effect on polydimethylsiloxane elastic modulus measured by custom-built compression instrument,” *Journal of Applied Polymer Science*, vol. 131, no. 22, 2014, doi: 10.1002/app.41050.

[101] F. C. P. Sales, R. M. Ariati, V. T. Noronha, and J. E. Ribeiro, “Mechanical Characterization of PDMS with Different Mixing Ratios,” *Procedia Structural Integrity*, vol. 37, pp. 383–388, Jan. 2022, doi: 10.1016/j.prostr.2022.01.099.

[102] N. Naserifar, S. S. Yerneni, L. E. Weiss, and G. K. Fedder, “Inkjet Printing of Curing Agent on Thin PDMS for Local Tailoring of Mechanical Properties,” *Macromolecular Rapid Communications*, vol. 41, no. 5, p. 1900569, 2020, doi: 10.1002/marc.201900569.

[103] Z. Cai, W. Qiu, G. Shao, and W. Wang, “A new fabrication method for all-PDMS waveguides,” *Sensors and Actuators A: Physical*, vol. 204, pp. 44–47, Dec. 2013, doi: 10.1016/j.sna.2013.09.019.

[104] A. Lamberti, S. L. Marasso, and M. Cocuzza, “PDMS membranes with tunable gas permeability for microfluidic applications,” *RSC Advances*, vol. 4, no. 106, pp. 61415–61419, 2014, doi: 10.1039/C4RA12934B.

[105] S. s. Madaeni, M. M. S. Badieh, and V. Vatanpour, “Effect of coating method on gas separation by PDMS/PES membrane,” *Polymer Engineering & Science*, vol. 53, no. 9, pp. 1878–1885, 2013, doi: 10.1002/pen.23456.

[106] K. Berean *et al.*, “The effect of crosslinking temperature on the permeability of PDMS membranes: Evidence of extraordinary CO2 and CH4 gas permeation,” *Separation and Purification Technology*, vol. 122, pp. 96–104, Feb. 2014, doi: 10.1016/j.seppur.2013.11.006.

[107] “Membranes | Free Full-Text | Thickness Effect on CO2/N2 Separation in Double Layer Pebax-1657®/PDMS Membranes.”.

[108] A. Ghadimi, M. Sadrzadeh, K. Shahidi, and T. Mohammadi, “Ternary gas permeation through a synthesized PDMS membrane: Experimental and modeling,” *Journal of Membrane Science*, vol. 344, no. 1, pp. 225–236, Nov. 2009, doi: 10.1016/j.memsci.2009.08.001.

[109] M. Sadrzadeh, K. Shahidi, and T. Mohammadi, “Effect of operating parameters on pure and mixed gas permeation properties of a synthesized composite PDMS/PA membrane,” *Journal of Membrane Science*, vol. 342, no. 1, pp. 327–340, Oct. 2009, doi: 10.1016/j.memsci.2009.07.015.

[110] L. Xu, H. Lee, D. Jetta, and K. W. Oh, “Vacuum-driven power-free microfluidics utilizing the gas solubility or permeability of polydimethylsiloxane (PDMS),” *Lab on a Chip*, vol. 15, no. 20, pp. 3962–3979, 2015, doi: 10.1039/C5LC00716J.

[111] A. Dharia *et al.*, “Silicon Micropore-Based Parallel Plate Membrane Oxygenator: SILICON MICROPORE MEMBRANE OXYGENATORS,” *Artificial Organs*, vol. 42, no. 2, pp. 166–173, Feb. 2018, doi: 10.1111/aor.12972.

[112] Y.-J. Won *et al.*, “Factors affecting pattern fidelity and performance of a patterned membrane,” *Journal of Membrane Science*, vol. 462, pp. 1–8, Jul. 2014, doi: 10.1016/j.memsci.2014.03.012.

[113] “Preparation and Application of Patterned Membranes for Wastewater Treatment | Environmental Science & Technology.”.

[114] J. Tong, C. A. Simmons, and Y. Sun, “Precision patterning of PDMS membranes and applications,” *J. Micromech. Microeng.*, vol. 18, no. 3, p. 037004, Feb. 2008, doi: 10.1088/0960-1317/18/3/037004.

[115] X. He, T. Wang, Y. Li, J. Chen, and J. Li, “Fabrication and characterization of micro-patterned PDMS composite membranes for enhanced ethanol recovery,” *Journal of Membrane Science*, vol. 563, pp. 447–459, Oct. 2018, doi: 10.1016/j.memsci.2018.06.015.

[116] J. K. Lee, H. H. Kung, and L. F. Mockros, “Microchannel Technologies for Artificial Lungs: (1) Theory,” *ASAIO Journal*, vol. 54, no. 4, pp. 372–382, Jul. 2008, doi: 10.1097/MAT.0b013e31817ed9e1.

[117] M. C. Kung, J.-K. Lee, H. H. Kung, and L. F. Mockros, “Microchannel Technologies for Artificial Lungs: (2) Screen-filled Wide Rectangular Channels,” *ASAIO Journal*, vol. 54, no. 4, pp. 383–389, Jul. 2008, doi: 10.1097/MAT.0b013e31817ed9c8.

[118] J.-K. Lee, M. C. Kung, H. H. Kung, and L. F. Mockros, “Microchannel Technologies for Artificial Lungs: (3) Open Rectangular Channels,” *ASAIO Journal*, vol. 54, no. 4, pp. 390–395, Jul. 2008, doi: 10.1097/MAT.0b013e31817eda02.

[119] D. M. Hoganson *et al.*, “Branched vascular network architecture: A new approach to lung assist device technology,” *The Journal of Thoracic and Cardiovascular Surgery*, vol. 140, no. 5, pp. 990–995, Nov. 2010, doi: 10.1016/j.jtcvs.2010.02.062.

[120] J. A. Potkay, M. Magnetta, A. Vinson, and B. Cmolik, “Bio-inspired, efficient, artificial lung employing air as the ventilating gas,” *Lab Chip*, vol. 11, no. 17, p. 2901, 2011, doi: 10.1039/c1lc20020h.

[121] T. Kniazeva, J. C. Hsiao, J. L. Charest, and J. T. Borenstein, “A microfluidic respiratory assist device with high gas permeance for artificial lung applications,” *Biomed Microdevices*, vol. 13, no. 2, pp. 315–323, Apr. 2011, doi: 10.1007/s10544-010-9495-1.

[122] T. Kniazeva *et al.*, “Performance and scaling effects in a multilayer microfluidic extracorporeal lung oxygenation device,” *Lab Chip*, vol. 12, no. 9, p. 1686, 2012, doi: 10.1039/c2lc21156d.

[123] T. Rieper, C. Müller, and H. Reinecke, “Novel scalable and monolithically integrated extracorporeal gas exchange device,” *Biomed Microdevices*, vol. 17, no. 5, p. 86, Oct. 2015, doi: 10.1007/s10544-015-9982-5.

[124] A. A. Gimbel *et al.*, “A high gas transfer efficiency microfluidic oxygenator for extracorporeal respiratory assist applications in critical care medicine,” *Artificial Organs*, vol. 45, no. 8, Aug. 2021, doi: 10.1111/aor.13935.

[125] J. A. Santos *et al.*, “Design and construction of three-dimensional physiologically-based vascular branching networks for respiratory assist devices,” *Lab on a Chip*, vol. 21, no. 23, pp. 4637–4651, 2021, doi: 10.1039/D1LC00287B.

[126] J. Santos *et al.*, "Toward Development of a Higher Flow Rate Hemocompatible Biomimetic Microfluidic Blood Oxygenator," *Micromachines*, vol. 12, no. 8, p. 888, Jul. 2021, doi: 10.3390/mi12080888.

[127] E. M. Vedula *et al.*, "Multilayer Scaling of a Biomimetic Microfluidic Oxygenator," *ASAIO J*, vol. 68, no. 10, pp. 1312–1319, Oct. 2022, doi: 10.1097/MAT.0000000000001647.

[128] B. C. Isenberg *et al.*, "A Clinical-Scale Microfluidic Respiratory Assist Device with 3D Branching Vascular Networks," *Advanced Science*, vol. 10, no. 18, p. 2207455, 2023, doi: 10.1002/advs.202207455.

[129] A. A. Setty *et al.*, "Toward Microfluidic Integration of Respiratory and Renal Organ Support in a Single Cartridge," *Artificial Organs*, vol. n/a, no. n/a, doi: 10.1111/aor.14603.

[130] L. J. Ma, E. A. Akor, A. J. Thompson, and J. A. Potkay, "A Parametric Analysis of Capillary Height in Single-Layer, Small-Scale Microfluidic Artificial Lungs," *Micromachines*, vol. 13, no. 6, Art. no. 6, Jun. 2022, doi: 10.3390/mi13060822.

[131] J. Lachaux *et al.*, "A compact integrated microfluidic oxygenator with high gas exchange efficiency and compatibility for long-lasting endothelialization," *Lab Chip*, vol. 21, no. 24, pp. 4791–4804, Dec. 2021, doi: 10.1039/D1LC00356A.

[132] M. Dabaghi *et al.*, "Microfluidic blood oxygenators with integrated hollow chambers for enhanced air exchange from all four sides," *Journal of Membrane Science*, vol. 596, p. 117741, Feb. 2020, doi: 10.1016/j.memsci.2019.117741.

3. Chapter 3: Scaled-up microfluidic lung assist device for artificial placenta application with high gas exchange capacity

3.1 Introduction

Premature births have a significant impact on respiratory health and mortality rates on preterm and term neonates. Newborns, especially those with very low birth weights and born before 28 weeks of gestation, have a very low chance of survival [1]. For instance, babies born before 24 weeks of gestation have more than a 50% chance of not surviving [1,2]. Additionally, one of the primary causes of morbidity associated with preterm delivery is respiratory failure due to insufficient surfactant production in underdeveloped lungs, leading to lung hypoplasia [3–5]. Premature neonates who experience respiratory failure often require mechanical ventilation for respiratory support. However, this treatment is invasive and has severe complications associated with it, including pulmonary injury, chronic lung disease, and diseases such as retinopathy of prematurity, intraventricular hemorrhage, or necrotizing enterocolitis [6]. These complications can lead to several long-term side effects. In the case of late-preterm and term infants, extracorporeal membrane oxygenation (ECMO) could be an alternative treatment option [7]. However, it is also invasive and requires central vascular access and surgery. Additionally, the hollow fiber-based blood oxygenators currently used in ECMO are not suitable for neonatal applications due to their high priming volume (>20 mL) and tortuous flow paths that can promote thrombotic reactions [7,8]. Furthermore, also have to be actively perfused with oxygen complicating the device and can result in hyperoxemia. The use of this technology can also result in other complications, such as cerebral injury with intracranial hemorrhage or stroke, poor somatic growth, and poor neurodevelopment [9–11].

The majority of clinical blood oxygenators use hollow fibers for gas exchange. Originally, blood flowed through the fibers in an enclosed jacket, but this caused high flow resistance and risks of hemolysis and thrombosis.[7]. To improve safety, modern designs have blood flow around the fibers while gases exchange inside them, coated with silicone or polymethylpentene to prevent plasma leakage. This reduces pressure drop but increases priming volume, making them unsuitable for neonates without blood transfusions. Additionally, this configuration leads to non-uniform blood flow and high shear regions, requiring high levels of heparinization, which is detrimental to

premature neonates [7,12,13]. To overcome these limitations, microfluidic blood oxygenator devices have been developed to provide a more streamlined and uniform flow of blood adjacent to a gas exchange membrane with optimal pressure drop, low priming volume, and reasonable gas exchange capability [12,14,15].

The artificial placenta concept on the other hand mimics the biological circulation of the blood in the fetus when inside the mother's womb and can be used to oxygenate fetal blood and eliminate carbon dioxide [6,16,17]. In addition to artificial placenta concept, there is a more complex system named as artificial womb which is an extracorporeal life support system that oxygenates the fetal blood, eliminates carbon dioxide, and supplies essential nutrients for the developing fetus to continue its growth until it attains a viable gestational age [18–22]. An ideal artificial placenta-type oxygenator would be a passive device operated by the arterio-venous pressure difference in the neonate and have a low priming volume to eliminate the need of blood transfusions [6]. [15,23–25]. Quantitatively, the operating parameters for an AP device should be flow rates of 20 to 30 ml/min/kg for a baby, delivering a maximum of 1.3 to 1.9 ml of oxygen per minute per kilogram of the baby's weight [15,24]. Such an AP device ought to possess a minimal priming volume (less than 10 ml per kg of body weight) to facilitate the use of saline as a filling solution instead of relying on blood transfusion[24]. This approach helps prevent significant blood dilution, subsequently avoiding a reduction in hematocrit levels. Hence, an optimal solution would involve a passive device driven by the neonate's heart (where the arteriovenous pressure differential usually ranges from 20 to 60 mmHg)[6,8]. Ideally, this device should have the capability to facilitate gas exchange in room air, essentially mirroring the concept of an artificial placenta. By linking this device to the umbilical vessels, it could effectively enhance the compromised gas exchange capacity of immature lungs during their crucial stages of growth and maturation[15].

In our previous work, we fabricated MBOs based on 5-inch master molds (limited by capabilities of mask aligner) and connected 16 of these devices in parallel to enable sufficient throughput required to support the needs of premature babies[15,26]. This configuration had lower residence time of blood in the device and higher priming volume associated with the fluidic blood distributors which was not optimal. Each MBOs served as a single oxygenator unit and 16 of them was needed to achieve the required gas exchange. High number of used oxygenator units required more connectors impacting the total priming volume and increasing the chance of the LAD's failure.

In this study, we have modified the fabrication process to produce 8-inch devices that have higher residence time for blood and lower priming volume due to reduced number of parallel units. master molds, resulted in increasing the effective gas exchange surface area from ~ 50 cm^2 to 159 cm^2. Using this approach, each scaled-up device has a gas exchange capacity of three smaller devices while the priming volume is significantly reduced assuming that 3 smaller devices would have the same gas exchange area of one scaled-up device (from ~ 0.8 mL to 1.6 mL for the scaled-up devices). Moreover, the design of the inlet/outlets with tapered configuration underwent significant design optimization to lower hydraulic resistance at the intersection between the blood vascular network and the entering or exiting blood. As a result, the huge upscaling in the size of our MBOs did not lead to a significant increase in the hydraulic resistance, thereby the pressure drop. Our tested LAD could achieve the highest gas exchange in room air and an oxygen environment compared to other microfluidic blood oxygenators[15,24,24,26–28,28–31].

3.2 Methods

3.2.1 Microfluidic blood oxygenator design

The MBOs were designed with a blood vascular network made up of two thin, non-porous PDMS membranes, forming a layer of interconnected microchannels (**Error! Reference source not found.**). For the experiments, two types of composite membranes made of porous polytetrafluoroethylene (PTFE) membranes and PDMS were utilized. The first membrane, referred to as composite membrane 1 or the top membrane, had a pore size of 1 μm, a porosity of 83%, and a thickness of approximately 35 μm. The second membrane, composite membrane 2 or the bottom membrane, had a pore size of 0.45 μm, a porosity of up to 90%, and a thickness of about 25 μm. The top and bottom membranes were 120 μm and 30 μm thick, respectively, and the network was designed to fit onto an 8-inch silicon wafer (see Figure). Similar to our previous studies, two different heights (105 μm and 195 μm) were chosen from the upper and lower designs criteria for the blood vascular network based on numerical simulations to optimize pumpless operation[15,26]. Heights lower than ~100 μm would cause significant increase in hydraulic resistances and pressure drops and heights greater than ~ 200 μm would compromise an efficient gas exchange and low priming volume. To support the membranes and form the microchannel network, an array of pillars measuring 1 × 1 mm with a spacing of 1 mm was placed inside the blood chamber (see **Error! Reference source not found.**C). The dimensions of the pillars and channels were optimized to

ensure a uniform velocity profile, low pressure drop, and low shear stress [26,30]. The thickness of the top membrane was optimized for device handling, while the bottom membrane was optimized for high gas exchange, resulting in the different thicknesses chosen.

To address the issue of high hydraulic resistance and pressure drop due to the inlet configuration, an optimized inlet with a tapered configuration for blood entering the blood vascular network (see **Error! Reference source not found.**) was incorporated [30]. Inlets with perpendicular c onfiguration to the blood vascular network are commonly used in oxygenator designs due to their convenience and ease of fabrication, but they often result in a significant redirection of blood, leading to high hydraulic resistance, pressure drop, and shear stress. To mitigate this, a tapered inlet configuration was designed to provide smooth access to the blood vascular network from the side of the blood channels, as numerical simulations from our previous studies showed that this design reduces shear stress and pressure drop[15,30]. In this work, the tapered design was further optimized to lower hydraulic resistance without noticeably impacting the priming volume. In the new design, the blood-contacting surface area of the tapered inlet was increased to smoothly introduce blood to the blood vascular network as depicted in **Error! Reference source not f ound.**D and E. Such a design avoids a sharp angle change in blood flow, which would reduce the hydraulic resistance, thereby lowering the pressure drop. In addition, numerical simulation done by COMSOL Multiphysics confirmed that changes made in the inlet design eliminated dead zones and reduced the shear stress significantly as seen in Figure 3.2. Additionally, the maximum shear stress in new inlet design did not surpass the shear stress threshold (~ 10 Pa[8]) tolerable with red blood cells even at a high blood flow rate of 40 mL/min while the previous design was not suitable for such high blood flow rate.

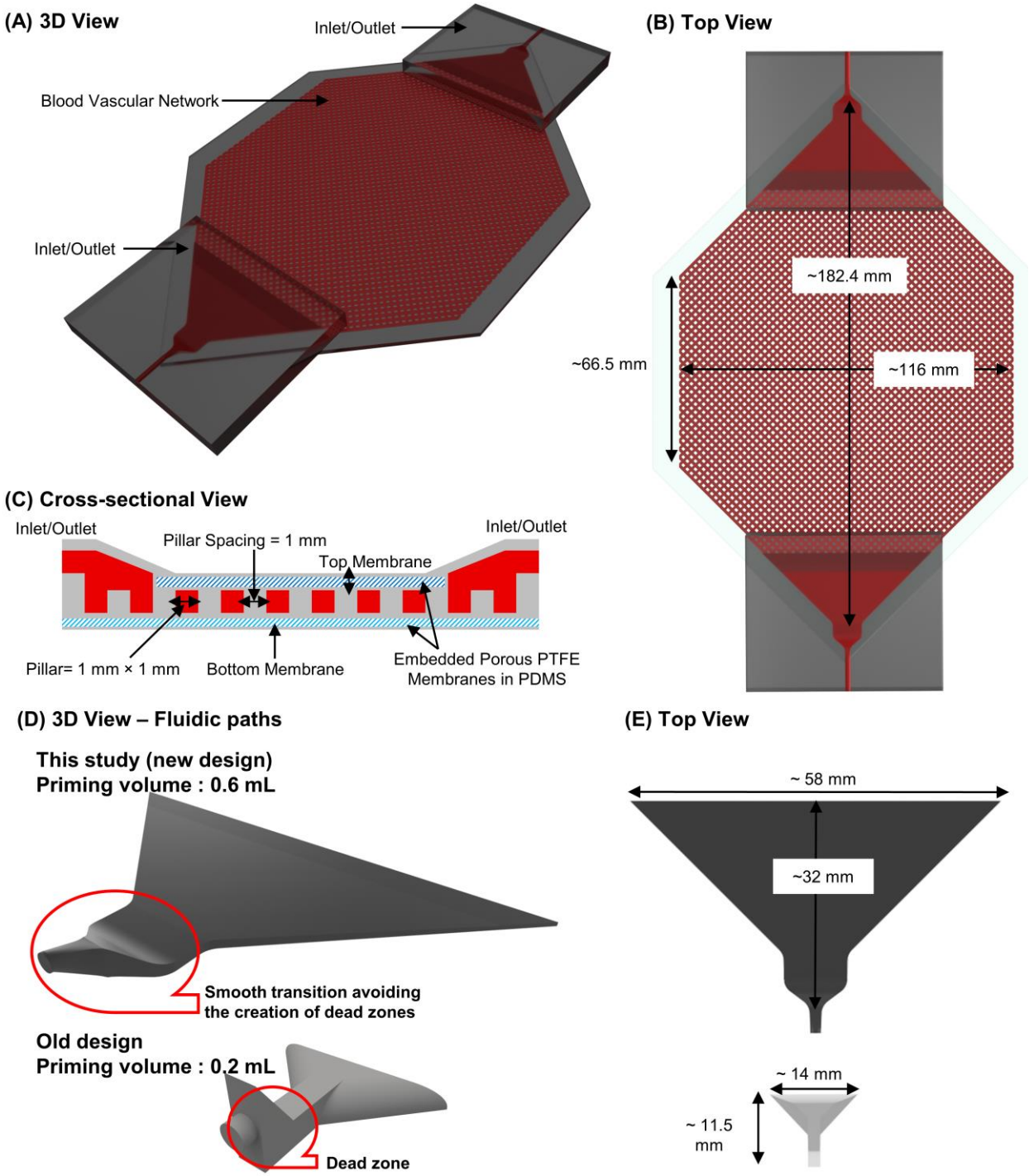

Figure 3.1: (A) A 3D schematic of scaled-up microfluidic blood oxygenator with double-sided blood gas exchange channels, (B) the top view of MBO representing the dimension of the blood vascular network, (C) the cross-sectional view of the MBO showing the top and bottom membranes with the dimensions of micro-pillars, (D) A 3D schematic of the new inlet design

versus the old design, and (E) the top of the new inlet design versus the old design.

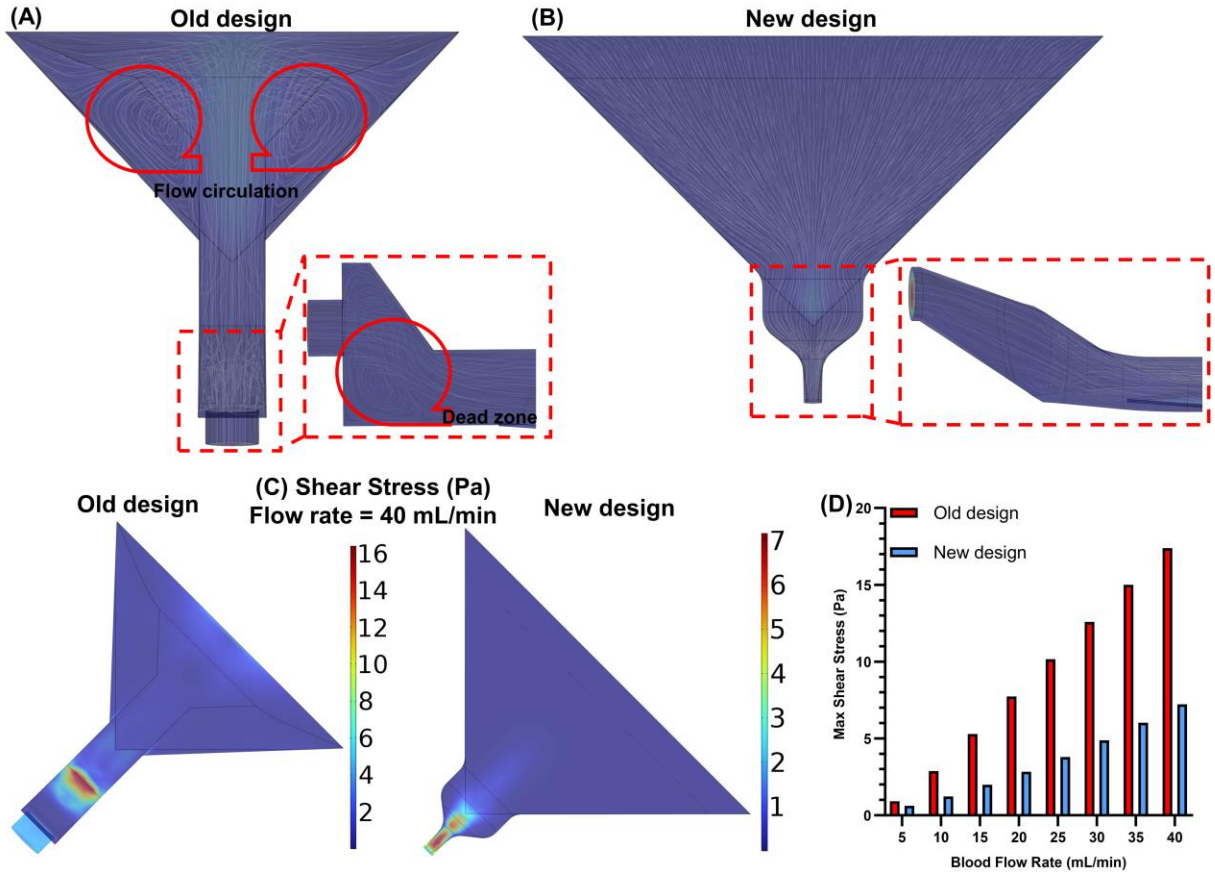

Figure 3.2: Numerical simulation using COMSOL Multiphysics. (A – B) The velocity streamlines in the old and new design showing that there is dead zone and circulation in the old design of the inlet/outlet. (C) Shear stress profile (top-view) highlighting shear stress difference between the old and the new design. (D) The maximum shear stress at various blood flow rates while the shear stress threshold is 10 Pa[8].

3.2.2 Microfluidic blood oxygenator fabrication

The negative mold for the blood vascular network was fabricated via the conventional photolithography using SU8 (3035 or 3050, MicroChem). A silane-based compound was applied to each silicon master mold using chemical vapor deposition techniques to decrease PDMS's stickiness to the master mold as reported in our previous work[30]. Briefly, the microfabricated mold was thoroughly rinsed with acetone for a few minutes, followed by a ten-minute rinsing in

isopropanol and rinsing with DI water. Then, the mold was dried with compressed air and placed on a hot plate at 150°C for 30 minutes to ensure that the master mold was completely dried. The master mold was exposed to oxygen plasma (900 mTorr, Harrick Plasma cleaner) for 2 minutes to activate the master mold's surface. Afterward, the mold was placed under a desiccator along with a petri dish containing a piece of kimwipe tissue soaked with 200 – 400 µL of trichloro (1H,1H,2H,2H-perfluorooctyl) silane (Sigma Aldrich) vacuumed to ~ 50 mm Hg. After an hour, the mold was removed and placed on a hot plate at 100°C for 3 hours to let unbonded silane molecules evaporate. After 5 -10 cycles of PDMS device fabrication, this process was repeated for each master mold.

To fabricate MBOs with double-sided microchannels using PDMS and porous PTFE membranes, we modified our fabrication technique to accommodate the fabrication of the scaled-up MBOs (Figure *3.3*). PDMS monomer and its curing agent were mixed in a ratio of 10:1 and placed in a desiccator to eliminate air bubbles. The PDMS was then spin-coated onto each master mold at 800 or 900 RPM for the device with the height of 195 and 105 µm, respectively, for one minute, and the mold was placed under a desiccator to remove air trapped inside the hollow pillar features (Figure *3.3*a). This step was repeated until all hollow pillars were filled with PDMS. The mold was cured on a hot plate at 85 °C for 30 minutes. Then, another layer of PDMS was spin-coated on the previous layer with an RPM of 2000 for 60 seconds, followed by embedding the porous PTFE membrane with a pore size of 1 µm (Figure *3.3*b). Then, the mold was placed on a leveled surface to allow PDMS uniformly diffuse through the PTFE membrane. Then, the PDMS was cured at 85 °C for 30 minutes and then, the top layer was peeled off from the master mold (Figure *3.3*c). Next, the bottom composite membrane was fabricated by placing a piece of PTFE membrane on a substrate and spin-coating PDMS onto the membrane at 6000 RPM for 5 minutes forming a thin layer of PDMS (~ 2 – 5 µm), which acted as an adhesive layer (Figure *3.3*d and e). The blood vascular network and PDMS membrane whose PDMS was still wet were brought into contact and allowed to cure overnight at room temperature, which led to strong bonding (Figure *3.3*f). The inlet/outlet with a tapered configuration was affixed to two opposite corners using wet PDMS as a glue (Figure *3.3*g). The bottom side of the blood vascular network (covered by the inlet/outlet) was cut and residual PDMS was removed from the other side to open the inlet using a scalpel, and two 1-mm-thick pieces of cured PDMS were used to seal the other sides (Figure *3.3*h).

Individual oxygenators were subjected to artificially elevated pressure testing to verify the strength of the bonding and composite PDMS membranes. The results of the testing showed that the fabricated oxygenators could easily withstand operating pressures ranging from 20-60 mm Hg and did not experience any failures at pressures below 300 mm Hg (the data is not shown here).

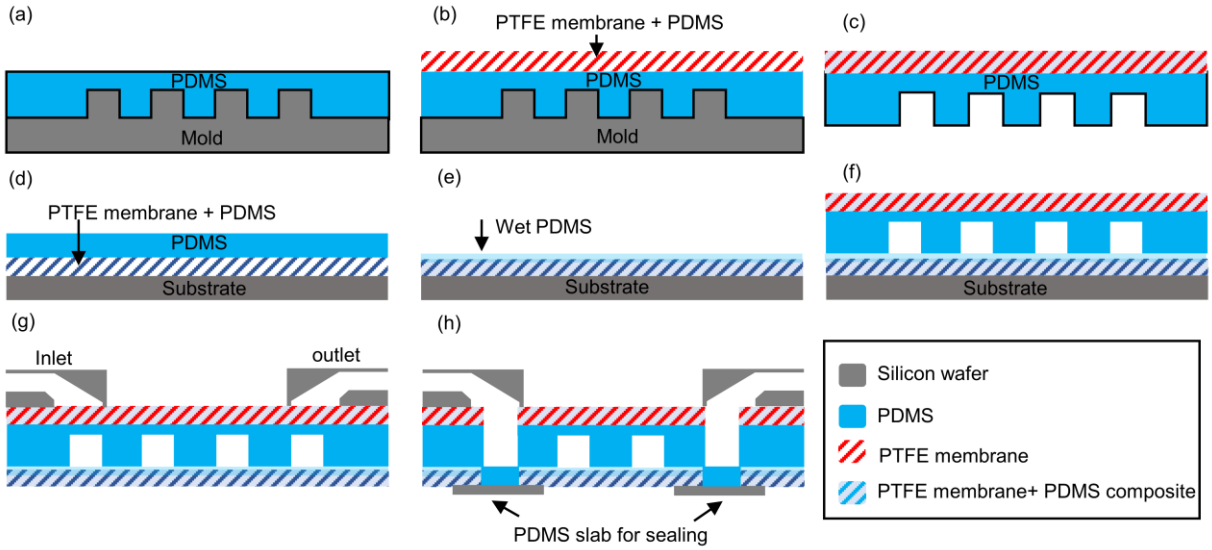

Figure 3.3: Step-by-step fabrication method of scaled-up MBOs based on a photolithography master mold using PDMS and porous PTFE membranes.

3.2.3 The assembly of LAD

The LAD was constructed by attaching eight MBOs in parallel to satisfy the design requirements and fulfill the anticipated gas exchange demands of a premature neonate with a weight of up to two kilograms, as presented in Figure *3.4*. To enhance the overall gas exchange capacity and operate the LAD at higher blood flow rates without affecting the pressure drop or oxygenation properties of the device, a parallel configuration was adopted. The use of flow distributors enabled a uniform blood distribution with no dead zone or high shear stress region, thereby avoiding any significant damage to red blood cells (hematocrit levels were measured before and after the experiment and remained consistent). The branching channel design was implemented based on Murray's law to ensure gentle flow distribution among the channels and prevent high pressure drop and shear stress, which could damage red blood cells. In contrast to our previous flow distributor designs, the width and height of branching channels were slightly reduced from the inlet to each of 8 outlets to provide better blood distribution with minimized shear stress and dead zones. To produce the flow

distributor, a 3D-printed mold (Formlab Form 3, Clear Resin) was used, and it was bonded to cured PDMS utilizing the flame-activation technique [32]. The LAD was assembled by connecting the MBOs to the flow distributors with a priming volume of ~ 1mL using low-priming-volume connectors (Figure *3.4*). Compared to our previous LAD[15], the priming volume of the blood distributor decreased from 2 mL to 1 mL and the diameter of connectors reduced by ~ 50% resulted in reducing the overall priming volume. Table 3.1 shows the comparison between the old and new LAD, highlighting that the total priming volume reduced from 18.4 mL to 14.88 mL. Before proceeding with the experiment, the LAD was perfused with normal saline solution with heparin and operated for one hour to confirm the absence of any device leakage and let heparin coat all surfaces [15].

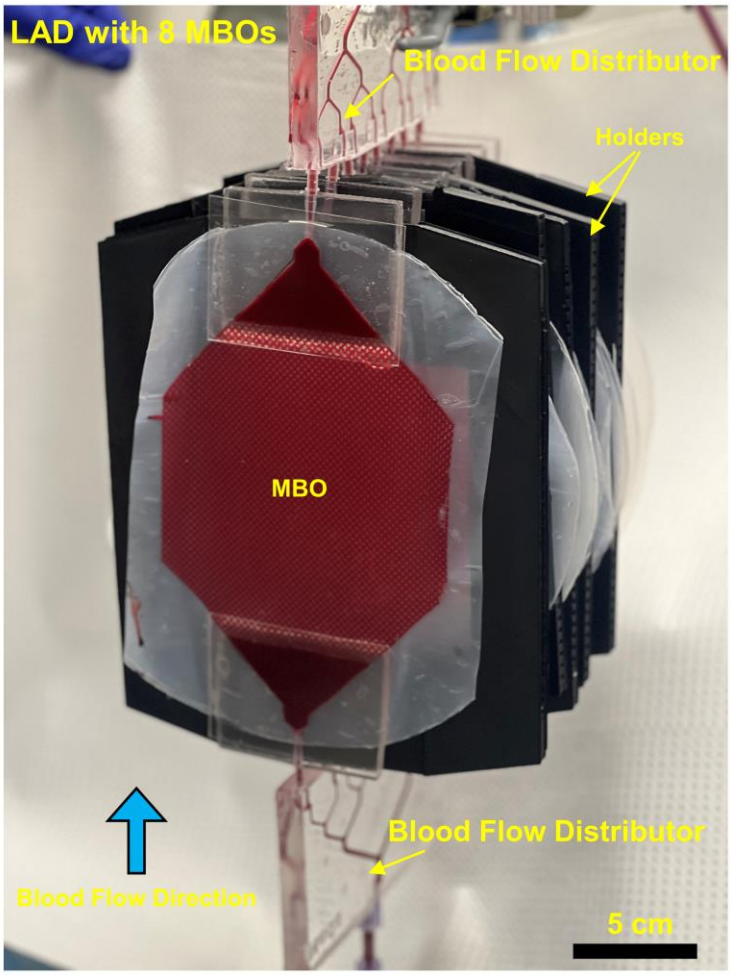

Figure 3.4: A picture of the assembled LAD with 8 scaled-up MBOs filled with porcine blood.

Table 3.1: Comparison between the LAD with 5" MBOs (old design) and the new LAD with 8" MBOs

	Priming volume (mL)	
	Old LAD with 5" MBOs	New LAD with 8" MBOs
MBOs	0.78 (n = 16)	1.57 (n = 8)
Flow distributors	2 (n = 2)	1 (n = 2)
Connectors	0.06 (n = 32)	0.02 (n = 16)
Total	18.4	14.88

3.2.4 Experimental Setup for Gas Exchange Testing with Blood

To assess the gas exchange capacity of our developed MBOs and LAD, we purchased porcine whole blood from Cedarlanelabs (porcine, whole blood, Sodium EDTA, donor, gender unspecified, 1 liter, 7204909-1LTR), which had been heparinized at a concentration of 3 units/mL. In order to replicate partially saturated arterial blood conditions in natural lungs, a hollow fiber membrane oxygenator (PDMSXA-1.0, PermSelect®, Ann Arbor, MI, USA) was used to adjust the oxygen saturation (SaO_2) level of the blood. A carbon dioxide/nitrogen gas mixture (5%/95% v/v) was supplied to the blood in the fibers at a flow rate of ~ 20 L/h, while the blood was circulated at a flow rate of 20-60 mL/min through the oxygenator to achieve an oxygen saturation level of between ~ 60% and ~68%. Once the desired SaO_2 was attained, the blood was transferred to a sealed bottle and refrigerated overnight to achieve equilibrium.

A diagram of the experimental setup is shown in Figure *3.5*. To record the pressure drop across the device, a TruWave Pressure Transducer (Edwards Lifesciences LLC, Irvine, CA, USA) was installed before the LAD, and a Spacelabs 90369 Patient Monitor (SpaceLabs Medical, Inc., Redmond, WA, USA) was used. Blood properties were assessed using a point-of-care blood gas analyzer (ABL800 FLEX blood gas analyzer) before and after the device to evaluate gas exchanges. The hematocrit level was randomly double-checked using a Complete MicroHematocrit System (StatSpin CritSpin, Norwood, MA, USA). The total content of oxygen in the blood was determined by measuring the amount of dissolved oxygen and the hemoglobin-bound oxygen, which were then added together.

When testing in room air, the LAD was exposed directly to the room air, and gas exchange measurements were recorded. When testing in an oxygen-enriched atmosphere with atmospheric

pressure, the LAD was placed in a Ziploc® bag and oxygen was perfused through the bag at a rate of 20 L/h. The bag was not completely sealed to allow excess gases to leave. The hematocrit level was monitored before and after LAD testing, and no significant changes were observed.

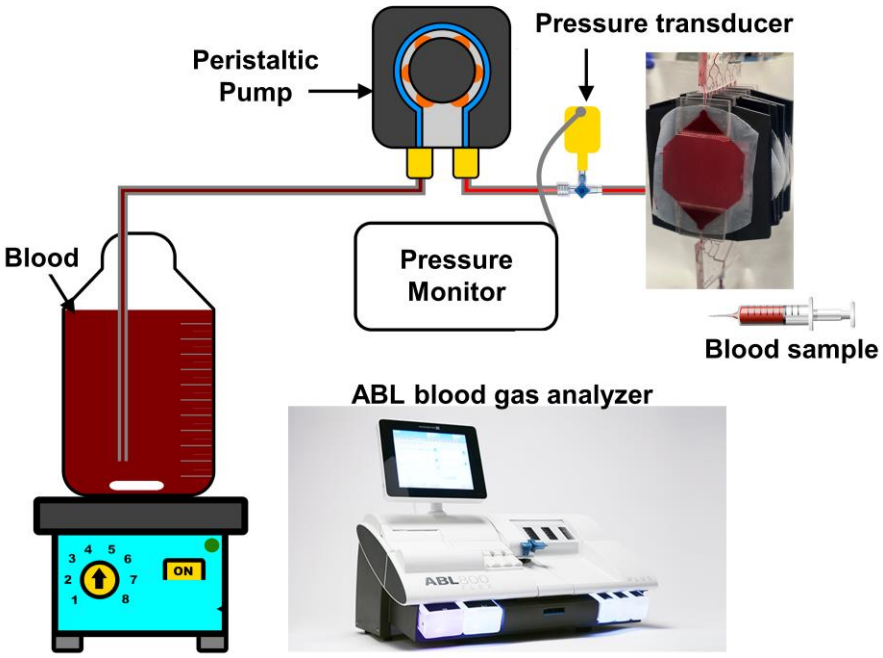

Figure 3.5: The experimental setup for assessing the gas exchange capacity of MBOs and LAD using porcine blood.

3.3 Results and Discussion

3.3.1 The performance of scaled-up microfluidic blood oxygenator using porcine blood

Two different heights of 105 µm and 195 µm were implemented in the fabrication of large MBOs. These devices were then tested using porcine blood to identify the suitable height that could generate a pressure drop within the operational range of 20-60 mmHg. Experimental tests were conducted at varying blood flow rates from 2 mL/min to 50 ml/min (Figure *3.6*). The results depicted in Figure *3.6* demonstrated a linear relationship between pressure drop and blood flow rates for all tested devices. As expected, the pressure drop was lower for the oxygenator with 195 µm channel height as compared to that with 105 µm. The highlighted region between two threshold lines in Figure *3.6* represents the operational or working pressure drop range that is required for the successful pumpless operation of the artificial placenta device. The operating flow rates for MBOs with the height of 105 µm was between ~ 3 mL/min and ~ 20 mL/min while this range for

MBOs with the height of 195 µm was from ~ 6 mL/min to ~ 35 mL/min. Notably, both MBOs could maintain their pressure drop in the optimal range at the most tested blood flow rates, making them suitable for the intended application. This achievement can be attributed to the significant design change and optimization in the inlet and outlet. Consequently, both MBOs with channel heights of 105 µm and 195 µm might be the optimal device for further experimentation and the LAD assembly.

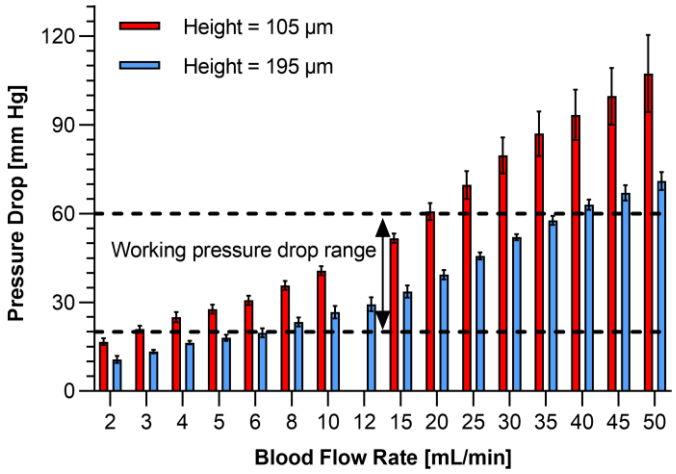

Figure 3.6: Pressure of scaled-up MBOs at different blood flow rates for two different heights of 105 µm and 195 µm. Data are mean ± SD, n = 3.

To further characterize the difference between MBOs with two different heights, an in vitro blood experiment was conducted to evaluate the gas exchange capacity of these devices while they were exposed to oxygen or room air. Gas exchange at blood flow rates identified for pumpless operation in oxygenators of different heights were tested from 2 mL/min to 15 mL/min and from 10 mL/min to 60 mL/min in room air and oxygen, respectively. The goal was to measure the increase in oxygen partial pressure (pO_2) and oxygen saturation level (SO_2) between the MBOs' inlet and outlet. Three devices per height were tested, and the average values were calculated for each condition, unless the less points were shown on the graphs. Testing was initially performed in an enriched oxygen environment, followed by exposing MBOs to room air. The results presented in Figure *3.7* demonstrate that blood oxygenation is consistently superior when MBOs are placed an enriched oxygen environment.

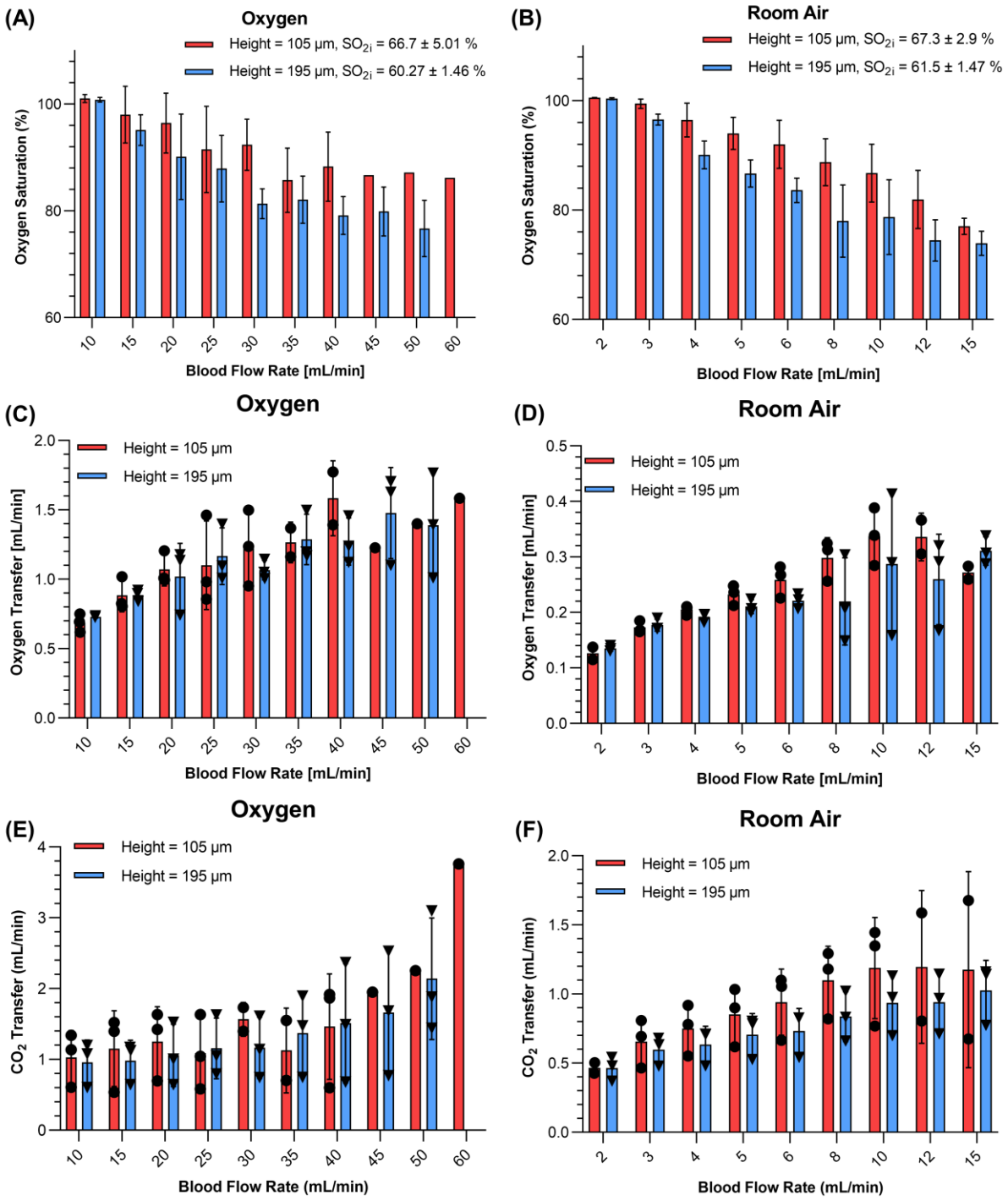

Figure 3.7: In vitro gas exchange results for scaled-up MBOs with two different heights of 105 µm and 195 µm. (A – B) Oxygen saturation level at different tested blood flow rates while the sweep gas was oxygen or room air. (C – D) Oxygen transfer at different tested blood flow rates while the sweep gas was oxygen or room air. (E – F) CO2 transfer or removal at different tested

blood flow rates while the sweep gas was oxygen or room air.

The results of the gas exchange experiments demonstrated that lowering the height of the blood vascular network had a positive impact on enhancing the oxygen saturation level, especially at higher blood flow rates and when the MBOs were exposed to room air. However, this effect was not significant at lower blood flow rates and when the MBOs were tested in oxygen, as depicted in Figure *3.7*. In both oxygen and room air conditions, the oxygen saturation achieved gradually decreases with the increase in blood flow rates, which is due to the reduced residence time of the blood in the oxygenator (Figure *3.7*A – B). Approximately, MBOs with a height of 105 μm have half the residence time as MBOs with a height of 195 μm. For example, at a blood flow rate of 10 mL/min, the residence times are 11.2 s for MBOs with a height of 195 μm and 6.0 s for those with a height of 105 μm. This difference may be due to the interaction between increased blood flow rates within the MBOs and the shortened residence time of individual red blood cells. We observed a similar behavior in our previous MBOs equipped with double-sided gas transfer diffusion[24,26]. We hypothesize that having both sides of the blood vascular network involved in gas exchange reduces the resistance of gas diffusion through membranes, ensuring better accessibility to the blood. Consequently, gas molecules face a significantly higher resistance reaching RBCs when they are farther from both the top and bottom membranes in devices with heights within the tested range. Within this height range, changes in height have a minimal effect on overall gas exchange. Thus, priming volume and pressure drops become the primary criteria for selecting the optimum device for LAD assembly. In addition, at higher blood flow rates, only the regions in proximity to the gas exchange membranes (both the top and bottom membranes) received a substantial influx of oxygen molecules before leaving the blood vascular network. Conversely, a significant portion of the blood, located away from the membranes (mostly the regions in the center of the blood vascular network), remains unsaturated as it exits the device. Alternatively, at higher blood flow rates, the flexibility of the membranes could result in an increased effective channel height, leading to a lower oxygen uptake than expectation for that height. Despite the reduction of oxygen saturation level by increasing blood flow rate, oxygen transfer or uptake slowly improved by raising the blood flow rate. This means that the rate of increase in the blood flow rate could partially compensate for the reduction in oxygen saturation level. It should be noted that both MBOs could increase oxygen saturation by more than 30 % at a very high blood flow rate of 20 mL/min when they were exposed to oxygen, which can be considered a significant improvement compared to all

reported single-layer microfluidic blood oxygenators. Carbon dioxide (CO_2) transfer or removal showed a similar trend as the oxygen uptake (Figure *3.7*E – F). However, CO_2 removal of MBOs tested in an oxygen rich environment reached a plateaued at the most blood flow rates. In contrast, CO_2 removal of MBOs exposed to room air gradually increased by increasing the blood flow rate.

At this point, both MBOs satisfied the need of gas transfer for a pumpless artificial placenta application. To obtain a reasonable oxygenation (an increase of at least ~ 30 % in oxygen saturation level), the LAD should be designed so that the blood flow rate per MBO does not exceed ~ 20 mL/min. As lowering the priming volume is desired, the MBOs with the channel height of 105 μm was selected for the LAD fabrication.

3.3.2 The LAD assembly and testing with porcine blood for evaluating the gas transfer capacity

The LAD was constructed by combining eight MBOs in a parallel configuration to meet design requirements for support the oxygenation needs of a neonate weighing up to 2 kg. The parallel arrangement was selected to facilitate a modular increase in blood flow capacity without having any negative impact on the pressure drop or oxygenation characteristics of the MBOs. In this parallel configuration for the LAD, a blood flow distributor was designed to distribute blood gradually among all eight MBOs without creating dead zones or high-shear stress regions. All MBOs were connected to the blood distributors using connectors with very low priming volume. Before assembling the LADs, several MBOs' pressure drop was measured at different flow rates using DI water and those that had the similar hydraulic behaviour were selected for assembling the LAD. Subsequently, the LAD was tested under enriched oxygen and room air conditions with porcine blood flowing at rates of 10 – 150 mL/min. The gas transfer capacity of the LAD was determined by measuring blood properties at both the inlet and outlet of the device as depicted in Figure 3.8.

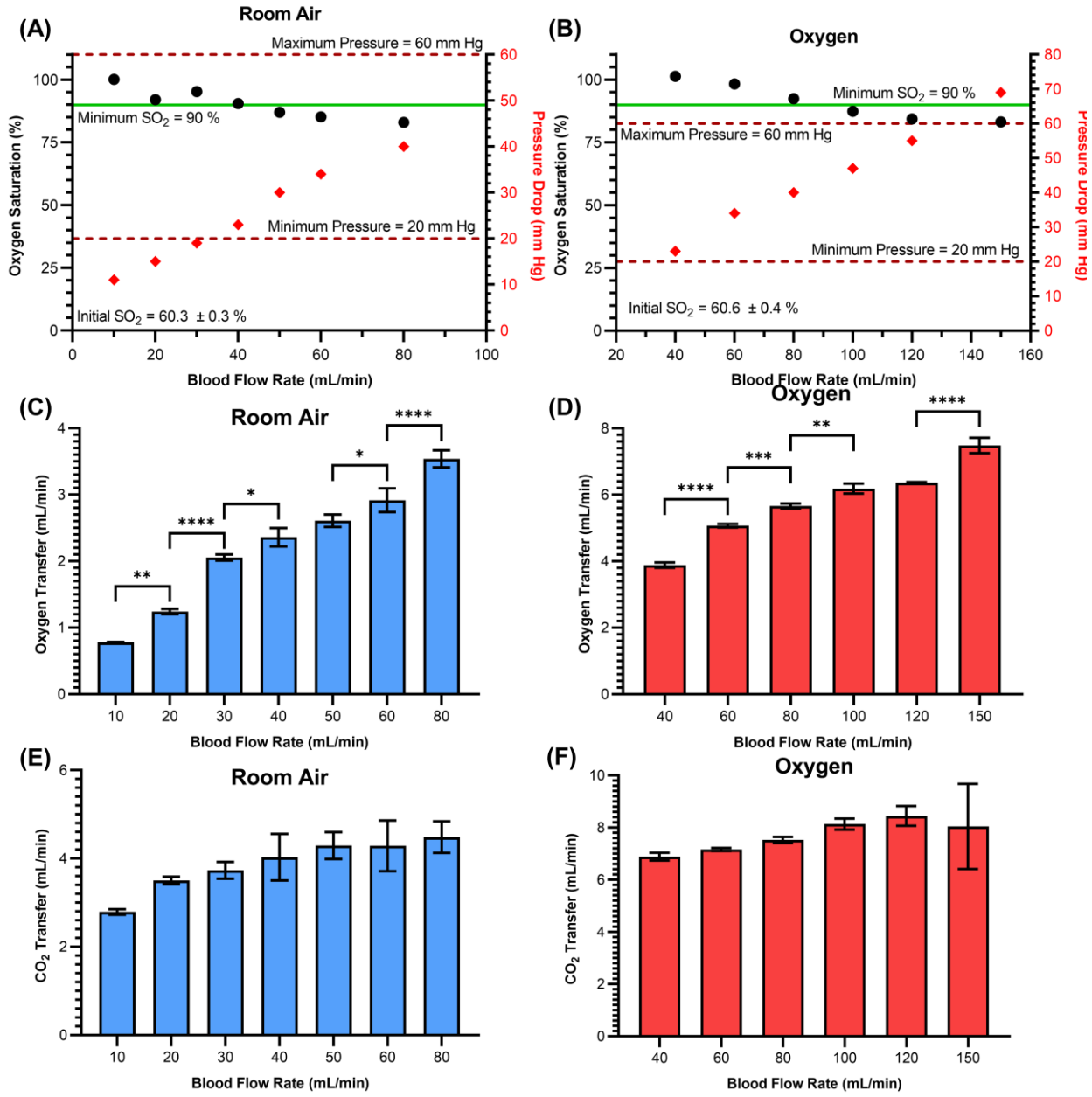

Figure 3.8: The in vitro assessment of the LAD made of 8 MBOs and two blood distributors. (A – B) The blood oxygen saturation level measured at the outlet of the LAD for different blood flow rates while the right y-axis indicates the pressure drop at the accompanied blood flow rates. The green line shows the minimum desired oxygen saturation level (90 %) and two dotted red lines indicate the operating blood pressure drop range for a pumpless operation. (C – D) Oxygen transfer of the LAD at various blood flow rates for Room air and the oxygen enriched environment. (E – F) CO_2 transfer of the LAD at various blood flow rates for Room air and the

oxygen enriched environment. Data are mean ± SD, n = 3.

The performance of the LAD was evaluated by conducting an in vitro blood experiment using porcine blood at different blood flow rates (Figure *3.8*). Specifically, the blood flow rates ranged from 10 to 80 mL/min in room air and from 40 to 150 mL/min in an enriched oxygen environment. The pressure drops of the LADs were measured under various flow rates, spanning from 10 to 150 ml/min. Notably, the increase in pressure drop exhibited a linear relationship with blood flow rates, as expected, and remained within the desired operating pressure drop range of 20-60 mm Hg (illustrated as a region between two dotted lines in Figure *3.8*A – B) for blood flow rates up to 120 mL/min. This range complies with the conditions necessary for the pumpless operation of an artificial placenta-type oxygenator, while also satisfying the required flow rates to adequately support a neonate weighing 2 kg.

The oxygen saturation level of blood before and after passing through the LAD at different blood flow rates in room air and oxygen is visualized in Figure *3.8*A – B. The results indicated a significant increase in blood oxygen saturation, ranging from ~ 41% to ~ 22%, within the blood flow rate range of 10 to 150 mL/min. In room air, the LAD could increase the oxygen saturation level above 90% at blood flow rates up to 40 mL/min while in oxygen condition, the blood flow rate increased to 80 mL/min. This relationship was observed due to the shorter residence time of blood in the LAD, resulting in reduced opportunities for oxygen molecules to be absorbed by red blood cells. Specifically, at a blood flow rate of 40 ml/min and a low pressure drop of 23 mm Hg, the LAD effectively raised the oxygen saturation level by ~ 30% in room air, satisfying the oxygenation needs of preterm neonates weighing 1 kg with respiratory distress syndrome (RDS). When the LAD was placed in an enriched oxygen environment, the LAD could raise the oxygen saturation level by ~ 32% at a blood flow rate of 80 mL/min and a low pressure drop of 40 mm Hg, which over satisfy the need of supporting a premature baby with a weight of 2 kg. It should be noted that the porcine blood had a high hematocrit level of ~ 47 %, which is very comparable to the hematocrit level of premature neonates.

These findings underscore the effectiveness of the LAD configuration in providing oxygenation support to preterm neonates of various weights up to 2 kg in an oxygen-rich environment. Moreover, the oxygen uptake demonstrated a positive correlation with increasing blood flow rates, up to 150 ml/min, in both room air and an enriched oxygen environment (as depicted in Figure

*3.8*C -D). This relationship signifies that a greater amount of oxygen was carried by the blood passing through the LAD while the blood flow rates were increased. For instance, at a blood flow rate of 40 ml/min, the LAD exhibited an oxygen uptake of 2.36 ml/min in room air and 3.88 ml/min in an oxygen-enriched environment. The tested LAD in this work could reach a high oxygen transfer value of 7.48 mL/min at a blood flow rate of 150 mL/min under oxygen conditions.

In addition, the release of carbon dioxide (CO_2), as calculated, exhibited an upward trend alongside increasing blood flow rates in both conditions, as illustrated in Figure *3.8*E – F. This behavior can be attributed to two primary factors: the diminishing thickness of the boundary layer near the membranes at higher blood flow rates and the augmented volume of CO_2-containing fluid traversing the membrane. Interestingly, exposing the LAD to pure oxygen, in comparison to ambient air, did not yield a significant effect on CO_2 release (CO2 removal did not change significantly with increasing blood flow rates), aligning with the typical behavior observed in numerous blood oxygenators. For instance, at a blood flow rate of 40 ml/min for an artificial placenta-type oxygenator, the CO_2 release of the LAD measured 4.03 ± 0.43 ml/min and 6.89 ± 0.12 ml/min, respectively for room air and oxygen conditions. Comparing too oxygen transfer, switching to oxygen as the sweep gas, the CO_2 transfer increased by ~ 70% while this value was 93% for oxygen transfer.

Table 3.2: A comparison was conducted between the present study and previous microfluidic blood oxygenators in the context of meeting the requirements of a pumpless artificial placenta-type oxygenator, characterized by a pressure drop of approximately 30 mm Hg. The comparison included scaling all devices accordingly. The representation of the number of single oxygenator units required to create an artificial placenta-type oxygenator was denoted as Nt. The priming volume for individual oxygenator units was indicated as PV_o.

Source	H [µm]	N_t	Surface Area [cm^2]	PV_o [mL]	ΔSO_2 [%]	O_2 Transfer [mL/min]	Blood Flow [mL/min]	ΔP [mmHg]	Supply gas
Hoganson 2011[33]	100	5	115	N/A	N/A	0.48	31.5	20	O_2
Rochow 2014[23]	80	20	305	2.5	N/A	1.04	30	32	O_2
	80	20	305	2.5	N/A	0.61	30	32	Air
Dabaghi 2018[24]	200	4	250	5	42	1.96	30	30	O_2
Thompson 2019[27]	30	6	189	2.8	38	1.13	30	33	O_2
Dabaghi 2019[30]	160	8	800	8	25	1.11	40	29	Air

	160	8	800	8	45	2.24	40	29	O_2
Dabaghi 2020[15]	180	16	750	12.5	29	1.54	40	25	Air
	180	16	750	12.5	43	3.37	40	25	O_2
This work	105	8	1200	12.5	30	2.36	40	23	Air
	105	8	1200	12.5	41	3.88	40	23	O_2

To be able to compare the current LAD with the previous artificial-placenta type oxygenators, different parameters such as priming volume, effective gas exchange surface area, oxygen transfer, and pressure drop are summarized for the most recent work in Table 3.2. As shown in this table, the new LAD presented in this work could provide an oxygen transfer of 2.36 mL/min in room air at a blood flow rate of 40 mL/min, which indicates ~ 53 % improvement compared to our previous tested LAD[15]. It should be noted that the priming volume of all MBOs for both LADs was ~ 12.5 mL, however, the new LAD consisted of only 8 single oxygenator units meaning that it requires a smaller number of connectors and a blood distributor with lower priming volume. In overall, the new designed LAD reached a superior gas transfer while the priming volume was significantly decreased. As the current LAD was designed to support premature neonates up to 2 kg, its priming volume meet the need of a pumpless operation without the need of blood transfusion, which is 10 mL/kg of baby body weight[15,24].

3.4 Conclusion

This study focuses on the development of a pumpless lung assist device (LAD) utilizing microfluidic blood oxygenators with large effective gas exchange surface area, specifically designed for preterm neonates experiencing respiratory failure. In vitro assessments were conducted using porcine blood samples to evaluate the gas exchange capacity of the LAD. The results demonstrated satisfactory gas transfer capabilities in room air and effective oxygenation in an oxygen-rich environment. The priming volume of all eight MBOs was ~ 12.5 mL and the redesigned blood inlet/outlet for the MBOs showed a significant impact on reducing the hydraulic resistance. As a result, we were able to lower the blood vascular network which helped enhancing gas transfer and lowering the priming volume. Moving forward, additional development steps for the LAD include implementing long-term strategies for hemocompatibility and biocompatibility measures, as well as exploring its application through the umbilical vessels in the newborn piglet model. These advancements aim to further enhance the device's performance and ensure its compatibility with the physiological requirements of preterm neonates that suffers from RDS.

3.5 References

1. Spencer, B.L.; Mychaliska, G.B. Milestones for Clinical Translation of the Artificial Placenta. *Seminars in Fetal and Neonatal Medicine* **2022**, *27*, 101408, doi:10.1016/j.siny.2022.101408.
2. De Bie, F.R.; Davey, M.G.; Larson, A.C.; Deprest, J.; Flake, A.W. Artificial Placenta and Womb Technology: Past, Current, and Future Challenges towards Clinical Translation. *Prenatal Diagnosis* **2021**, *41*, 145–158, doi:10.1002/pd.5821.
3. Zimmer, K. Artificial Wombs Are Science Fiction: But Artificial Placentas Are on the Horizon. *IEEE Spectrum* **2021**, *58*, 22–29, doi:10.1109/MSPEC.2021.9393995.
4. Spencer, B.L.; Mychaliska, G.B. Updates in Neonatal Extracorporeal Membrane Oxygenation and the Artificial Placenta. *Clinics in Perinatology* **2022**, *49*, 873–891, doi:10.1016/j.clp.2022.07.002.
5. Blauvelt, D.G.; Abada, E.N.; Oishi, P.; Roy, S. Advances in Extracorporeal Membrane Oxygenator Design for Artificial Placenta Technology. *Artificial Organs* **2021**, *45*, 205–221, doi:10.1111/aor.13827.
6. Rochow, N.; Chan, E.C.; Wu, W.-I.; Selvaganapathy, P.R.; Fusch, G.; Berry, L.; Brash, J.; Chan, A.K.; Fusch, C. Artificial Placenta - Lung Assist Devices for Term and Preterm Newborns with Respiratory Failure. *Int J Artif Organs* **2013**, *36*, 377–391, doi:10.5301/ijao.5000195.
7. Dabaghi, M.; Rochow, N.; Saraei, N.; Mahendran, R.K.; Fusch, G.; Chan, A.K.C.; Brash, J.L.; Fusch, C.; Selvaganapathy, P.R. Miniaturization of Artificial Lungs toward Portability. *Advanced Materials Technologies* **2020**, *5*, 2000136, doi:10.1002/admt.202000136.
8. Wu, W.-I.; Rochow, N.; Chan, E.; Fusch, G.; Manan, A.; Nagpal, D.; Selvaganapathy, P.Ravi.; Fusch, C. Lung Assist Device: Development of Microfluidic Oxygenators for Preterm Infants with Respiratory Failure. *Lab Chip* **2013**, *13*, 2641, doi:10.1039/c3lc41417e.
9. Amodeo, I.; Di Nardo, M.; Raffaeli, G.; Kamel, S.; Macchini, F.; Amodeo, A.; Mosca, F.; Cavallaro, G. Neonatal Respiratory and Cardiac ECMO in Europe. *Eur J Pediatr* **2021**, *180*, 1675–1692, doi:10.1007/s00431-020-03898-9.
10. Wild, K.T.; Burgos, C.M.; Rintoul, N.E. Expanding Neonatal ECMO Criteria: When Is the Premature Neonate Too Premature. *Seminars in Fetal and Neonatal Medicine* **2022**, *27*, 101403, doi:10.1016/j.siny.2022.101403.
11. Wild, K.T.; Hedrick, H.L.; Rintoul, N.E. Reconsidering ECMO in Premature Neonates. *FDT*

2020, *47*, 927–932, doi:10.1159/000509243.

12. Potkay, J.A. The Promise of Microfluidic Artificial Lungs. *Lab Chip* **2014**, *14*, 4122–4138, doi:10.1039/C4LC00828F.
13. Chen, W.; Zheng, H.; Yan, Z.; Chen, R. Shape Design of an Artificial Pump-Lung Using High-Resolution Hemodynamic Simulation with High-Performance Computing. *Physics of Fluids* **2023**, doi:10.1063/5.0140986.
14. Astor, T.L.; Borenstein, J.T. The Microfluidic Artificial Lung: Mimicking Nature's Blood Path Design to Solve the Biocompatibility Paradox. *Artificial Organs* **2022**, *46*, 1227–1239, doi:10.1111/aor.14266.
15. Dabaghi, M.; Rochow, N.; Saraei, N.; Fusch, G.; Monkman, S.; Da, K.; Shahin-Shamsabadi, A.; Brash, J.L.; Predescu, D.; Delaney, K.; et al. A Pumpless Microfluidic Neonatal Lung Assist Device for Support of Preterm Neonates in Respiratory Distress. *Adv. Sci.* **2020**, *7*, 2001860, doi:10.1002/advs.202001860.
16. Sahoo, T.; Gulla, K.M. Artificial Placenta: Miles to Go before I Sleep…. *American Journal of Obstetrics & Gynecology* **2019**, *221*, 368–369, doi:10.1016/j.ajog.2019.06.037.
17. Usuda, H.; Watanabe, S.; T, H.; Saito, M.; Sato, S.; Ikeda, H.; Kumagai, Y.; Choolani, M.C.; Kemp, M.W. Artificial Placenta Technology: History, Potential and Perception. *Placenta* **2022**, doi:10.1016/j.placenta.2022.10.003.
18. Schoberer, M.; Arens, J.; Lohr, A.; Seehase, M.; Jellema, R.K.; Collins, J.J.; Kramer, B.W.; Schmitz-Rode, T.; Steinseifer, U.; Orlikowsky, T. Fifty Years of Work on the Artificial Placenta: Milestones in the History of Extracorporeal Support of the Premature Newborn. *Artificial Organs* **2012**, *36*, 512–516, doi:10.1111/j.1525-1594.2011.01404.x.
19. Usuda, H.; Watanabe, S.; Saito, M.; Sato, S.; Musk, G.C.; Fee, M.E.; Carter, S.; Kumagai, Y.; Takahashi, T.; Kawamura, M.S.; et al. Successful Use of an Artificial Placenta to Support Extremely Preterm Ovine Fetuses at the Border of Viability. *American Journal of Obstetrics and Gynecology* **2019**, *221*, 69.e1-69.e17, doi:10.1016/j.ajog.2019.03.001.
20. Bryner, B.; Gray, B.; Perkins, E.; Davis, R.; Hoffman, H.; Barks, J.; Owens, G.; Bocks, M.; Rojas-Peña, A.; Hirschl, R.; et al. An Extracorporeal Artificial Placenta Supports Extremely Premature Lambs for 1week. *Journal of Pediatric Surgery* **2015**, *50*, 44–49, doi:10.1016/j.jpedsurg.2014.10.028.
21. Khulbe, Y.; Gupta, S.; Javed, B.; Neyazi, A.; Padhi, B.K. Artificial Womb: Opportunities and

Challenges for Public Health. *International Journal of Surgery* **2023**, *109*, 618, doi:10.1097/JS9.0000000000000208.

22. Huang, Z.; Xiao, T.; Zhou, W. Artificial Womb: A Paradigm Shift for Saving Extremely Premature Infants. *Chinese Medical Journal* **2023**, *136*, 1759–1761, doi:10.1097/CM9.0000000000002745.
23. Rochow, N.; Manan, A.; Wu, W.-I.; Fusch, G.; Monkman, S.; Leung, J.; Chan, E.; Nagpal, D.; Predescu, D.; Brash, J.; et al. An Integrated Array of Microfluidic Oxygenators as a Neonatal Lung Assist Device: In Vitro Characterization and In Vivo Demonstration: Neonatal Lung Assist Device. *Artificial Organs* **2014**, *38*, 856–866, doi:10.1111/aor.12269.
24. Dabaghi, M.; Fusch, G.; Saraei, N.; Rochow, N.; Brash, J.L.; Fusch, C.; Ravi Selvaganapathy, P. An Artificial Placenta Type Microfluidic Blood Oxygenator with Double-Sided Gas Transfer Microchannels and Its Integration as a Neonatal Lung Assist Device. *Biomicrofluidics* **2018**, *12*, 044101, doi:10.1063/1.5034791.
25. Matharoo, H.; Dabaghi, M.; Rochow, N.; Fusch, G.; Saraei, N.; Tauhiduzzaman, M.; Veldhuis, S.; Brash, J.; Fusch, C.; Selvaganapathy, P.R. Steel Reinforced Composite Silicone Membranes and Its Integration to Microfluidic Oxygenators for High Performance Gas Exchange. *Biomicrofluidics* **2018**, *12*, 014107, doi:10.1063/1.5014028.
26. Dabaghi, M.; Saraei, N.; Fusch, G.; Rochow, N.; Brash, J.L.; Fusch, C.; Selvaganapathy, P.R. An Ultra-Thin Highly Flexible Microfluidic Device for Blood Oxygenation. *Lab Chip* **2018**, *18*, 3780–3789, doi:10.1039/C8LC01083H.
27. Thompson, A.J.; Ma, L.J.; Plegue, T.J.; Potkay, J.A. Design Analysis and Optimization of a Single-Layer PDMS Microfluidic Artificial Lung. *IEEE Trans. Biomed. Eng.* **2019**, *66*, 1082–1093, doi:10.1109/TBME.2018.2866782.
28. Malankowska, M.; Pellejero, I.; Julian, I.; Rho, H.S.; Pinczowski, P.; Tiggelaar, R.M.; Gardeniers, H.; Mallada, R.; Pina, M.P. On the Improvement of Alveolar-Like Microfluidic Devices for Efficient Blood Oxygenation. *Adv. Mater. Technol.* **2021**, *6*, 2001027, doi:10.1002/admt.202001027.
29. Thompson, A.J.; Marks, L.H.; Goudie, M.J.; Rojas-Pena, A.; Handa, H.; Potkay, J.A. A Small-Scale, Rolled-Membrane Microfluidic Artificial Lung Designed towards Future Large Area Manufacturing. *Biomicrofluidics* **2017**, *11*, 024113, doi:10.1063/1.4979676.
30. Dabaghi, M.; Saraei, N.; Fusch, G.; Rochow, N.; Brash, J.L.; Fusch, C.; Ravi Selvaganapathy,

P. An Ultra-Thin, All PDMS-Based Microfluidic Lung Assist Device with High Oxygenation Capacity. *Biomicrofluidics* **2019**, *13*, 034116, doi:10.1063/1.5091492.

31. Malankowska, M.; Julian, I.; Pellejero, I.; Rho, H.S.; Schlautmann, S.; Tiggelaar, R.M.; Pina, M.P.; Gardeniers, H.J.G.E.; Mallada, R. Understanding Blood Oxygenation in a Microfluidic Meander Double Side Membrane Contactor. *Sensors and Actuators B: Chemical* **2019**, *288*, 414–424, doi:10.1016/j.snb.2019.02.110.
32. Ghaemi, R.; Dabaghi, M.; Attalla, R.; Shahid, A.; Hsu, H.-H.; Selvaganapathy, P.R. Use of Flame Activation of Surfaces to Bond PDMS to Variety of Substrates for Fabrication of Multimaterial Microchannels. *J. Micromech. Microeng.* **2018**, *28*, 087001, doi:10.1088/1361-6439/aabd29.
33. Hoganson, D.M.; Pryor II, H.I.; Bassett, E.K.; Spool, I.D.; Vacanti, J.P. Lung Assist Device Technology with Physiologic Blood Flow Developed on a Tissue Engineered Scaffold Platform. *Lab Chip* **2011**, *11*, 700–707, doi:10.1039/C0LC00158A.

4. Chapter 4: Hierarchical microfluidic blood oxygenators with rounded channel cross sections fabricated using backside diffused photolithography technique and its characterization

4.1 Introduction

Premature births have a profound impact on the respiratory well-being and mortality rates of both preterm and term neonates, posing a grave concern in their care after the birth[1–3]. The chances of survival for newborns, especially those with extremely low birth weights and born before 28 weeks of gestation, are dismally low. To illustrate, infants delivered before 24 weeks of gestation face a daunting probability of over 50% of not making it[4]. Respiratory failure, stemming from inadequate surfactant production in underdeveloped lungs, emerges as a leading cause of morbidity in preterm deliveries, contributing to lung hypoplasia[5]. When premature neonates encounter respiratory failure, they often require invasive mechanical ventilation for respiratory support[6,7]. However, this treatment modality carries significant risks, such as pulmonary injury, chronic lung disease, and the development of conditions like retinopathy of prematurity, intraventricular hemorrhage, or necrotizing enterocolitis[8]. These complications can have long-lasting effects. In the case of late-preterm and term infants, extracorporeal membrane oxygenation (ECMO) could be considered as an alternative treatment option when the mechanical ventilation is not sufficient[9,10]. Nevertheless, ECMO also presents invasiveness as a challenge, necessitating central vascular access and surgical intervention. Additionally, the current hollow fiber-based blood oxygenators employed in ECMO are unsuitable for neonatal applications due to their high priming volume (>20 mL) and substantial pressure drop, requiring the use of an external pump for perfusion[10]. Moreover, their gas exchange mechanism relies on oxygen, which adds further complexities. The utilization of ECMO can also give rise to additional complications, including cerebral injury such as intracranial hemorrhage or stroke, inadequate somatic growth, and impaired neurodevelopment[11–13].

Commercially available blood oxygenators commonly rely on hollow fibers as the primary component for facilitating gas exchange. Most modern hollow fiber based oxygenators use the design that blood flows in the outer jacket surrounding the fibers, while gas exchange takes place within the hollow fibers[14–16]. Although the modern configuration of hollow fiber-based

oxygenators reduces pressure drop by lowering hydraulic resistance, it comes with drawbacks such as increased priming volume and potential impact on gas exchange efficiency. Considering all these matters, these conventional hollow fiber-based blood oxygenators may not be the most suitable option for providing respiratory support for term and preterm neonates who cannot stand interventions like blood transfusions[10,17].

Researchers have miniaturized blood oxygenators using microfabrication technologies, leading to advanced microfluidic blood oxygenators (MBOs)[10,18]. They offer enhanced efficiency in gas exchange, providing precise oxygen control, especially vital for neonatal patients. [19–21]. Their design minimizes priming volume, essential for neonates with limited blood volume, reducing risks related to blood transfusions [22,23]. MBOs ensure controlled and uniform blood flow, avoiding issues like stagnation zones or excessive shear stress, and lessening the need for high anticoagulation levels—beneficial for premature neonates prone to bleeding. [23,24]. While MBOs show great potential, efforts continue to refine their design and long-term performance, positioning them as pivotal in advancing neonatal respiratory care.

Conventional photolithography is the most common method to fabricate the master mold needed for manufacturing MBOs [25,26]. Photolithography offers precise manufacturing capabilities for microfluidic blood oxygenators. It allows for the creation of microscale features with exceptional accuracy and control, crucial for well-defined fluid channels and gas exchange structures [27,28]. Nevertheless, photolithography is essentially a 2D patterning method and it is difficult to pattern smoothly varying hierarchical flow networks that can mimic vascular channels using this method. Multistep and multilayer lithography can be use to fabricate microfluidic networks with larger inlets and central channel and progressively smaller capillaries however, the transitions between these layers are abrupt leading to generation of stagnation zones [10]. Furthermore, conventional lithography fabricated microfluidic designs have high velocity and shear stress at the inlet and outlet regions, increasing the pressure drop in the device and introducing local high shear stress that can promote thrombotic reactions. As a result, a more complex photolithographic approach should be obtained to fabricate oxygenators with various channel heights, which requires the deposition of several layers of photoresists with different thicknesses. Although this approach can create a network of channels with different heights, it will also create local stagnation zones and high shear stress regions at the intersection regions between channels with various heights.

An innovative approach developed to achieve multilevel hierarchical microchannels is a technique known as backside lithography [29–31]. A diffuser is used between the mask and the resist to diffuse the collimated light, forming a smooth circular exposure profile. The depth of this profile depends on the width of the features in the mask. This method enables the formation of smooth circular cross-sections and tapering during transitions from large channels to smaller capillaries, resulting in a more biomimetic structure. However, the integration of thin gas exchange membranes onto such microfluidic networks has not been demonstrated before coupled with a light diffuser technique diverges from conventional methods by exposing a photoresist through a lithography mask placed on the surface of a transparent substrate, rather than sandwiching the mask to a photoresist-coated wafers[32,33].

Traditionally, the backside photolithography approach introduces an additional step involving the creation of the mask directly on the sample's surface. This can be achieved through various techniques, such as deposition and engraving or lift-off microstructures on a glass substrate[29,31]. By exposing a uniform resin thickness from the backside of the glass wafer, a comparable resolution to front-face conventional photolithography can be achieved when similar exposure doses are followed. By incorporating the synergy of backside photolithography and a light diffuser, a master mold with 3D structures can be created[29]. The inclusion of a diffuser plays a pivotal role in achieving height gradation in relation to width (hierarchy channels). When an optical diffuser is employed, the light emitted from its surface disperses based on its angular diffusion profile[34,35]. The quality of the optical diffuser, particularly its angular diffusion profile, plays a critical role in this technique, influencing its effectiveness. Previous studies have established a direct connection between the profiles achieved in negative photoresists, specifically SU-8, and the intensity curves of polar diffusion[29]. Notably, researchers have demonstrated the impressive capability of obtaining angles of up to 45° between the photoresist and the substrate by utilizing an opal diffuser. This finding highlights the potential of the technique in creating distinct features that deviate from the conventional photolithography process. The main drawback associated with this technique is the need to fabricate a Cr-based mask on a glass substrate for each master mold production. This process is burdensome, time-consuming, and costly. To overcome these challenges, we have implemented an alternative approach by utilizing inexpensive film masks. This enables the creation of a hierarchical blood vascular network with varying heights through a single backside exposure fabrication step.

Here, we develop a new fabrication process where microfluidic channel network formed using diffuse backside lithography has been integrated with thin gas permeable membranes on two sides to form a microfluidic blood oxygenator with double-sided gas transfer diffusion. With this technique, we were able to generate channels with diverse heights ranging from hundreds of microns to a few microns using only one backside exposure and an opal diffuser. Thin membranes were integrated on the top (~ 60 µm) and bottom (~ 45 µm) of this network to produce microfluidic blood oxygenators, resulting in a total thickness of ~ 200 µm. These oxygenators were capable of efficiently oxygenating blood even at high flow rates up to 15 mL/min for single oxygenator unit. By employing these advancements, we aim to address the limitations of previous methods and pave the way for improved fabrication techniques in the field of microfluidics, particularly in the development of sophisticated blood oxygenation systems.

4.2 Methods

4.2.1 Master mold fabrication using backside photolithography

A glass wafer was cleaned with acetone and isopropanol followed by heating on a hot plate up to 120 °C. A thin layer of SU8 around 10 µm (SU8 3005, Kayaku Advanced Materials, Inc., Westborough, MA, USA) was spin-coated on the cleaned glass wafer, baked, and exposed to serve as the support layer for better adhesion. Then, a thick layer of SU8 around 500 µm (SU8 3050, Kayaku Advanced Materials, Inc., Westborough, MA, USA) was deposited on the glass wafer followed by soft baking. For UV exposure, the film mask was placed on the back of the glass wafer with deposited SU8, and the opal diffuser was located on the top of the film mask. To achieve channels with different heights and width, various UV exposure energies from 600 mJ/cm^2 to 1500 mJ/cm^2 was tried. After UV exposure, wafers were hard baked at 105 °C and developed. A chemical vapor deposition technique was used to apply a silane-based compound that served as a mold release agent onto each master mold using our previous technique[36]. The procedure involved several steps. First, the microfabricated mold underwent a thorough rinsing with acetone for several minutes, followed by a ten-minute rinse in isopropanol and a subsequent rinse with DI water. Afterward, the mold was dried using compressed air and placed on a hot plate set at 150°C for 30 minutes to ensure complete drying. To activate the surface of the master mold, it was exposed to oxygen plasma (900 mTorr, Harrick Plasma cleaner) for a duration of 2 minutes. Following activation, the mold was placed in a desiccator alongside a petri dish containing a piece of kimwipe

tissue soaked in 200 – 400 µL of trichloro (1H,1H,2H,2H-perfluorooctyl) silane (Sigma Aldrich). The system was then subjected to a vacuum of approximately 50 mm Hg. After an hour, the mold was removed from the setup and transferred to a hot plate set at 100°C for 3 hours, allowing any unbonded silane molecules to evaporate. This entire process was repeated for each master mold after every 5-10 cycles of PDMS device fabrication.

4.2.2 Microfluidic blood oxygenator fabrication with hierarchical channels

The double-sided MBOs (dsMBOs) were designed with a blood vascular network made up of two thin, non-porous PDMS membranes, forming a layer of interconnected microchannels. For the experiments, two composite membranes made of ultra-thin stainless steel mesh (with a thickness of 39 ± 2 µm, a pore size of 45 µm, and a porosity of 49%; purchased from Asada Mesh Co. Ltd.) and PDMS were utilized. After preliminary optimization, the master mold was made by exposing the resist to UV energy of 1500 mJ/cm^2 to fabricate the dsMBOs for blood experiments This UV exposure energy resulted in blood channel (capillaries) with an average height of ~ 90 µm at the center, which is ideal for proper gas exchange while a low-pressure drop can be achieved.

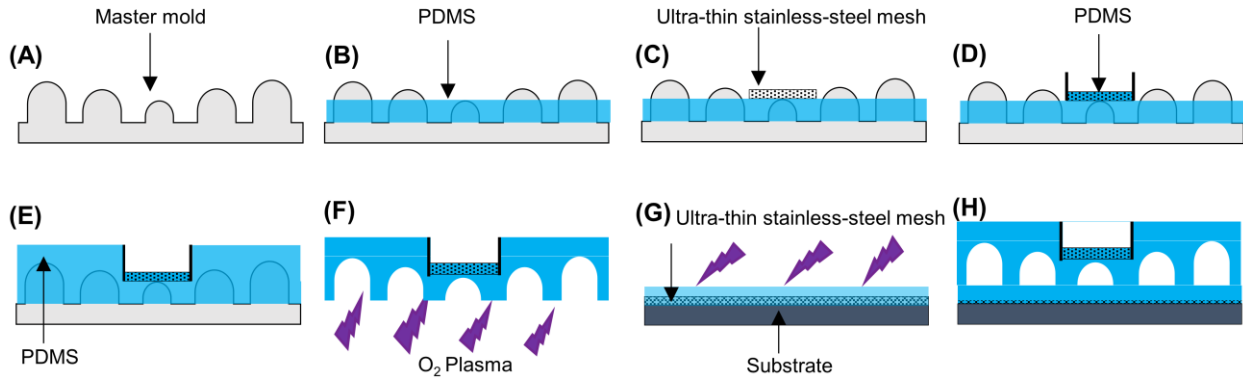

Figure 4.1: Step-by-step fabrication method of dsMBOs based on back-side photolithography master mold using PDMS and ultra-thin stainless-steel mech.

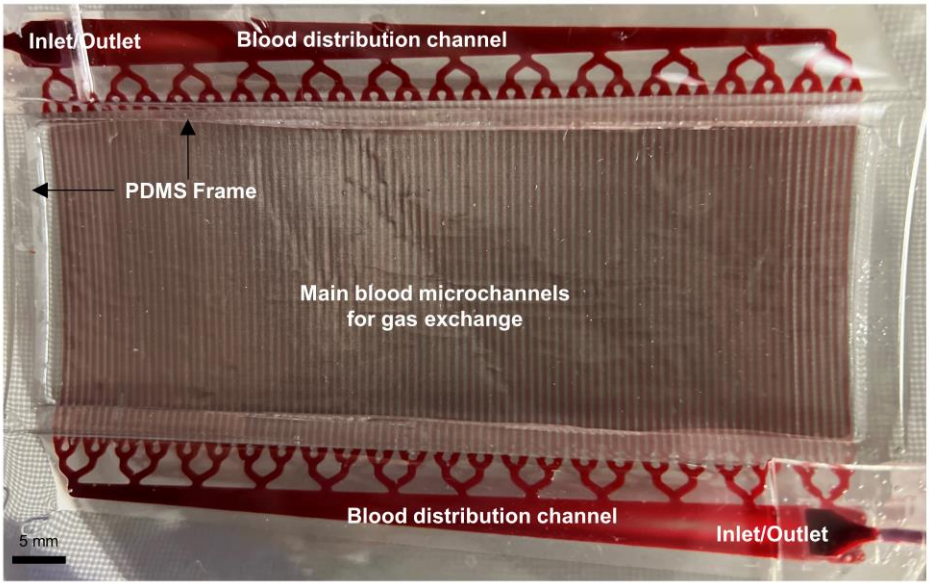

Figure 4.2: A picture of dsMBO with hierarchy blood channels filled with porcine blood

In order to produce double-sided microchannel-based oxygenators (dsMBOs) utilizing PDMS and ultra-thin stainless-steel mesh, we made modifications to our fabrication technique to accommodate the creation of dsMBOs with hierarchical channels. The height of channels in the current master mold varies, ranging from approximately 500 µm at the inlet/outlet regions to around 90 µm at the center (Figure 4.1A). This presents a challenge as it prevents the fabrication of a double-sided MBO by simply spin-coating PDMS on top of the master mold. To address this issue, we incorporated the following steps: Initially, a mixture of PDMS monomer and curing agent, in a ratio of 10:1, was prepared and placed in a desiccator to eliminate any air bubbles. The PDMS mixture was then spin-coated onto each master mold at a speed of 700-900 RPM for one minute, followed by curing on a hot plate (Figure 4.1B). At this stage, only the center channels were covered with PDMS, leaving the remaining channels exposed. Subsequently, an additional layer of PDMS was spin-coated on top of the previous layer at an RPM of 4000 for 60 seconds. This was followed by the placement of ultra-thin stainless-steel mesh, specifically covering the center channels (Figure 4.1C). The PDMS was then cured at 85 °C for 30 minutes. A PDMS frame was positioned around the center channels and ultra-thin stainless-steel mesh to prepare the device for pouring PDMS onto the exposed channels (Figure 4.1D – E). For the bottom composite membrane, a thin layer of PDMS was spin-coated (RPM 4000, 1 minute spinning), and a piece of ultra-thin stainless-steel mesh was placed on top. Another thin spin-coating of PDMS was applied after the first layer was baked. Once the poured thick PDMS on the exposed channels had cured,

the inlet/outlet with a tapered configuration was affixed to two opposite corners using wet PDMS as an adhesive. Finally, the product was released from the master mold. The bottom side of the blood vascular network (covered by the inlet/outlet) was cut, and any remaining PDMS was carefully removed from the other side to open the inlet using a scalpel. Subsequently, both the top layer and bottom layer were exposed to oxygen plasma and bonded together (Figure 4.1F – H). The final device filled with porcine blood is shown in Figure 4.2.

To ensure the strength of the bonding and composite PDMS membranes, individual oxygenators underwent pressure testing under artificially elevated conditions. The test results demonstrated that the fabricated oxygenators could withstand operating pressures ranging from 20-60 mm Hg without experiencing any failures. Furthermore, no failures were observed at pressures below 300 mm Hg (the data is not presented here).

4.2.3 The assembly of LAD

To meet the design requirements and fulfill the anticipated gas exchange demands of a premature neonate weighing up to two kilograms, the LAD (Lung Assist Device) was constructed by incorporating eight MBOs in parallel, as shown in Figure 4.3. In order to enhance the overall gas exchange capacity and facilitate operation at higher blood flow rates while maintaining optimal pressure drop and oxygenation properties, a parallel configuration was implemented. The utilization of flow distributors ensured uniform blood distribution without the presence of stagnation zones or high shear stress regions, thereby mitigating any potential damage to red blood cells (hematocrit levels were measured pre- and post-experiment and remained consistently stable). To achieve gentle flow distribution among the channels and prevent excessive pressure drop and shear stress that could harm red blood cells, the design of the branching channels adhered to Murray's Law. For the production of the flow distributor, a 3D-printed mold (Formlab Form 3, Clear Resin) was employed, which was subsequently bonded to cured PDMS through the application of the flame-activation technique. The assembly of the LAD involved the interconnection of the MBOs with the flow distributors utilizing low-priming-volume connectors. Prior to commencing the experiment, a thorough perfusion of the LAD was conducted using a normal saline solution containing heparin, and the device was operated for one hour to confirm the absence of any leakage and facilitate the uniform coating of all surfaces with heparin.

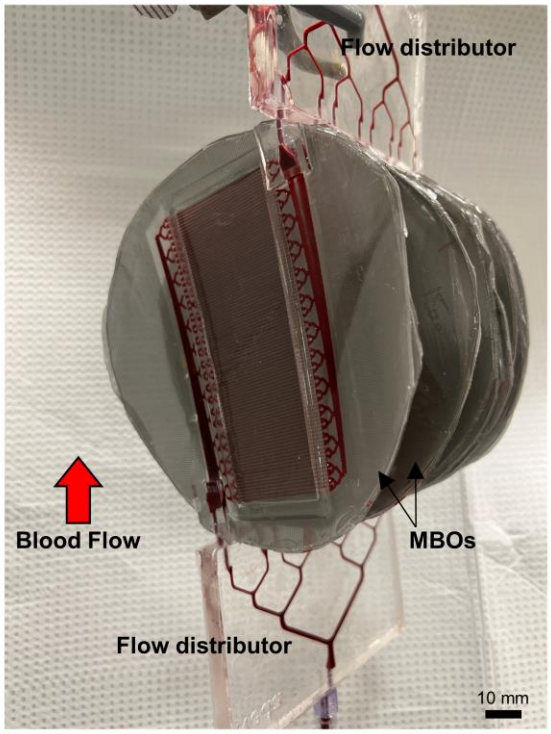

Figure 4.3: A picture of the assembled LAD with MBOs having hierarchy blood channels filled with porcine blood.

4.2.4 Experimental Setup for Gas Exchange Testing with Blood

In order to evaluate the gas exchange capacity of the developed MBOs and LAD, porcine whole blood was procured from Cedarlanelabs (product: porcine, whole blood, Na EDTA, donor, gender unspecified, 1 liter, 7204909-1LTR) and heparinized at a concentration of 3 units/mL. We utilized a hollow fiber membrane oxygenator (PDMSXA-1.0, PermSelect®, Ann Arbor, MI, USA) to adjust the oxygen saturation (SaO_2) level of the blood. The blood around the fibers was exposed to a flow of carbon dioxide/nitrogen gas mixture (5%/95% v/v) at a rate of approximately 10 - 20 L/h, while the blood circulated through the oxygenator at a flow rate of 10-60 mL/min to achieve an oxygen saturation level of around 60 ± 5%. Once the desired SaO_2 level was attained, the blood was transferred to a sealed bottle and refrigerated overnight to establish equilibrium. To measure the pressure drop across the device, we installed a TruWave Pressure Transducer (Edwards Lifesciences LLC, Irvine, CA, USA) before the LAD and MBOs, and a Spacelabs 90369 Patient Monitor (SpaceLabs Medical, Inc., Redmond, WA, USA) was employed for data recording. The blood properties were evaluated using a point-of-care blood gas analyzer (ABL800 FLEX blood

gas analyzer) before and after passing through the device to assess the gas exchanges. The total oxygen content in the blood was determined by measuring the amount of dissolved oxygen and the oxygen bound to hemoglobin, which were then combined. For testing in room air, the LAD was directly exposed to the room air, and we recorded the measurements of gas exchange. When testing in an oxygen-enriched atmosphere at atmospheric pressure, the LAD was placed inside a Ziploc® bag, and oxygen was perfused through the bag at a rate of 20 L/h. The bag was intentionally left slightly unsealed to allow for the release of excess gases and maintain atmospheric pressure for oxygen conditions.

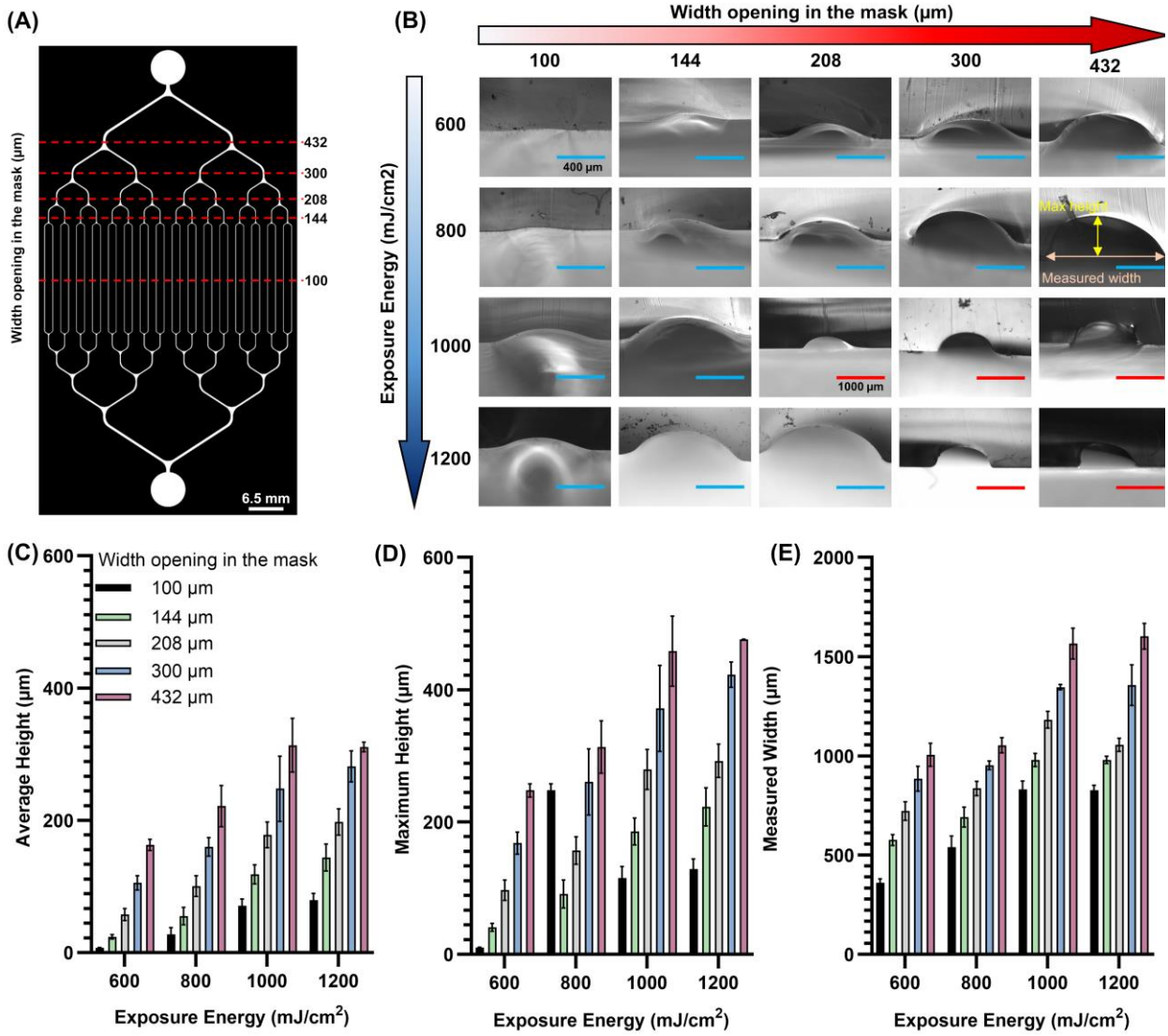

Figure 4.4: (A) the design used for optimizing fabrication process included microchannels with various width, (B) the cross-sectional images of microchannels from different width opening in

the mask and exposure energy, (C) the average height of channels based on width opening in the mask and exposure energy, (D) the maximum height of channels based on width opening in the mask and exposure energy, and (E) the measured width of channels based on width opening in the mask and exposure energy.

4.3 Results and Discussion

4.3.1 The impact of exposure energy on channel dimensions

The proposed fabrication method in this work was based on the backside photolithography method that uses SU8 photoresists to pattern and forms micro features using a high-resolution mask and UV exposure unit[29]. Here, an optical light diffuser was placed between the mask and the resist to diffuse the light radially from the mask openings and achieve hierarchical channel fabrication. We optimized exposure energy and the mask designs to find the relationship between with, height, and exposure energy. To characterize the size of micro features, we designed a hierarchical blood vascular network that had channels with various widths and used microscopy to visualize and measure the dimension of micropatterns for each master mold as shown in Figure 4.4.

The width and height of microchannel was found to increase as the width opening in the mask and exposure energy was increased as seen in Figure 4.4B. The quantified average height, maximum height, and width obtained are shown in Figure 4.4C – D. For example, at an exposure energy of 1200 mJ/cm^2, increasing the width opening in the mask from 100 µm to 400 µm resulted in the width of the microchannel increasing from approximately 800 µm to around 1600 µm (doubled), while the average height increased from approximately 80 µm to about 310 µm (four times higher). At a lower exposure energy of 600 mJ/cm^2, increasing the width opening in the mask from 100 µm to 400 µm led to the width of the microchannel increasing from around 350 µm to approximately 1000 µm (tripled), while the average height increased from about 8 µm to approximately 160 µm (20 times higher). These findings demonstrate that varying the exposure energy had a greater impact on the height rather than the width of the microchannels, and this effect was more pronounced at lower exposure energy. We observed that when the width opening in the mask exceeded approximately 1000 µm, the resulting channel height matched the thickness of the deposited SU8. As the width of opening increased in the mask (greater than few hundred of microns), the corresponding channels' height would be the same as the thickness of deposited

SU8,defining a threshold. Therefore, to control the height of blood branching channels, which their opening in the mask were wider than the threshold and do not contribute to gas exchange but greatly affect hydraulic resistance and pressure drop, the thickness of the deposited SU8 should be adjusted to achieve the desired dimensions and control these parameters.

Increasing the exposure energy resulted in channels that were wider and deeper. To further investigate the impact of these changes on hydraulic resistance behaviour, we measured the pressure drop of MBOs at various flow rates based on the design shown in Figure 4.4A. As seen in Figure 4.5, increasing exposure energy had noticeable effect on the pressure drop. At lower exposure energy, which resulted in narrower microchannels with lower heights, the pressure drop was high even at lower flow rates. While there was a minor difference between MBOs that were exposed at two higher energy of 1000 and 1200 mJ/cm^2 suggesting that as the impact of increasing exposure energy at higher exposure energy would be minor. At lower exposure energy levels, smaller and shallower channels form, resulting in a significant increase in hydraulic resistance and pressure drop. As the energy exposure increases, these changes become smaller and less noticeable, with a reduced impact on hydraulic resistance. Therefore, if pressure drop is the key parameter for selecting the optimum design, greater exposures that lead to wider and deeper channels would be preferred.

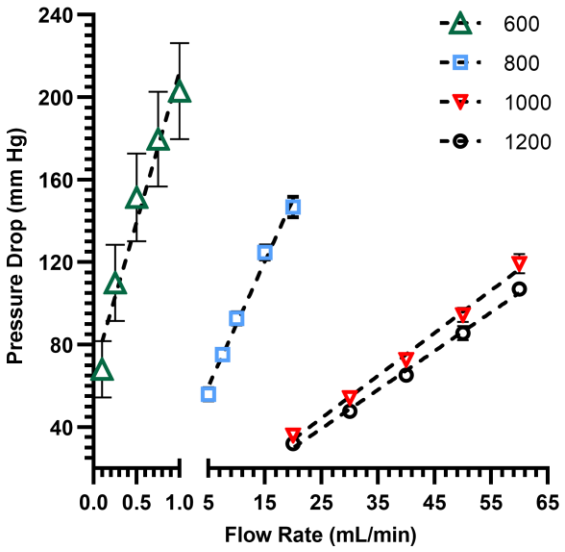

Figure 4.5: Pressure drop of MBOs exposed at various UV energy at different flow rates. Data are mean ± SD, n = 4.

4.3.2 The performance of MBOs with hierarchy blood channels using porcine blood

The design has been optimized to accommodate a greater number of gas exchange channels within 6-inch master molds. Additionally, we have slightly increased the exposure energy to 1500 mJ/cm^2 in order to enhance the channel height. This would result in achieving higher gas exchange at higher blood flow rates, as depicted in Figure 4.6A. This design contained 96 microchannels at the center and every 8 neighbor channels were connected to the main blood distributing channels whose dimensions were inspired by Murray's Law. In this optimized design, the channels branch out into three generations to reach the central channels. Compared to the previous optimizing design, the number of bifurcations has decreased from 5 to 3. The width of the main blood distribution channels varied from 1 mm to 5 mm to ensure uniform blood distribution across all 96 microchannels. Blood entered from a wider cross-section and exited the device from the opposite wider side. Choosing this design allowed us to minimize the priming volume required for branching channels and the space needed for the surrounding. It should be noted that because of the size limitation, more than 96 channels could not be accommodated. Beside the height of microchannels, the length of microchannels affected the amount of gas transfer. In order to assess the impact of length on the gas exchange, a simulation was operated while the length and the blood flow rate varied using a previously developed numerical model [21]. As shown in Figure 4.6B, increasing

the length of microchannels improved SO_2 at the outlet. However, the impact of increasing the length of microchannels became smaller when the channel's length was greater or equal to 40 mm. This was expected as the length decreased, the blood residence time would decrease as well, thereby red blood cells would not have enough time to pick up enough oxygen. As the length of 70 mm for microchannels would bring the outer channels were close to the edge of wafer, we decided to fabricate MBOs with channel's length of 55 mm.

To further characterize dsMBOs with hierarchy blood channels, an in vitro blood experiment was conducted to evaluate the gas exchange capacity of these devices while they were exposed to oxygen or room air. Various blood flow rates were tested from 1 mL/min to 5 mL/min and from 7 mL/min to 18 mL/min for room air and oxygen, respectively. The goal was to measure the increase in oxygen partial pressure (pO_2) and oxygen saturation level (SO_2) between the MBOs' inlet and outlet. Three devices were tested, and the average values were calculated for each condition, unless the less points were shown on the graphs. Testing was initially performed in an enriched oxygen environment, followed by exposing MBOs to room air. The results presented in Figure 4.7 demonstrate that blood oxygenation is consistently superior when MBOs are placed an enriched oxygen environment as expected. As blood flow rate increased, the pressure drop also increased with a linear trend (Figure 4.7A). Previously we demonstrated that the introduction of double-sided devices would noticeably enhance the gas transfer [37]. To further confirm that our new fabrication approach was successful in the creation of double-sided MBOs with hierarchy blood channels, we fabricated devices with thick top PDMS layer for comparison purposes (named as single-sided MBOs (ssMBOs)). As seen in Figure 4.7B, dsMBOs increased the oxygen saturation level significantly higher than ssMBOs. For instance, at a high blood flow rate of 15 mL/min, dsMBOs raised oxygen saturation level to ~ 93 % from ~ 70 % while ssMBOs could only raise the oxygen saturation to ~ 75 % from ~ 65 %.

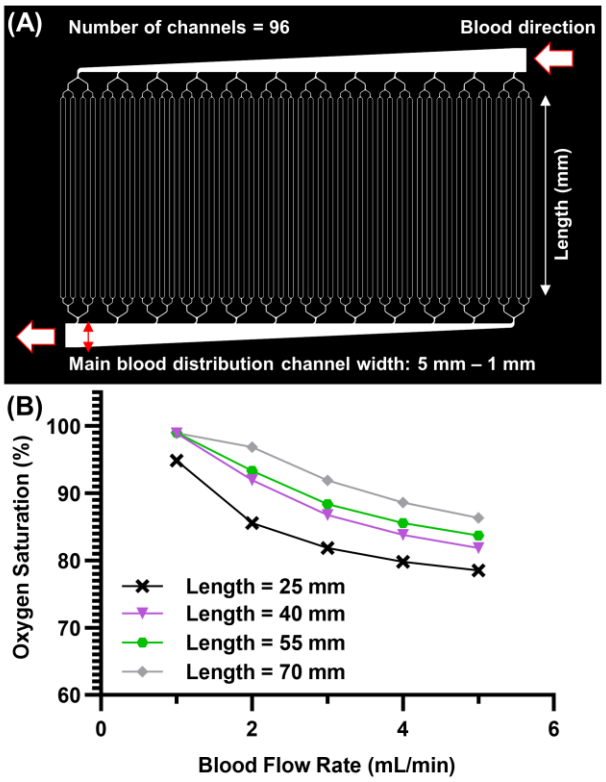

Figure 4.6: (A) the design of finalized MBOs for blood experiments containing 96 microchannels at the center with a length of 55 mm. (B) Simulated oxygen saturation result at the outlet at various blood flow rates while the length of microchannels varies from 25 mm to 70 mm.

The dsMBOs with hierarchy blood channels were also tested in room air and their results were compared with simulation results as shown in Figure 4.7. Simulation results closely matched the experimental data.

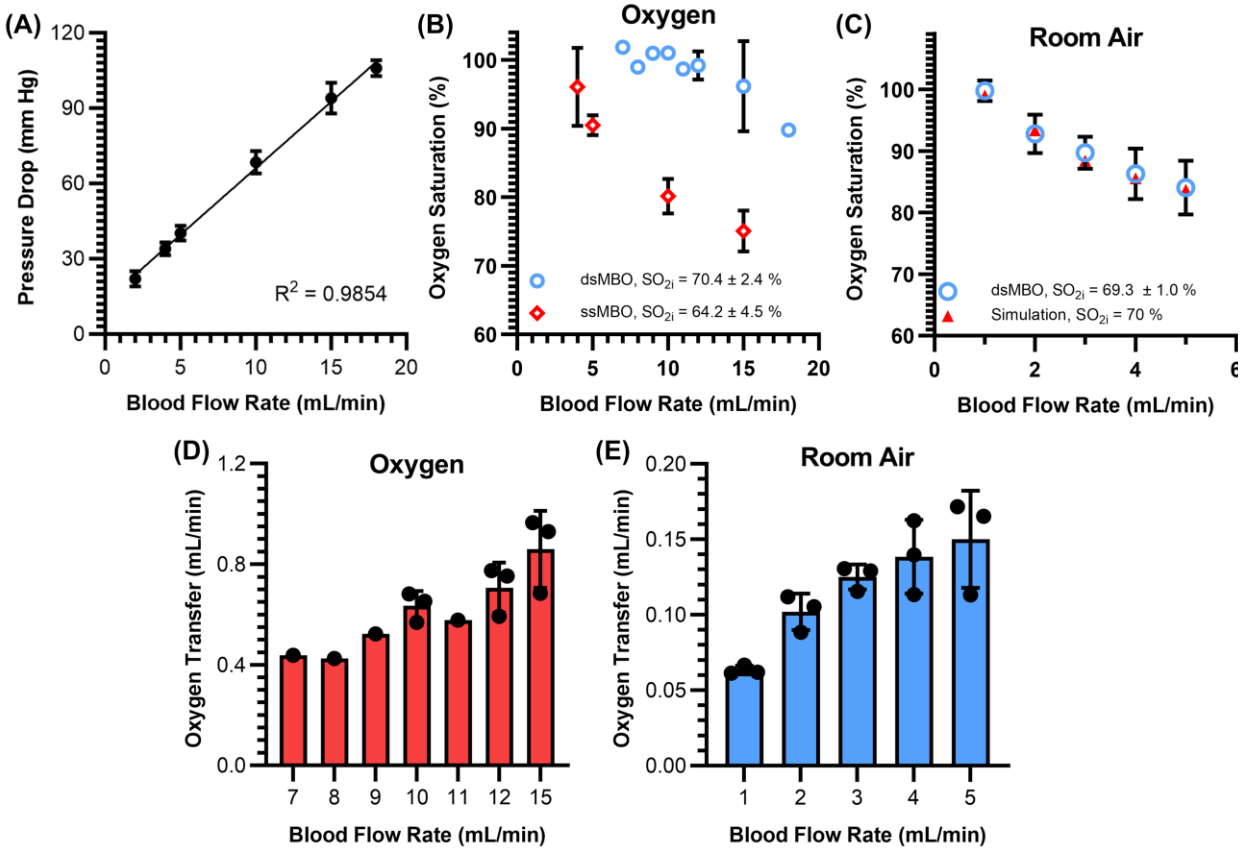

Figure 4.7: In vitro gas exchange results for MBOs. (A) pressure drop at various blood flow rates (B – C) Oxygen saturation level at various blood flow rates while the sweep gas was oxygen or room air. (D – E) The amount of oxygen transfer at various tested blood flow rates while the sweep gas was oxygen or room air.

In both oxygen and room air conditions, the oxygen saturation levels showed a gradual decrease as the blood flow rates increased, indicating that the blood within the blood vascular network did not have sufficient time to acquire an optimal amount of oxygen for complete oxygenation (Figure 4.7B - C). Up to a blood flow rate of 10 mL/min, oxygen saturation consistently remained at approximately 100% under oxygenated conditions. However, increasing blood flow rates resulted in a decrease in oxygen saturation In contrast, ssMBOs were unable to achieve full blood oxygenation even at a low flow rate of 4 mL/min. As we have previously demonstrated, the incorporation of double-sided gas transfer channels has a significant impact on oxygenation[37]. Under room air conditions, oxygen saturation began to decline at lower blood flow rates due to the reduced oxygen pressure difference between the blood and the sweep gas. This observation can be attributed to the interplay between the increased blood flow rates within the MBOs and the reduced

residence time of individual red blood cells. At higher blood flow rates, only the regions in close proximity to the gas exchange membranes (both top and bottom membranes) receive a substantial supply of oxygen molecules before exiting the blood vascular network. On the other hand, a significant portion of the blood, mainly located in the central regions of the blood vascular network, remains unsaturated as they left the device. However, the flexibility of the membranes at higher blood flow rates can be considered negligible as ultra-thin stainless steel mech reinforced both the bottom and top membranes[38]. Therefore, no significant increase in the effective channel height would be observed, which would result in lower-than-expected oxygen uptake for that specific height. Despite the decrease in oxygen saturation levels with increasing blood flow rates, the oxygen transfer gradually improved with higher blood flow rates (Figure 4.7D – E). This is due to higher volume of blood at lower saturation being exposed to the oxygen transported through the membrane at higher flow rates.

4.3.3 The LAD assembly and testing with porcine blood for evaluating the gas transfer capacity

In the context of an artificial placenta application, an LAD should oxygenate blood, raising the oxygen saturation level by approximately 30%, while maintaining a pumpless flow rate of at least 30 mL/min/kg of body weight[37,39]. Considering the oxygenation criteria, the LAD was constructed by combining eight dsMBOs with hierarchy blood channels in a parallel configuration, specifically designed to cater to the oxygenation needs of neonates weighing up to 2 kg. This parallel arrangement allows for convenient modular scaling of the blood flow capacity, while ensuring optimal pressure drop and oxygenation characteristics of the developed MBOs in this study. To facilitate efficient blood distribution without any stagnation zones or high-shear stress regions, a dedicated blood flow distributor was designed. The MBOs were seamlessly connected to the blood distributors using connectors with minimal priming volume. Before the LAD assembly, pressure drop measurements were performed on multiple MBOs using DI water, enabling the selection of MBOs with similar hydraulic behavior. Subsequently, the LAD underwent rigorous testing under both enriched oxygen and room air conditions, with porcine blood flowing at rates ranging from 5 to 100 mL/min. The gas transfer capacity of the LAD was assessed by analyzing blood properties at both the inlet and outlet of the device, as depicted in Figure 4.8 and Figure 4.9.

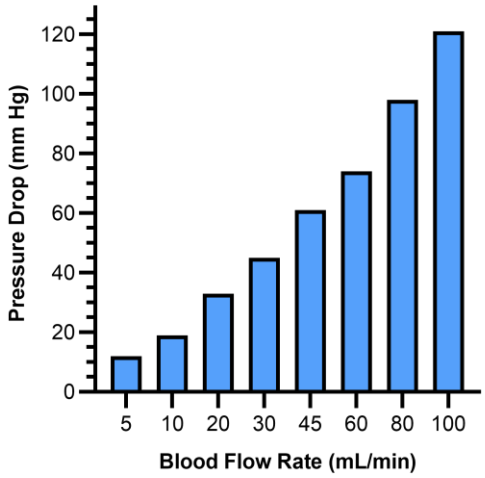

Figure 4.8: Pressure drop of the tested LAD at different flow rates.

The performance assessment of the LAD involved conducting an in vitro blood experiment using porcine blood at varying blood flow rates (Figure 4.8). The room air condition encompassed flow rates ranging from 5 to 30 mL/min, while the enriched oxygen environment involved flow rates ranging from 30 to 100 mL/min. Throughout these experiments, the pressure drops of the LADs were meticulously measured across a range of flow rates, from 5 to 100 mL/min. The increase in pressure drop exhibited a linear correlation with the blood flow rates, conforming to expectations. Moreover, the observed pressure drop values fell within the desired operating range of 20-60 mm Hg up to flow rate of ~ 50 mL/min. This compliance with the operating pressure drop criteria ensures the suitability of the LAD for pumpless operation as an artificial placenta-type oxygenator, while still accommodating the necessary flow rates to adequately support a neonate weighing ~ 2 kg.

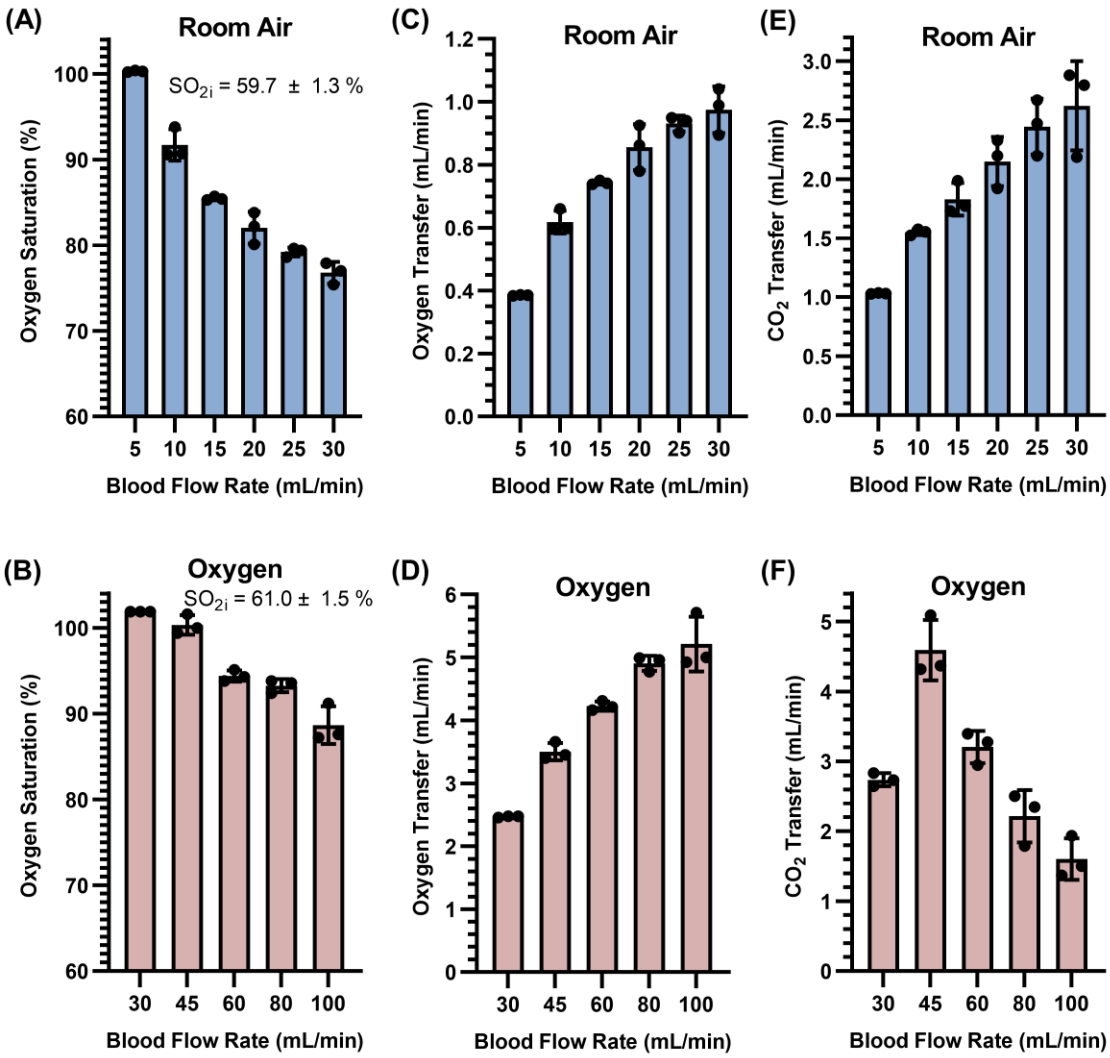

Figure 4.9: The in vitro evaluation was conducted on the LAD consisting of eight MBOs and two blood distributors. (A – B) The blood oxygen saturation level was measured at the outlet of the LAD for different blood flow rates. (C – D) The oxygen transfer of the LAD was assessed at various blood flow rates in both room air and an oxygen-enriched environment. (E – F) Similarly, the CO_2 transfer of the LAD was evaluated at various blood flow rates in room air and the oxygen-enriched environment. The presented data represents the mean ± standard deviation, with a sample size of three (n = 3).

Figure 4.9A – B illustrates the changes in blood oxygen saturation before and after passing through the LAD, considering various blood flow rates in both room air and oxygen conditions. The findings demonstrate a significant increase in blood oxygen saturation within the range of 30 to 80

mL/min, above 90% under oxygen conditions, which can be considered sufficient for supporting premature neonates. Under room air conditions, the LAD was capable of achieving oxygen saturation levels above 90% at blood flow rates up to 10 mL/min, whereas under oxygen conditions, the corresponding flow rate increased to 80 mL/min. This correlation can be attributed to the shorter residence time of blood in the LAD, limiting the absorption of oxygen molecules by red blood cells. Notably, at a blood flow rate of 30 mL/min and a low pressure drop of ~ 45 mm Hg, the LAD effectively increased the oxygen saturation level by around 40% in oxygen (fully oxygenation), meeting the oxygenation requirements of 1 kg preterm neonates with respiratory distress syndrome (RDS). The hydraulic resistance and pressure drop of the LAD can be lowered without sacrificing the gas exchange efficiency of the developed LAD. To achieve such that, thicker SU8 can be deposited to increase the height of blood distribution channels and the width of branching channels can be increased to lower their resistance. None of them changes will have any impact on the gas transfer as the dimension of the microchannels at the center do not depend on the thickness of deposited SU8.

These findings highlight the effectiveness of the developed LAD in providing oxygenation support to preterm neonates weighing up to 2 kg, particularly in an environment rich in oxygen (without considering pressure drop). Furthermore, the results demonstrated a positive correlation between oxygen uptake and increasing blood flow rates, up to 100 ml/min, both in room air and an oxygen-enriched setting (as depicted in Figure 4.9C - D). This correlation indicates that a higher amount of oxygen was carried by the blood as it passed through the LAD with increased flow rates. For example, at a blood flow rate of 30 ml/min, the LAD exhibited an oxygen uptake of 0.98 ml/min in room air and 2.47 ml/min in an oxygen-enriched environment. In this study, the tested LAD achieved a remarkable oxygen transfer value of 5.21 mL/min at a blood flow rate of 100 mL/min under oxygen conditions.

The increase in oxygen transfer or exchange in blood oxygenators with higher blood flow rates can be attributed to several factors: (I) Steeper concentration gradient for oxygen: With increased blood flow rates, a more pronounced concentration gradient for oxygen is established between the sweep gas and the blood. This steep gradient facilitates faster diffusion of oxygen molecules across the membrane or gas-liquid interface, leading to an augmented oxygen transfer. (II) Amplified surface area: Blood oxygenators typically possess a large surface area available for gas exchange. As blood

flow rates escalate, a greater volume of blood comes into contact with this surface area, providing more opportunities for oxygen molecules to diffuse into the blood and thereby enhancing overall oxygen transfer. (III) Improved mixing: Higher blood flow rates promote more thorough mixing of blood nearby the membranes. This improved mixing enhances the exposure of deoxygenated blood to fresh oxygen, facilitating efficient oxygen transfer. It is important to note that the relationship between blood flow rates and oxygen transfer may reach a point of diminishing returns. Beyond a certain threshold, further increases in blood flow rates may not yield significant improvements in oxygen transfer due to limitations in other factors, such as the oxygen-carrying capacity of blood or the diffusion capacity of the sweep gas.

Additionally, the data obtained from measuring CO_2 transfer revealed a consistent increase as blood flow rates increased in room air. However, when oxygen was introduced, the CO_2 transfer increased at the beginning but started to drop with increasing blood flow rates, as depicted in Figure 4.9E and F. In blood oxygenators, the phenomenon of CO_2 transfer or exchange initially increasing but subsequently decreasing with higher blood flow rates can be attributed to two primary factors: (I) Boundary layer thickness: At lower blood flow rates, the boundary layer near the oxygenator membranes tends to be thicker. This thicker boundary layer hampers the transfer of CO_2 from the blood to the sweep gas. As blood flow rates rise, the boundary layer thickness diminishes, leading to more effective CO_2 transfer initially. (II) Volume of CO_2-containing fluid: With increased blood flow rates, a larger volume of fluid carrying CO_2 passes through the membrane or gas-liquid interface. Initially, this increased volume of CO_2-containing fluid enhances CO_2 transfer due to a greater exposure of CO_2 to the sweep gas. However, beyond a certain point, further increases in blood flow rates may result in a saturation effect. In this case, the sweep gas becomes overwhelmed by the volume of CO_2-containing fluid, causing a decrease in CO_2 transfer.

When transitioning the sweep gas from room air to pure oxygen in blood oxygenators, the CO_2 transfer or exchange tends to decrease. This decline can be attributed to the following factors: (I) Partial pressure gradient of gases: CO_2 transfer in blood oxygenators relies on the partial pressure difference between the blood and the sweep gas. When room air, which typically has a lower oxygen concentration, serves as the sweep gas, a larger partial pressure gradient for CO_2 transfer is established. This results in more efficient CO_2 removal from the blood. However, when pure oxygen is used as the sweep gas, the partial pressure gradient for CO_2 transfer decreases, leading

to a reduction in CO_2 exchange efficiency. (II) Competitive effect of oxygen and CO_2: Pure oxygen in the sweep gas increases the concentration of oxygen molecules. This can create a competitive effect between oxygen and CO_2 molecules for binding sites on the oxygenator membrane. As a consequence, the availability of binding sites for CO_2 decreases, impairing the transfer of CO_2 and causing a decrease in CO_2 exchange. It is important to note that the decrease in CO_2 transfer when switching from room air to pure oxygen as the sweep gas may be advantageous in specific contexts. For instance, in certain medical procedures or research studies where the retention of CO_2 or the maximum oxygenation is desired, reducing CO_2 transfer can be beneficial. However, if the goal is efficient CO_2 removal, maintaining room air as the sweep gas may be more effective.

4.4 Conclusion

The primary focus of this study is to develop a pumpless lung assist device (LAD) specifically designed for preterm neonates suffering from respiratory failure. The device utilizes microfluidic blood oxygenators, which offer a substantial surface area for effective gas exchange. In addition, a novel backside photolithography technique was developed to create a large master mold with rounded cross-section channels and a hierarchical blood vascular network. This innovative approach eliminated the need for expensive chromium (Cr) masks by using cost-effective film photolithography masks to achieve channels of varying heights. Consequently, the fabrication process became more affordable and allowed for faster exploration of different channel designs. By utilizing this technique, channels ranging from a few microns to a few hundred micrometers could be produced using a single exposure. In vitro experiments using porcine blood samples were conducted to evaluate the MBO’s and LAD's gas transfer capabilities. The findings demonstrated satisfactory gas exchange in normal air and efficient oxygenation in an environment rich in oxygen. Moving forward, the future development of the LAD will involve implementing long-term strategies to ensure compatibility with blood and tissue, as well as exploring its application through the umbilical vessels using a newborn piglet model. These advancements aim to enhance the device's performance and cater to the physiological requirements of preterm neonates with respiratory distress syndrome (RDS).

4.5 References

1. Debevec, T.; Narang, B.J.; Manferdelli, G.; Millet, G.P. Premature Birth: A Neglected Consideration for Altitude Adaptation. *Journal of Applied Physiology* **2022**, *133*, 975–978, doi:10.1152/japplphysiol.00201.2022.

2. Lammertink, F.; Vinkers, C.H.; Tataranno, M.L.; Benders, M.J.N.L. Premature Birth and Developmental Programming: Mechanisms of Resilience and Vulnerability. *Frontiers in Psychiatry* **2021**, *11*.

3. de Mendonça, E.L.S.S.; de Lima Macêna, M.; Bueno, N.B.; de Oliveira, A.C.M.; Mello, C.S. Premature Birth, Low Birth Weight, Small for Gestational Age and Chronic Non-Communicable Diseases in Adult Life: A Systematic Review with Meta-Analysis. *Early Human Development* **2020**, *149*, 105154, doi:10.1016/j.earlhumdev.2020.105154.

4. Walani, S.R. Global Burden of Preterm Birth. *International Journal of Gynecology & Obstetrics* **2020**, *150*, 31–33, doi:10.1002/ijgo.13195.

5. Naumburg, E.; Söderström, L. Increased Risk of Pulmonary Hypertension Following Premature Birth. *BMC Pediatrics* **2019**, *19*, 288, doi:10.1186/s12887-019-1665-6.

6. Ofman, G.; Pradarelli, B.; Caballero, M.T.; Bianchi, A.; Grimaldi, L.A.; Sancilio, A.; Duenas, K.; Rodriguez, A.; Ferrero, F.; Ferretti, A.; et al. Respiratory Failure and Death in Vulnerable Premature Children With Lower Respiratory Tract Illness. *The Journal of Infectious Diseases* **2020**, *222*, 1129–1137, doi:10.1093/infdis/jiaa046.

7. Razak, R.; Adisasmita, A. Low Birth Weight and Asphyxia Neonatorum Risk: A Case-Control Study.; Atlantis Press, June 19 2020; pp. 384–387.

8. Cannavò, L.; Rulli, I.; Falsaperla, R.; Corsello, G.; Gitto, E. Ventilation, Oxidative Stress and Risk of Brain Injury in Preterm Newborn. *Ital J Pediatr* **2020**, *46*, 100, doi:10.1186/s13052-020-00852-1.

9. De Bie, F.R.; Davey, M.G.; Larson, A.C.; Deprest, J.; Flake, A.W. Artificial Placenta and Womb Technology: Past, Current, and Future Challenges towards Clinical Translation. *Prenatal Diagnosis* **2021**, *41*, 145–158, doi:10.1002/pd.5821.

10. Dabaghi, M.; Rochow, N.; Saraei, N.; Mahendran, R.K.; Fusch, G.; Chan, A.K.C.; Brash, J.L.; Fusch, C.; Selvaganapathy, P.R. Miniaturization of Artificial Lungs toward Portability. *Advanced Materials Technologies* **2020**, *5*, 2000136, doi:10.1002/admt.202000136.

11. Van Ommen, C.H.; Neunert, C.E.; Chitlur, M.B. Neonatal ECMO. *Frontiers in Medicine* **2018**, *5*.

12. Ijsselstijn, H.; van Heijst, A.F.J. Long-Term Outcome of Children Treated with Neonatal Extracorporeal Membrane Oxygenation: Increasing Problems with Increasing Age. *Semin Perinatol* **2014**, *38*, 114–121, doi:10.1053/j.semperi.2013.11.009.

13. Zwischenberger, J.B.; Nguyen, T.T.; Upp, J.R.; Bush, P.E.; Cox, C.S.; Delosh, T.; Broemling, L. Complications of Neonatal Extracorporeal Membrane Oxygenation. Collective Experience from the Extracorporeal Life Support Organization. *J Thorac Cardiovasc Surg* **1994**, *107*, 838–848; discussion 848-849.

14. Teber, O.O.; Altinay, A.D.; Mehrabani, S.A.N.; Tasdemir, R.S.; Zeytuncu, B.; Genceli, E.A.; Dulekgurgen, E.; Pekkan, K.; Koyuncu, İ. Polymeric Hollow Fiber Membrane Oxygenators as Artificial Lungs: A Review. *Biochemical Engineering Journal* **2022**, *180*, 108340, doi:10.1016/j.bej.2022.108340.

15. He, T.; He, J.; Wang, Z.; Cui, Z. Modification Strategies to Improve the Membrane Hemocompatibility in Extracorporeal Membrane Oxygenator (ECMO). *Adv Compos Hybrid Mater* **2021**, *4*, 847–864, doi:10.1007/s42114-021-00244-x.

16. Doyle, A.J.; Hunt, B.J. Current Understanding of How Extracorporeal Membrane Oxygenators Activate Haemostasis and Other Blood Components. *Frontiers in Medicine* **2018**, *5*.

17. Blauvelt, D.G.; Abada, E.N.; Oishi, P.; Roy, S. Advances in Extracorporeal Membrane Oxygenator Design for Artificial Placenta Technology. *Artificial Organs* **2021**, *45*, 205–221, doi:10.1111/aor.13827.

18. Potkay, J.A. The Promise of Microfluidic Artificial Lungs. *Lab Chip* **2014**, *14*, 4122–4138, doi:10.1039/C4LC00828F.

19. Ma, L.J.; Akor, E.A.; Thompson, A.J.; Potkay, J.A. A Parametric Analysis of Capillary Height in Single-Layer, Small-Scale Microfluidic Artificial Lungs. *Micromachines* **2022**, *13*, 822, doi:10.3390/mi13060822.

20. Thompson, A.J.; Ma, L.J.; Plegue, T.J.; Potkay, J.A. Design Analysis and Optimization of a Single-Layer PDMS Microfluidic Artificial Lung. *IEEE Trans. Biomed. Eng.* **2019**, *66*, 1082–1093, doi:10.1109/TBME.2018.2866782.

21. Dabaghi, M.; Saraei, N.; Fusch, G.; Rochow, N.; Brash, J.L.; Fusch, C.; Selvaganapathy, P.R. Microfluidic Blood Oxygenators with Integrated Hollow Chambers for Enhanced Air Exchange from All Four Sides. *Journal of Membrane Science* **2020**, *596*, 117741, doi:10.1016/j.memsci.2019.117741.

22. Astor, T.L.; Borenstein, J.T. The Microfluidic Artificial Lung: Mimicking Nature's Blood Path Design to Solve the Biocompatibility Paradox. *Artificial Organs* **2022**, *46*, 1227–1239, doi:10.1111/aor.14266.

23. Isenberg, B.C.; Vedula, E.M.; Santos, J.; Lewis, D.J.; Roberts, T.R.; Harea, G.; Sutherland, D.; Landis, B.; Blumenstiel, S.; Urban, J.; et al. A Clinical-Scale Microfluidic Respiratory Assist Device with 3D Branching Vascular Networks. *Advanced Science* **2023**, *10*, 2207455, doi:10.1002/advs.202207455.

24. Vedula, E.M.; Isenberg, B.C.; Santos, J.; Lai, W.; Lewis, D.J.; Sutherland, D.; Roberts, T.R.; Harea, G.T.; Wells, C.; Teece, B.; et al. Multilayer Scaling of a Biomimetic Microfluidic Oxygenator. *ASAIO J* **2022**, *68*, 1312–1319, doi:10.1097/MAT.0000000000001647.

25. *Microfluidics and Nanofluidics Handbook: Fabrication, Implementation, and Applications*; Mitra, S.K., Chakraborty, S., Eds.; CRC Press: Boca Raton, Fla, 2012; ISBN 978-1-4398-1672-1.

26. Chen, C.; Hirdes, D.; Folch, A. Gray-Scale Photolithography Using Microfluidic Photomasks. *Proceedings of the National Academy of Sciences* **2003**, *100*, 1499–1504, doi:10.1073/pnas.0435755100.

27. Raj M, K.; Chakraborty, S. PDMS Microfluidics: A Mini Review. *Journal of Applied Polymer Science* **2020**, *137*, 48958, doi:10.1002/app.48958.

28. Gale, B.K.; Jafek, A.R.; Lambert, C.J.; Goenner, B.L.; Moghimifam, H.; Nze, U.C.; Kamarapu, S.K. A Review of Current Methods in Microfluidic Device Fabrication and Future Commercialization Prospects. *Inventions* **2018**, *3*, 60, doi:10.3390/inventions3030060.

29. Fenech, M.; Girod, V.; Claveria, V.; Meance, S.; Abkarian, M.; Charlot, B. Microfluidic Blood Vasculature Replicas Using Backside Lithography. *Lab on a Chip* **2019**, *19*, 2096–2106, doi:10.1039/C9LC00254E.

30. Toepke, M.W.; Kenis, J.A. Multilevel Microfluidics via Single-Exposure Photolithography. *J. Am. Chem. Soc.* **2005**, *127*, 7674–7675, doi:10.1021/ja050660+.

31. Kang, M.; Hwan Byun, J.; Na, S.; Li Jeon, N. Fabrication of Functional 3D Multi-Level Microstructures on Transparent Substrates by One Step Back-Side UV Photolithography. *RSC Advances* **2017**, *7*, 13353–13361, doi:10.1039/C6RA28812J.

32. Hafeez, H.; Ryu, H.-Y.; An, I.S.; Oh, H.-K.; Ahn, J.-H.; Park, J.-G. Dimensionally Controlled Complex 3D Sub-Micron Pattern Fabrication by Single Step Dual Diffuser Lithography (DDL). *Microelectronic Engineering* **2015**, *143*, 25–30, doi:10.1016/j.mee.2015.02.053.

33. Lee, J.-H.; Choi, W.-S.; Lee, K.-H.; Yoon, J.-B. A Simple and Effective Fabrication Method for Various 3D Microstructures: Backside 3D Diffuser Lithography. *J. Micromech. Microeng.* **2008**, *18*, 125015, doi:10.1088/0960-1317/18/12/125015.

34. Kim, H.-D.; Yoon, G.-W.; Yeon, J.; Lee, J.-H.; Yoon, J.-B. Fabrication of a Uniform Microlens Array over a Large Area Using Self-Aligned Diffuser Lithography (SADL). *J. Micromech. Microeng.* **2012**, *22*, 045002, doi:10.1088/0960-1317/22/4/045002.

35. Rengarajan, V.; Geng, J.; Huang, Y. Fabrication of Tapered 3D Microstructure Arrays Using Dual-Exposure Lithography (DEL). *Micromachines* **2020**, *11*, 903, doi:10.3390/mi11100903.

36. Dabaghi, M.; Saraei, N.; Fusch, G.; Rochow, N.; Brash, J.L.; Fusch, C.; Ravi Selvaganapathy, P. An Ultra-Thin, All PDMS-Based Microfluidic Lung Assist Device with High Oxygenation Capacity. *Biomicrofluidics* **2019**, *13*, 034116, doi:10.1063/1.5091492.

37. Dabaghi, M.; Fusch, G.; Saraei, N.; Rochow, N.; Brash, J.L.; Fusch, C.; Ravi Selvaganapathy, P. An Artificial Placenta Type Microfluidic Blood Oxygenator with Double-Sided

Gas Transfer Microchannels and Its Integration as a Neonatal Lung Assist Device. *Biomicrofluidics* **2018**, *12*, 044101, doi:10.1063/1.5034791.

38. Matharoo, H.; Dabaghi, M.; Rochow, N.; Fusch, G.; Saraei, N.; Tauhiduzzaman, M.; Veldhuis, S.; Brash, J.; Fusch, C.; Selvaganapathy, P.R. Steel Reinforced Composite Silicone Membranes and Its Integration to Microfluidic Oxygenators for High Performance Gas Exchange. *Biomicrofluidics* **2018**, *12*, 014107, doi:10.1063/1.5014028.

39. Rochow, N.; Chan, E.C.; Wu, W.-I.; Selvaganapathy, P.R.; Fusch, G.; Berry, L.; Brash, J.; Chan, A.K.; Fusch, C. Artificial Placenta - Lung Assist Devices for Term and Preterm Newborns with Respiratory Failure. *Int J Artif Organs* **2013**, *36*, 377–391, doi:10.5301/ijao.5000195.

5. Chapter 5: Conclusion and Recommendations for Future Work

5.1 Conclusion

This thesis explores the development of several microfluidic blood oxygenators, targeting the limitations associated with their traditional counterparts found in existing literature and as listed in Chapter 1. Key challenges like constrained throughput, diminished gas exchange in room air, intricate blood channel configurations, issues with scaling, and extensive build-up volume are systematically tackled within this research.

Traditional microfluidic blood oxygenators were limited in their capacity, often managing volumes under 20 mL/min. Their performance diminished significantly at higher blood flow rates, especially when room air was the chosen sweep gas. To address this, the central goal of this thesis was the scale-up and integration of these oxygenators into a modular lung assist device (LAD) to ensure it aligns with the demands of clinical applications. One of the main challenges with microfluidic lung assist devices has been to ensure ample gas transfer at a low-pressure drop for pumpless functionality, without necessitating a large priming volume of blood. In the first part of this thesis, we enhanced the gas exchange efficiency of our placenta-type microfluidic LAD. By employing a fabrication method, we produced large-area thin film microfluidic blood oxygenators (MBO) that offer a larger gas exchange surface area. The constructed LAD, using these sacled-up MBOs, displayed a notable rise in oxygen saturation levels: an increase of 30% at a 40 ml/min flow rate with a 23 mm Hg pressure drop in room air. This is adequate for aiding at least 1 kg preterm neonates facing respiratory challenges. In a pure oxygen atmosphere, the LAD's capacity expands to support neonates up to 2 kg. Testing showcased the LAD's ability to manage blood flow rates as high as 150 ml/min, elevating oxygen saturation by approximately 20%. This equates to an oxygen transfer rate of 7.48 mL/min in oxygen-rich settings, ranking among the top for placenta-type devices. Such efficiency positions this LAD as an invaluable tool for assisting neonates (1-2 kg) in respiratory distress. This importance achieved while the new LAD also reduced the priming volume from 18.4 mL to 14.88 mL. This study highlighted the importance of scaling up the size of MBOs to increase throughput and also reduce the number of connectors required for assembling a LAD. The scaled-up MBOs were fabricated based on 8-inch master molds, but there is potential to extend the size of these master molds to 12 inches. Such an increase would pave the way for MBOs that can accommodate higher blood flow rates, possibly sufficient to support one kg babies without the

need for a LAD assembly. It is worth noting that it would be ideal to develop a 12-inch master mold with channels of varying heights from the inlet/outlet towards the center of the mold to diminish hydraulic resistance.

Historically, photolithography was the go-to method for fabricating master molds for MBOs. However, a significant drawback of standard photolithography is its inability to produce micro features of varied heights in a single step. This leads to oxygenators with uniform channel heights throughout, resulting in increased velocity, shear stress, and, consequently, elevated pressure drops at the inlets and outlets. This non-uniformity can also induce localized high shear stress, heightening the risk of thrombotic reactions. While more intricate photolithography techniques can achieve varied channel heights, they can inadvertently introduce stagnation zones and high shear stress at intersecting channels, particularly where the heights differ. To circumvent these issues, we innovated a backside photolithography approach for fabricating double-sided MBOs with hierarchy blood channels. This method was used to fabricate a large master mold featuring rounded channels and a hierarchical blood vascular system. Replacing the traditional expensive chromium mask, we leveraged cost-effective film photolithography masks, allowing for varied channel heights. This economical approach accelerated our design exploration while keeping costs low. Remarkably, our method enabled the fabrication of channels ranging from mere microns to several hundred micrometers with a single exposure. The hallmark of this research is the incorporation of thin membranes on both sides of the microchannels designated for gas exchange. Due to the hierarchical structuring of these microchannels, there is a notable height disparity ranging from the inlet/outlet zones (approximately 600 µm) to the central gas exchange channels (around 100 µm). This presents a challenge when using traditional fabrication techniques for double-sided MBOs. We have introduced a novel microfabrication technique to overcome this obstacle, paving the way for the first MBOs with hierarchical blood microchannels and dual-sided gas transfer diffusion. The limitations of this fabrication method and its capacity for future work is discussed in the next section.

5.2 Recommendations for future works

While the microfluidic blood oxygenators highlighted in this study have demonstrated potential in addressing the oxygenation requirements of preterm neonates with RDS within an artificial placenta setting, their transition to clinical applications for adult patients remains to be realized.

One of the most significant challenges has been the need for enhanced oxygenation capacity. Despite our concentrated efforts in this thesis, which led to a marked improvement in gas exchange, making it viable for a 2 kg neonate, there is an evident demand for even greater capacity. This expansion would not only cater to a broader patient demographic but would also allow for the design and implementation of more compact devices. Parallel to these developments, there is a pressing need to enhance the device's hemocompatibility and to devise strategies to mitigate clot formation within the oxygenator. It is crucial to note that the development of hemocompatibility methods and surface modification strategies were beyond the scope of this thesis, but their incorporation is essential for the device's future success. Furthermore, creating efficient vascular access systems that facilitate seamless and efficient integration of the oxygenator with the human body, especially with minimal pressure drops, remains a priority. As we envision these oxygenators becoming more mainstream, it is imperative to innovate and adopt manufacturing technologies that allow for consistent, reliable, and large-scale production. Delving into these areas could significantly influence the progression of microfluidic blood oxygenators, making them apt for a more diverse patient group.

5.2.1 Optimizing Design and Scalability of MBOs with Hierarchical Blood Microchannels

In this thesis, the MBOs featuring hierarchical blood microchannels and double-sided gas diffusion showcased successful blood oxygenation at a significant flow rate of 15 mL/min in oxygen-rich settings. A noticeable challenge, however, was the elevated hydraulic resistance, signaling a need for design optimization. A potential reason for this resistance could be the dimensions of the blood distribution channels, which are solely for blood distribution and not for gas transfer. Adjusting the width and optimizing the angles of these channels relative to the primary inlet/outlet channel could decrease hydraulic resistance without affecting gas exchange efficacy. Moreover, refining the SU8 deposition thickness when fabricating master molds could reduce the height of the two predominant blood channels linked to the inlet/outlet, resulting in a decrease in the overall priming volume but retaining the MBOs' gas exchange capabilities. By implementing these adjustments, we can achieve reductions in hydraulic resistance, pressure drop, and priming volume. On another note, the current design is restricted by a 6-inch master mold, limiting gas exchange microchannels to 96. Transitioning to an 8-inch mold or even 12-inch mold would accommodate more of these channels, promoting enhanced gas transfer at increased blood flow rates.

The PDMS framework, tailored for the double-sided iteration of these MBOs, offers the potential to incorporate inlets/outlets. This would enable the stacking of multiple MBOs without the necessity for connectors, simplifying LAD assembly. Such an integration would not only minimize areas of blood contact and overall priming volume but also pave the way for a more streamlined and compact LAD design.

5.2.2 Fabrication of unified device through additive manufacturing techniques

While photolithography stands out for its proficiency in 2D designs, its dimensional constraints call for the investigation of other fabrication techniques. The innovative fabrication method presented in this thesis, which introduces rounded cross-sectional microchannels and a hierarchical network of blood channels, is nonetheless limited when it comes to sculpting true 3D designs. The developed fabrication method can be considered as a 2.5D technique to realize channels with more complex geometries. Here, additive manufacturing shines as a superior choice, providing a route to devise larger devices endowed with true intricate 3D attributes. This versatile technique can be used in two pivotal ways: one, to fashion expansive master molds with 3D geometries and elaborate designs, and two, to engineer an integrated double-sided oxygenator employing sacrificial material printing. The advantage of additive manufacturing lies in its ability to carve out detailed 3D structures with an impressive accuracy that scales down to mere micrometers. It is particularly advantageous for generating large-scale microfluidic blood oxygenators requiring channels that subtly slope from the inlet and outlet zones towards the central gas exchange region. However, a caveat to consider is the inherent roughness of 3D-printed components, a characteristic potentially detrimental for devices intended for blood processing. To ameliorate this, surface modification procedures must be synergized with this fabrication method to refine surface textures, thereby mitigating any thrombotic risks.

Additionally, the use of a sacrificial material offers a pioneering pathway to conceive an integrated LAD. This process commences with a 3D printer delineating the vascular pathways or blood microchannels with a material that is soluble, either in water or select chemicals. The capability to layer these constructs atop one another in a single session is a significant advancement. Once established, the PDMS envelopes these intricate 3D designs. When the sacrificial material is dissolved, what remains is a seamless device, primed for use, and devoid of any necessity for extra bonding. An added layer of sophistication can be infused by deploying multi-material printing,

allowing layers composed of distinct materials to be differentiated and removed with varying solvents, paving the way for even more intricate designs. This methodology reaps multifaceted rewards: it obviates the need for bonding, facilitates tailor-made device sizing, and dispenses with the assembly of singular oxygenator units and connectors, all while shaving of priming volume.